AXIAL LOAD BEHAVIOUR OF THIN WALLED STEEL SECTIONS WITH OPENINGS

BY

AVNASH SINGH BANWAIT

AXIAL LOAD BEHAVIOUR

OF

THIN WALLED STEEL SECTIONS WITH OPENINGS

By

Avnash Singh Banwait

A Thesis

Submitted to the School of Graduate Studies

in Partial Fulfilment of the Requirements

for the Degree

Master of Engineering

McMaster University

April 1987

MASTER OF ENGINEERING (1987) McMASTER UNIVERSITY
(Civil Engineering) Hamilton, Ontario

TITLE: Axial Load Behaviour of Thin Walled Sections with Openings

AUTHOR: Avnash Singh Banwait (B.Sc. Eng.)

SUPERVISOR: Dr. K.S. Sivakumaran

NUMBER OF PAGES: xv, 130

ABSTRACT

In the application of cold formed steel structural members, holes are usually cut in the webs of sections for passing pipes or conduits. The Canadian standard for the design of cold formed steel sections does not provide sufficient design information for these conditions. However, the American Iron and Steel Institute has recently provided design guidelines for sections with circular perforations based on limited available experimental data.

The purpose of this study is to determine the effect of size and shape of openings on the axial load behaviour of cold formed sections having different flat width-to-thickness ratios of webs.

A total of fifty five stub column tests were performed to provide design guidelines for stiffened plates with openings. Cold formed lipped channel steel sections were selected for the tests. Circular, square or slotted holes were cut in the centres of the webs. The diameter, or width of the openings, varied from 0 to 0.6 times the flat width of the web. The tests were performed under axial compression and centering of the specimen was done with the help of strain gauges. Load versis axial shortening and out-of-plane deflection curves are plotted. Experimental buckling loads of the sections are obtained using the strain reversal method. Ultimate loads of the stub columns are

calculated using the effective width approach given in North American codes. An empirical relationship was derived from the experimental data for the effect of square or circular openings in the web on the strength of cold formed sections.

It was found that the buckling load of a section decreases with respect to the buckling load of an unperforated section when size (diameter or width) of the opening is 20% of the flat width of the web but increases as the size of the opening is increased to 60%. The ultimate strength of sections with circular and square openings changes insignificantly when the size of the openings is 20% of the flat width of web. However, it drops to about 87% when the opening size is increased to 60%.

The shape of the opening influences the degree of reduction in strength. The shapes in increasing order of influence are circular, square and slotted openings. The maximum drop in compressive strength, about 14%, was for the section with a slotted opening, of width of about 48% of the web flat width. It also shows the importance of both the longitudinal and transverse dimensions of the opening. The design guidelines provided by the American Iron and Steel Institute (1986) are conservative. The equation proposed herein accurately predicts the effect of square or circular perforations on the strength of the cold formed steel sections.

ACKNOWLEDGEMENTS

I would like to express my gratitude to my supervisor, Dr. K. S. Sivakumaran, for suggesting this research topic and for his constant guidance and encouragement throughout my work.

I thank Dr. R. M. Korol for his valuable advice during the initial stages of this research.

Thanks are also due to Mr. David Perrett, Mr. Peter Koudys, and Mr. Ross McAndrew for their timely help in preparation of the specimens during the experimental work. Thanks also to Bailey Metal Products Limited, Toronto, and Brockhouse Limited, Bramalea, for their donations of material for test specimens. I also want to thank the Department of Civil Engineering and Engineering Mechanics, for providing funds and laboratory facilities, and the Natural Sciences and Engineering Research Council for supporting this research project.

I wish to thank Dr. Sikander Azam for his moral support and encouragement.

Finally, I am thankful to my beloved wife, Kuldeep, for typing test data and for being patient during this research.

To my dear parents

TABLE OF CONTENTS

Table of Contents (continued)

List of Tables

List of figures

List of Figures (continued)

List of Figure (continued)

List of figures (continued)

LIST OF SYMBOLS

B -Effective width of an element.

B_i -Effective width of web, flanges, and lips, for i=1, 2 and 3 respectively.

B_p -Effective width of perforated web.

B_{un} -Effective width of an unperforated web.

C -A constant in equation 5.12.

d -Diameter of a perforation.

E -Modulus of elasticity of steel.

f -Stress in a plate element.

f_{max} -Maximum stress in a plate element.

f_y -Yield strength of steel.

f_u -Ultimate strength of steel.

h -Height of the straight portion of a perforation.

I_{min} -Minimum required moment of inertia of a stiffener about its own centroidal axis parallel to the end stiffened element.

k -Buckling coefficient.

n -A constant in equation 5.12.

L -Length of the specimen.

P -Axial compressive load.

P_{aisi} -Ultimate axial compressive load calculated as per AISI-1986.

P_{csa} -Ultimate axial compressive load of a specimen calculated by modifying provisions of CAN3-S136-M84.

P_{cr} -Critical or Buckling load of a specimen.

P_t -Experimental compressive axial ultimate load of the specimen.

P_1 -Calculated ultimate loads of specimens using equations 5.4 and 5.16.

P_2 -Calculated ultimate loads of specimens using equation 5.7 and 5.16.

P_3 -Loads obtained by dividing loads P_2 by a factor.

$\bar{P}$ -Load at any data point selected as a pivotal point.

r -Radius of the perforation.

R -Reduction factor defined in equation 5.9

R_w -Ratio of W_p and W_{un}.

t -Base metal thickness.

W -Flat width of the element (width of an element exclusive of rounded corners).

W_i -Flat width of web,flanges, and lips, for i= 1, 2, and 3 respectively.

W_{lim} -Limiting value of flat width for fully effective compressive elements.

W_p -Flat width of a perforated web.

W_{un} -Flat width of an unperforated web.

Δ_0 -Initial imperfection at the centre of a plate element.

Δ_t -Total out-of-plane deflection at the centre of the plate element.

Δ -Measured out-of-plane deflection at the centre of of the plate element.

$\bar{\Delta}$ -Measured out-of-plane deflection at the center of a plate element at a data point, selected as pivotal point.

Ψ -A function in equation 4.1.

CHAPTER 1

INTRODUCTION

1.1 GENERAL BACKGROUND

Presently, there are two families of steel sections in use, namely, hot rolled steel shapes and cold formed steel sections. The hot rolled sections are commonly used for heavy construction. However, the usually available shapes of hot rolled sections such as WWF, W, M, S, C, MC and HSS, and their sizes, are limited due to production difficulties. The use of cold formed steel structural sections is becoming increasingly popular, especially for construction of houses and low rise commercial buildings. The members are cold formed to various shapes from steel sheets, strips, plates, or flat bars, using roll forming and press braking, or bending brake operations. The choice of the shape of the cross section, and grade of steel, may depend upon the type of loading conditions and preference of the designer. The thickness of material may vary, but, in general, the cold formed structural sections have greater width to thickness ratios than the hot rolled shapes. Therefore, as will be explained later, the cold formed sections are more susceptible to local buckling than the hot rolled shapes.

The use of cold formed steel sections started in

the middle of the nineteenth century. However, these thin walled sections were not widely used because of a lack of knowledge about their behaviour. With the development of the aircraft industry in the early twentieth century, much research work was done on thin walled structures to help design as light an aircraft as possible. The material used in aircraft structural components was aluminium, due to its better weight to strength ratio over steel, but the basic principles used in the analysis of aluminium thin walled structures are applicable for steel structures as well.

Cold formed steel sections were also widely used in the production of automobile bodies. Knowledge gained from the aircraft and automobile industries increased their use in building construction. Consequently, the American Iron and Steel Institute issued the first design guidelines for the use of cold formed steel sections in 1946. Since then, their use in building construction has grown many fold (YU, 1985). At present, in addition to building and bridge construction, cold formed steel sections are used in car bodies, railway coaches, storage racks, grain bins, highway products, transmission towers and poles, and drainage facilities.

In light building construction, cold formed steel is preferred over hot rolled steel for the following reasons (YU, 1985):

(a) Favourable weight-to-span ratio can be obtained

by forming different shapes as desired by loading conditions.

(b) Load carrying panels and decks can provide a useful surface for floor, roof and wall construction. These may also provide an enclosed cell for passing electrical and other conduits.

(c) Nestable sections can be produced allowing for economical packing, shipping, and construction.

Cold formed steel sections also have advantages over the traditional light construction materials such as wood and concrete. These include economy in foundations, fast construction, accurate detailing, elimination of form work, enclosure for ducts and pipes, etc.

Brief descriptions of the methods of cold forming and design considerations of cold formed compression members are presented in the following sections.

1.2 METHODS OF COLD FORMING

Two primary methods used in the manufacture of cold formed sections are:

1.2.1 COLD ROLL-FORMING

This is the most widely used method for mass production of cold formed steel sections. With this method, a section is formed continuously by gradually feeding the steel sheet through sucessive pairs of rolls, which act as

male and female dies. Each pair of rolls progressively forms the section from the sheet. Depending upon the geometry of the section, 5 to 16 pairs of rolls may be used. The usual speed of forming a section may vary between 10 to 25 m/min. But it can be as high as 100 m/min. The cross-section produced by cold roll-forming can be held within very close dimensional tolerances, normally plus or minus 0.4 mm. Hence, the members are usually uniform in cross-section.

1.2. 2 PRESS BRAKE OPERATION

This method is preferable when the section to be formed is of simple configuration, and with relatively wide plate components. It is usually used if the required quantity is less than 1000 linear meters. The equipment used in the press brake operation consists of a moving top beam and stationary bottom bed, on which dies applicable to the particular cold formed steel shape are mounted. In general, press beds are limited to a length up to 3 meters. Some of the more powerful machines can form section up to 8 meters in length (Walker, 1975).

There are other less popular ways of cold forming. A method used for manufacturing simple sections such as angles, Z-sections, and channels is the bending brake operation. However, it is not suitable for more complex sections. Other production methods for cold-forming include drawing and extrusions. These methods are not economical in

mass production of prismatic steel sections and are not commonly used.

1.3 DESIGN CONSIDERATIONS FOR THE COLD FORMED STEEL SECTIONS

Cold formed steel sections are used to frame either a part, or the entire building. Some typical applications in building construction are:

1. as individual structural framing members, such as joists, girders, girts, studs, and columns.
2. as surface members such as roof and floor decks and wall panels.
3. as standardized steel buildings.

Naturally, the design considerations vary with the application. Here, only those related to the cold formed members, specifically columns subjected to axial compressive loads are discussed.

Compression members comprising of cold formed sections are prone to three types of failure for which it is essential to design against:

(a) overall buckling

(b) local buckling

(c) combination of the above two.

1.3.1 OVERALL COLUMN BUCKLING OF COLD FORMED MEMBERS

Overall member buckling generally occurs in slender columns. The cold formed compression members may buckle in one of the following modes:

1. flexural buckling about the axis of weakest bending stiffness.
2. torsional buckling may occur because the torsional stiffness of an open thin walled section is proportional to the cube of the wall thickness; consequently, cold formed sections consisting of thin elements may be relatively weak against torsion.
3. A combination of torsional and flexural deformations is called lateral-torsional buckling. This occurs in sections where the shear centre does not coincide with the centroid, which is common for many cold formed steel sections.

For hot rolled sections the most common mode of buckling is overall flexural buckling. This occurs because most hot rolled shapes have at least one axis of symmetry, and the sections are so proportioned that flexural buckling can occur prior to torsional buckling (Chilver, 1961).

Well-established theories exist for the design of cold formed members which fail in overall column buckling. Therefore, this study is not concerned with this problem.

1.3.2 LOCAL BUCKLING AND POST BUCKLING STRENGTH

The plate components of cold formed steel members usually have high width to thickness ratios (the thickness of cold formed sections made from steel sheets ranges from 0.4 to 6.4 mm, whereas steel plates or bars may be as thick

as 25 mm). These thin plate elements may buckle locally at stress levels less than the overall buckling stress, when subjected to compression, shear, bending or bearing loads. Local buckling is said to take place when the plate elements of a thin walled section buckle without any overall bending, or twisting of the member as a whole. It is assumed that during local buckling, the common edges of component plate elements remain straight, and the original angle between adjacent plates at their common edge is maintained. Buckling will occur in all the plate elements of the section simultaneously. The wave length of buckles in all the plate elements will be the same. Exceptions to this phenomenon occur when sections have large variations in plate thickness, or the angle between the plate elements is very shallow (Allen and Bulson, 1980).

Plate components of hot rolled sections have comparatively low width to thickness ratios. These components do not normally exhibit local buckling instability prior to overall buckling instability.

For an ideal plate buckling may be produced due to compressive forces which act along the middle surface of the plate when the membrane strain energy at a certain critical load level is converted into the strain energy of bending. At this point, (point B of Curve I, Fig.1.1) large deformations perpendicular to the surface of the plate take place (Cook, 1981). However, in plates adequately supported

at the edges, buckling does not necessarily mean failure, since plates have appreciable reserve strength due to the membrane action. For proper utilisation of this additional strength, analysis of post-buckling behaviour is required (Lee and Harris, 1978). During this stable post buckling the member will continue to carry additional loads. However, there will be a redistribution of stress after buckling. Edges of the plate components continue to take load until they yield. The ultimate strength of these cold formed members can be many times higher than the buckling load (Yu, 1985 and Chilver, 1961).

The sudden change in geometrical shape of the plate at the time of buckling, from flat to curved surface as described in the previous paragraph, is only possible for perfectly flat plates loaded along the middle surface. However, in practice, plates have imperfections or may be loaded eccentrically. The behaviour of such plates is a gradual transition from pre-buckling to post-buckling as shown by Curve II of fig. 1.1.

In North America, design of cold formed steel structural members is governed by the Canadian Standards Association (1984) publication "Cold Formed Steel Structural Members, CAN3-S136-M84" and American Iron and Steel Institute (1986) publication "Specification for the Design of Cold-Formed Steel Structural Members". Accordingly, the strength of a compression member is obtained by adding the

strength of individual flat plate elements including the curved part on the edges. The resistance of an individual plate element including post buckling strength is calculated using the effective width equation given in the codes. The effective width equation is based on work by Winter (1947).

1.4 EFFECT OF HOLES ON LOCAL BUCKLING AND POST-BUCKLING STRENGTHS

In cold formed members used in buildings, holes are usually provided in webs and/or flanges, for duct work, piping and bridging. For steel storage racks, holes are often used for easy assembly. The effect of holes on the strength of thin walled columns is complex. The presence of a hole may increase, or decrease, the buckling load of a member, depending on its size, shape or location. It may also reduce the post buckling strength of individual plate components and, hence, the ultimate strength of the member.

As per CAN3-S136-M84, guidelines exist only for the compression members without any openings. No provisions exist in this code for the design of perforated plate elements. AISI (1986) does, however, provide guidelines to account for the effect of a circular hole punched in the centre of a web whose flat width-to-thickness ratio is up to 70. However, these provisions are based on limited data.

1.5 OBJECTIVES AND SCOPE OF RESEARCH

As discussed above, the unperforated cold formed steel sections can be designed for local, or overall buckling, by using the guidelines of relevant codes. The present study was undertaken in view of the need for proper design guidelines for perforated members, and the limited research done on the behaviour of perforated cold formed structural members under compression. This study is concerned with the behaviour of cold formed members with openings. It was decided to study, experimentally, the effects of the following parameters on the behaviour of these members before, and after, local buckling. The parameters under consideration are;

a. size of a hole.

b. shape of a hole.

c. flat width to thickness ratio of the compressive element with the hole.

The tests were performed on both the perforated and the unperforated cold formed stub columns. From the experimental data, the following curves are drawn:

1. load vs axial shortening of the sections.
2. load vs out-of-plane deflection of the web at a point adjoining the opening at mid-height of the member.

The results also include the local buckling loads and ultimate strengths. Experimental buckling loads of all

the specimens are determined by using strain reversal and maximum membrane methods only. The guidelines provided in CAN3-S136-M84 for the calculation of effective width of unperforated elements are used to calculate the ultimate strength of unperforated sections. In calculating the ultimate strength of the perforated sections, these guidelines are modified to incorporate the effect of openings. The ultimate strength of both unperforated and perforated sections is determined by using AISI (1986) guidelines. Strengths of sections predicted by the above methods are compared with the experimental values. Finally, from the experimental data of this study, an empirical relationship is derived to determine the effect on the strength of a section due to a circular or square opening in its web. This relationship is also verified by experimental data obtained by other ivestigators and is available in literature. This empirical relationship is valid for a stiffened plate having flat width-to-thickness ratio upto 112. The size of opening (square or circular) may be upto 0.6 times the flat width of the plate.

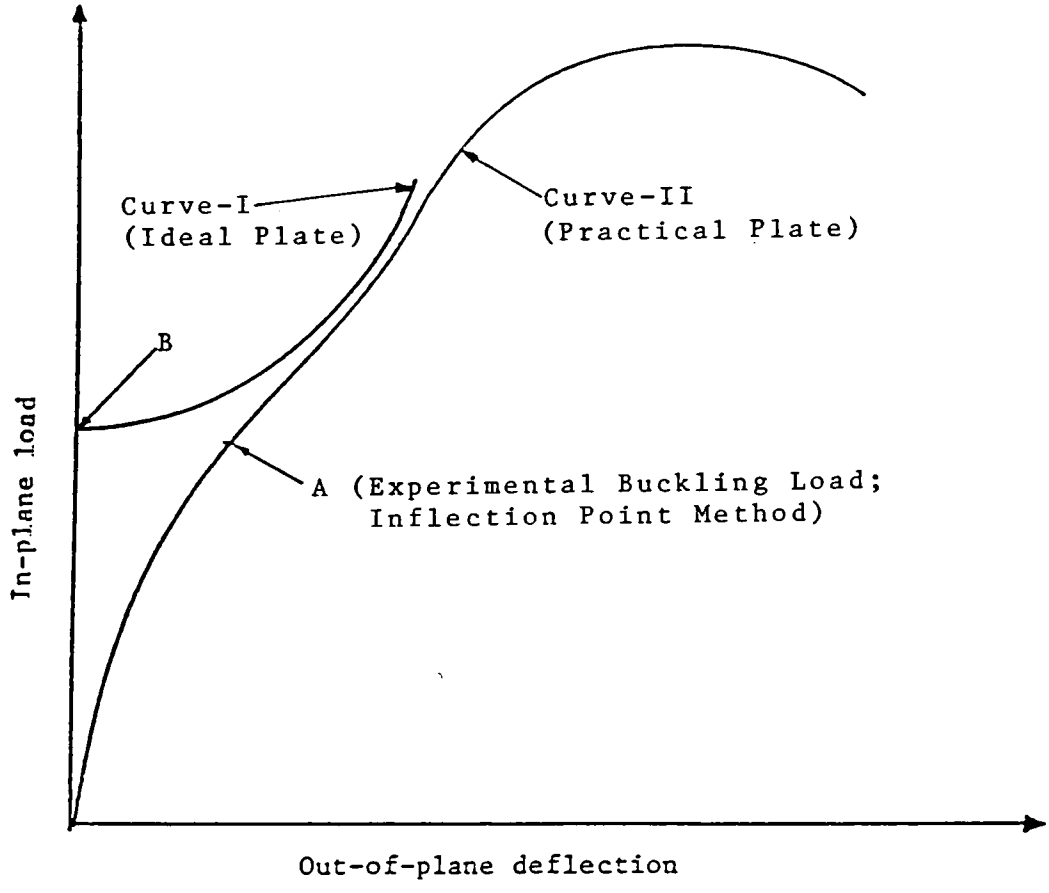

Fig. 1.1 Buckling and Post Buckling behaviour of a thin plate

CHAPTER 2

EXPERIMENTAL PROGRAM

2.1 INTRODUCTION

This chapter provides detailed information on the stub column tests performed on cold formed lipped channel sections. The lipped channel section (Fig. 2.1) was selected for test specimens since it is one of the most commonly used shapes for compression members in structural frames and as wall studs. The lips act as stiffeners of the flanges. The sizes of the cross-section were selected from the available sizes manufactured by industry, however, they have different values of flat width-to-thickness ratios of the webs. A total of 55 specimens were tested, and depending on the sizes of the cross-sections, all the specimens were divided into three different sets, namely, Preliminary Tests, Set I, and Set II, consisting of 3, 28, and 24 specimens, respectively. The material for the three specimens of the preliminary tests was provided by Brockhouse Canada Ltd., Bramalea, Ontario. The rest of the specimens were provided by Bailey Metal Products limited, Toronto, Ontario. The preliminary stub column tests were done to study the general behaviour of the specimens.

Descriptions of the specimens, experimental set-up including the details of the instruments used, and the

testing procedures, are shown in the following sections. Test results are presented in the next chapter, and their analysis is given in subsequent chapters.

2.2 DESCRIPTION OF SPECIMENS

The dimensions (Fig. 2.1) of the specimens for each set are shown in Table 2.1. The lengths of the specimens were chosen with the help of the stub column test procedures provided in Technical Memorandum No.3 of the Column Research Council (1976), now known as the Structural Stability Research Council. For cold formed sections having thin walled plate elements, the stub column test is aimed at determining the effect of local buckling, as well as the effect of cold forming on column performance. Therefore, the length of the stub column test specimen for cold formed sections should be:

a) less than twenty times the minimum radius of gyration.

b) more than three times the largest dimension of the cross-section of the specimen.

The first condition for limiting the length of the specimen is to preclude overall member buckling (flexural, torsional, or a combination of the two) and the second condition is to ensure that the specimen be sufficiently long so that it has the same initial residual stress pattern as a much longer member cut from the same stock (Column Research Council 1976).

However, in most of the sections available from industry, as is the case for the specimens of this study, both conditions cannot be simultaneously satisfied. This is because the dimension of twenty times the minimum radius of gyration is less than three times the maximum dimension of the section. While determining the length of the specimens, it was thought that the effect of residual stresses on a cold formed steel section may not be significant. Moreover, as will be explained in the succeeding paragraph, there was difficulty in finding the appropriate location for mounting instruments, such as strain gauges and displacement transducers. Therefore, only the first condition is satisfied, that is, the maximum length of the specimen is less than twenty times the minimum radius of gyration.

As stated earlier, another factor which governs the selection of length is the location of failure of the section. To evaluate buckling loads of the specimens, and to plot load vs maximum lateral deflection graphs, it is desirable to know the failure location before testing. It is known that the length of the half buckle wave of a specimen lies between the dimension of flange, and the dimension of the web, provided, the angle between the web and the flange is not too large (Allen and Bulson, 1980). As a first trial, therefore, to obtain the crest of the buckle at the mid-height of section, the length of a specimen was taken equal to three times the average value of the widths of flange and

web. However, during the preliminary tests it was found that the length of the section had to be reduced slightly from that previously calculated as above to obtain failure in the middle of the section.

The specimens were cut to lengths, within a tolerance of 1 mm, as shown in Table 2.1. In Set I, the length of the specimen with the slotted hole was kept at 223 mm, due to the large length of the opening along the length of the specimen (Fig. 2.1). The specimens were cut to length with a power band saw, at right angles to the longitudinal axis. Wooden blocks were inserted into the sections to avoid vibrations and to make a slow and smooth cut. The ends of the specimens were lapped with 180 grain sand paper and were checked to see whether these were normal to the longitudinal axis of specimens.

The flat widths (Fig. 2.1) W_1, W_2 and W_3, of the plate elements of the specimens are given in Table 2.1. These were obtained by deducting the rounded corners from the total widths (external or face-to-face) of the plate elements. The width of one side of a rounded corner is equal to three times the plate thickness of the specimen, since the internal radius of the right angle bend is twice the thickness. The total widths of the plate elements of the specimens were obtained from the brochures of the manufacturers. The dimensions given in the brochure were verified by measuring widths of plate elements of each

specimen with vernier calipers (least count 0.0254 mm). The measured values were very close to the values given by the manufacturers brochures (maximum variation of 0.3mm in a plate element). This, however, did not change the calculated results by more than 0.6%, which is negligible. Therefore, the dimensions as shown in Table 2.1, are used in this study for calculations and comparisons.

The design calculations of the cold formed sections are always done using the base metal thickness of galvanized sheet steel. The base metal thicknesses, shown in Table 2.1 for Sets I and II, were obtained by deducting the average thickness of the galvanized coating from the total average thickness of the plate components. The thickness of the coating on the sheet steel was determined as per provisions of ASTM A90-81 " Standard Test Method for Weight of Coating on Zinc-Coated (Galvanized) Iron or Steel Articles (ASTM, 1985). Accordingly, three samples each for Set I and II of 65 mm diameter plate were cut from the sections and weighed. To strip off the galvanized coating, these samples were then dipped in a 50% solution of hydrochloric acid until the bubbles stopped forming. Specimens were then washed with tap water, dried, and weighed again. The difference between the final and initial weights of a specimen is the weight of the coating. The thickness was then calculated as per guidelines in the ASTM standard. The average thickness of the coating was found to be 0.033 mm and 0.05 mm for

specimens of Sets I and II, respectively. The base metal thickness of specimens for the Preliminary Tests was taken from the brochure of the manufacturer (Brockhouse Ltd.).

Various sizes and shapes of openings were made in the centre of the webs of the specimens. Typical openings are shown in Figures 2.2 and 2.3. The slotted openings were made by the manufacturer, while circular and square openings in the centre of the webs were made in the laboratory using a milling machine. Care was taken during these operations to avoid undue initial stresses.

The specimens were numbered according to the shape and size of the perforation in the web. The first letters A, B, and C stand for the circular, square and slotted hole, respectively. The letter D indicates the specimen with no opening. The second number 2, 4, or 6 denotes the approximate percentage of hole size to flat width of the web of the specimen (For example, 4 stands for a hole width, or diameter of forty percent of the flat width of the web). The third number 1, 2, or 3 stands for the first, second, and third specimens of the same type, respectively. The identification numbers of the specimens and hole sizes are shown in Table 2.2.

2.3 MATERIAL PROPERTIES

Steel properties (shown in Table 2.1) such as yield stress f_y, ultimate strength f_u, and initial modulus of

elasticity E, for specimen Sets I and II, were determined in the laboratory. The yield stress and the ultimate strength were obtained from tensile coupons cut from individual plate elements (web and flanges only) as per guidelines provided in ASTM A370-77 "Standard Methods and Definition for Mechanical Testing of Steel Products (ASTM, 1985). Accordingly, stress-strain curves for all tensile coupons were drawn with autographic instruments mounted on the Tinius-Olson Universal testing machine. These curves were truncated at a strain of about 1%. For ultimate strength calculations, load readings at failure of the test coupons were recorded. The initial part of the stress-strain curves for Set I and II were straight lines. At about 70 % and 80 % of yield stress values for Set I and Set II, respectively, the material appeared to start yielding slowly, and the straight lines deviated into curves showing a reduction in slope (modulus of material). There was a sharp bend in the stress strain curves near the yield stress, and the curves became almost flat with a sharp reduction in slope. A very small upward slope showing strain hardening of the material appeared toward the end.

Due to gradually yielding material, the yield stress of each coupon was obtained by the 0.2% offset method. Using this method, a straight line is drawn parallel to the initial straight portion of the stress-strain curve. The starting point of this line is at 0.2% strain. The yield

stress is that corresponding to a point where the above drawn line intersects the stress-strain curve. For Sets I and II, the design values of the yield stress and ultimate strength are obtained by a weighted average procedure. To do so, the sum of the multiplication of yield stress or ultimate strength of individual plate components and their coressponding widths are obtained. This sum is divided by the sum of the widths of the plate elements.

Initial modulus of elasticity values are obtained from the slopes of the stress-strain curves drawn to determine the yield stress. All material properties for Preliminary Tests were adopted from the brochure of the manufacturer.

2.4 INSTRUMENTATION

The experimental set-up is shown in Figures 2.4 to 2.6. The location of instruments, such as strain gauges and diplacement transducers mounted on a specimen, is shown in Fig. 2.1. The following instruments were used for tests.

Loading Machine

A 600 kN capacity Tinius-Olson Universal testing machine was employed to determine material properties and to test stub column specimens. A load range of 20%, with 120 kN as the full load, was adopted for Sets I and II. For Preliminary Tests, a load range of 300 kN was employed because of the higher strength of these specimens.

Displacement Transducers and Dial Gauges

Four displacement transducers of Durham Instruments Type GCD 121-1000 and two of Hewlett Packard Type 7DCDT-1000 were used to measure axial shortening of the specimen and lateral deflection of the web.

Spring loaded dial gauges (least count 0.001 mm) were used to measure the displacement of flanges.

Strain Gauges

Foil type strain gauges having a gauge factor of 2.11 were used. For corners, strain gauges of 5 mm gauge length were used. For the middle of the flanges and for the tip of the hole, 10 mm gauge length strain gauges were adopted to obtain a better average of the strain recorded at these locations, because failure might occur at slightly different positions than the centre line at mid-height.

Locations for mounting the strain gauges, transducers, and dial gauges on the specimen were first marked. To bare the metal at strain gauge mounting locations, an area about twice the size of the strain gauge was cleaned off galvanized coating. The strain gauges were bonded to the specimens as per the procedures of the strain gauge manufacturing company.

Data Recording System

A 40 channel data acquisition system, Autodata Nine:3A/110VAC, was used to record readings of transducers

and strain gauges.

2.5 TESTING PROCEDURE

Since the specimens were subjected to concentric loads, it was decided to center them with respect to loads. To do so, the specimens were placed on a well ground plate at approximately the central position under the head of the testing machine. A ground plate was not used on top of the specimen as the head of the machine was grounded smooth. The exact centering of the specimen was performed by loading the specimen at loads of 30, 20, and 15 kN for Preliminary Tests, Set I and Set II, respectively. Initial and final voltage readings of the four strain gauges located at the four corners at mid-height of the specimens were recorded. Multiplying the difference between the final and initial voltage readings of a strain gauge by the gauge factor gives the value of strain at a gauge location. The mean value of these strains and their deviations from the mean value were obtained. The position of the specimen was shifted until the maximum deviation from mean value for a particular loading range was less than 5%. This limit is difficult to achieve. To help center the specimen to meet this condition, the specimen had to be removed occasionally from the testing machine and the ends lapped again with a fine sand paper on a flat surface. When the specimen was finally centered, four wedges were inserted between the loading head and frame of

the testing machine while the machine was still loaded at the centering load. The insertion of these wedges prevented rotation of the loading head during the remaining stages of the loading cycle.

The load on the specimen was then reduced to 0.6 kN and the transducers were mounted. The initial readings of all measuring devices were recorded and the load on the specimen increased slowly at an interval of 2 to 3 kN. After loading the specimen at each interval, the load was allowed to stabilize for a maximum of three minutes, then the readings of the transducers were taken. This process was continued until the specimen failed and the load began to drop off. After the peak load, only displacement measurements were taken at intervals of about 5 kN. Because this was done while the load was still dropping with the machine still running at the same rate, small errors could be expected in the readings taken after the failure load was reached. Generally, the readings were taken until the load dropped to about 25% of the failure load. The results of these tests are given in Chapter 3.

Table 2.1 Dimensions and material properties of specimens

Item	Specimen Set		
	P	I	II
L (mm)	432	200	265
W1 (mm)	189.48	82.46	144.68
W2 (mm)	62.48	31.66	33.55
W3 (mm)	18.54	7.89	8.84
t (mm)	2.286	1.602	1.287
W1/t	82.89	51.48	112.42
W2/t	27.33	19.77	26.07
W3/t	8.11	4.93	6.87
E (GPa)	203	205	210
fy (MPa)	345	340.6	262.6
fu (MPa)	-	443.6	336.0

Table 2.2 Designation of specimens and shapes and sizes of holes in their webs.

Test No.	Set No.	Shape of hole	Specimen Designation	r (mm)	d (mm)	h (mm)
1			A-2-1			
2	I	Circle	A-2-2	8.25	16.5	-
3			A-2-3			
4			A-4-1			
5	I	Circle	A-4-2	16.5	33.0	-
6			A-4-3			
7			A-6-1			
8	I	Circle	A-6-2	24.75	49.5	-
9			A-6-3			
10			B-2-1			
11	I	Square	B-2-2	-	16.5	16.5
12			B-2-3			
13			B-4-1			
14	I	Square	B-4-2	-	33.0	33.0
15			B-4-3			
16			B-4-4			
17			B-6-1			
18			B-6-2			
19	I	Square	B-6-3	-	49.5	49.5
20			B-6-4			
21			B-6-5			
22			C-I-1			
23	I	Slotted	C-I-2	19.0	38.0	64.0
24		(fig. 2.1)	C-I-3			
25			C-I-4	just one size of opening		
26			D-0-1			
27	I	No Hole	D-0-2	-	-	-
28			D-0-3			

Table 2.2 continued----

Test No.	Set No.	Shape of hole	Specimen Designation	r (mm)	d (mm)	h (mm)
29			A-2-1			
30	II	Circle	A-2-2	14.5	29.0	-
31			A-2-3			
32			A-4-1			
33	II	Circle	A-4-2	29.0	58.0	-
34			A-4-3			
35			A-6-1			
36	II	Circle	A-6-2	43.5	87.0	-
37			A-6-3			
38			B-2-1			
39	II	Square	B-2-2	-	29.0	29.0
40			B-2-3			
41			B-4-1			
42	II	Square	B-4-2	-	58.0	58.0
43			B-4-3			
44			B-6-1			
45	II	Square	B-6-2	-	87.0	87.0
46			B-6-3			
47			C-I-1			
48	II	Slotted	C-I-2	19.0	38.0	64.0
49			C-I-3			
50			D-0-1			
51	II	No Hole	D-0-2	-	-	-
52			D-0-3			
53	P	Circle	A-3-1	28.6	57.2	-
54	P	Circle	A-6-1	57.2	114.4	-
55	P	No Hole	D-0-1	-	-	-

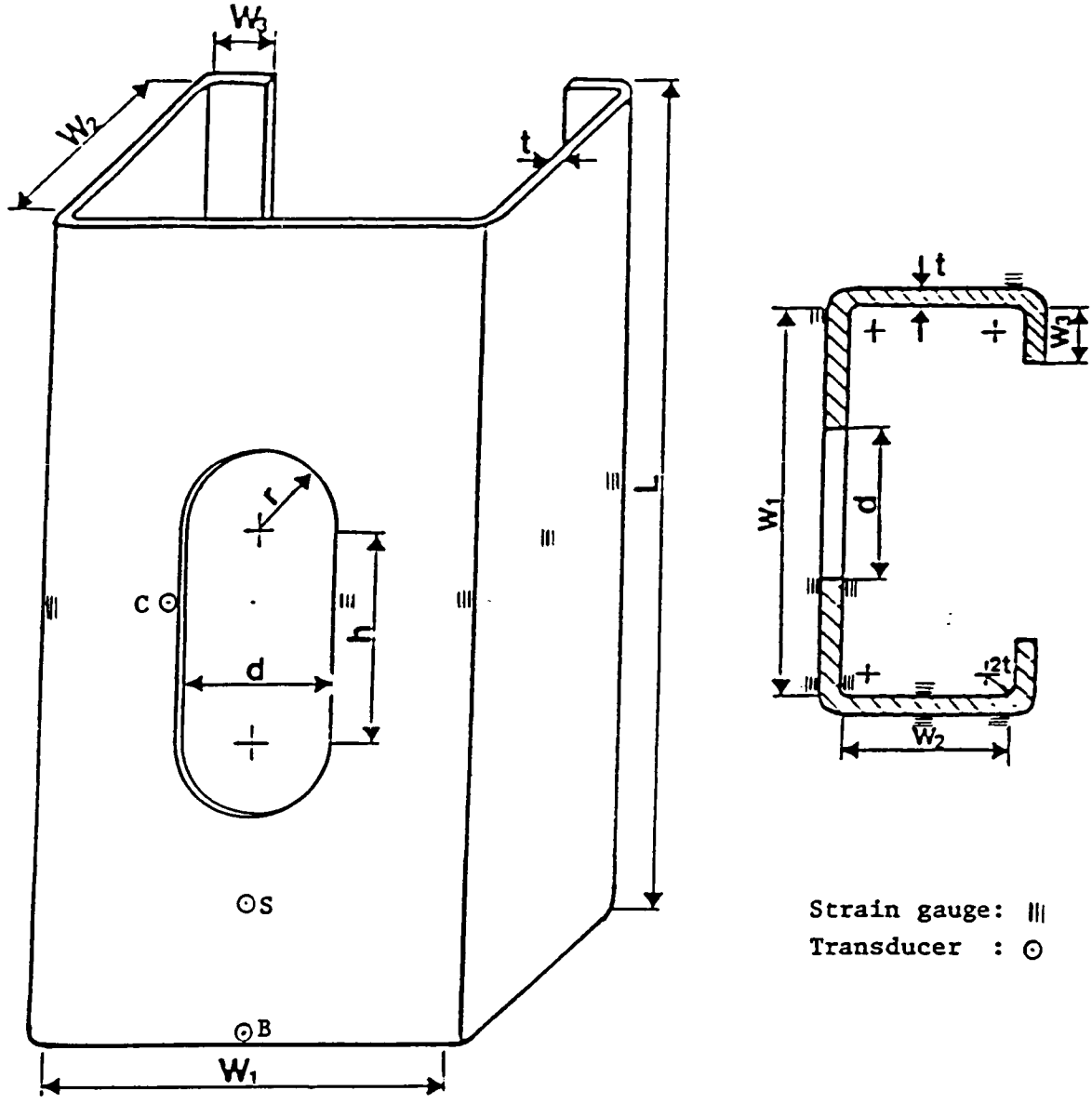

Fig. 2.1 Typical dimensions of a Stub Column Specimen and locations of strain gauges and displacement tranducers

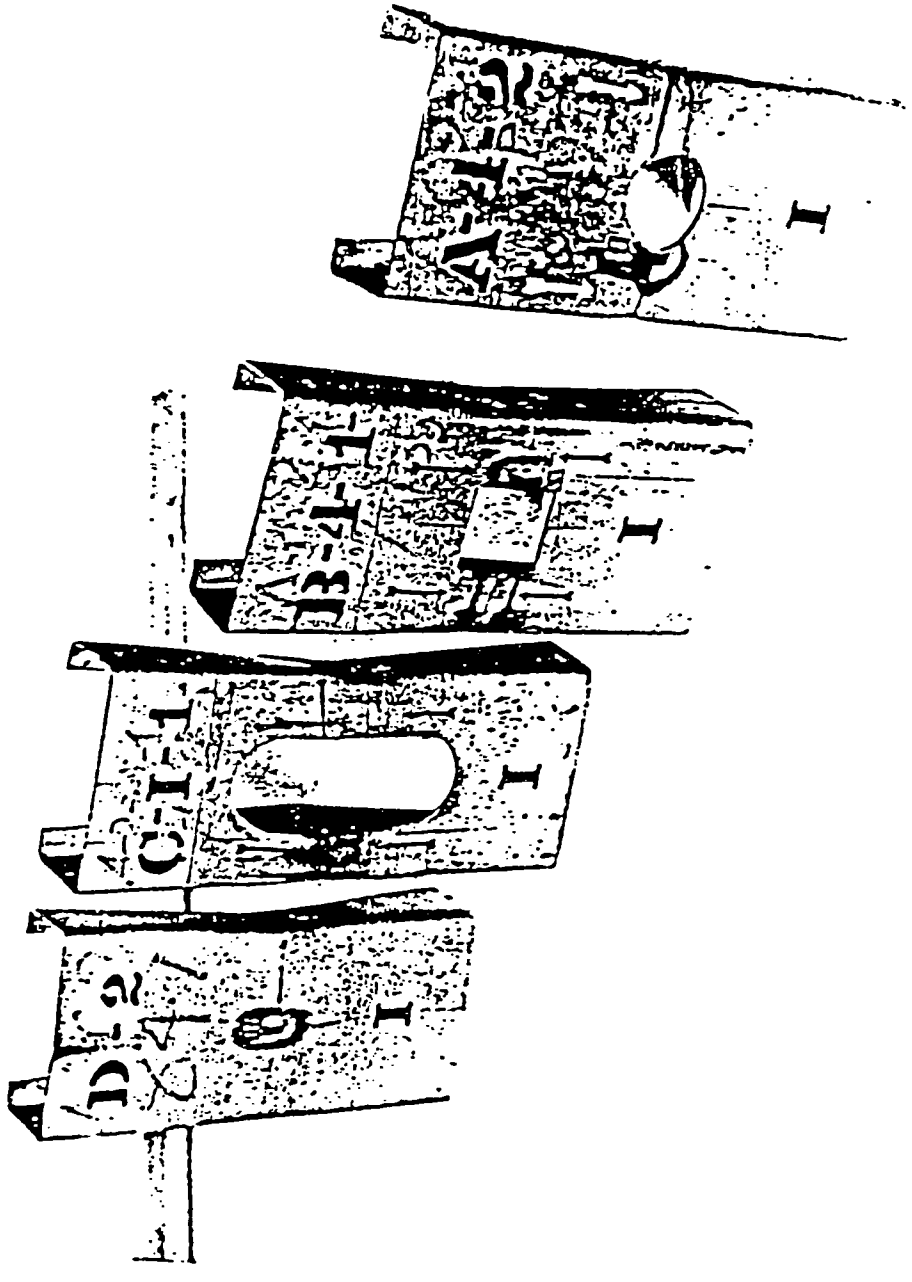

Fig. 2.2 Test Specimens of Set I (after failure) showing typical openings

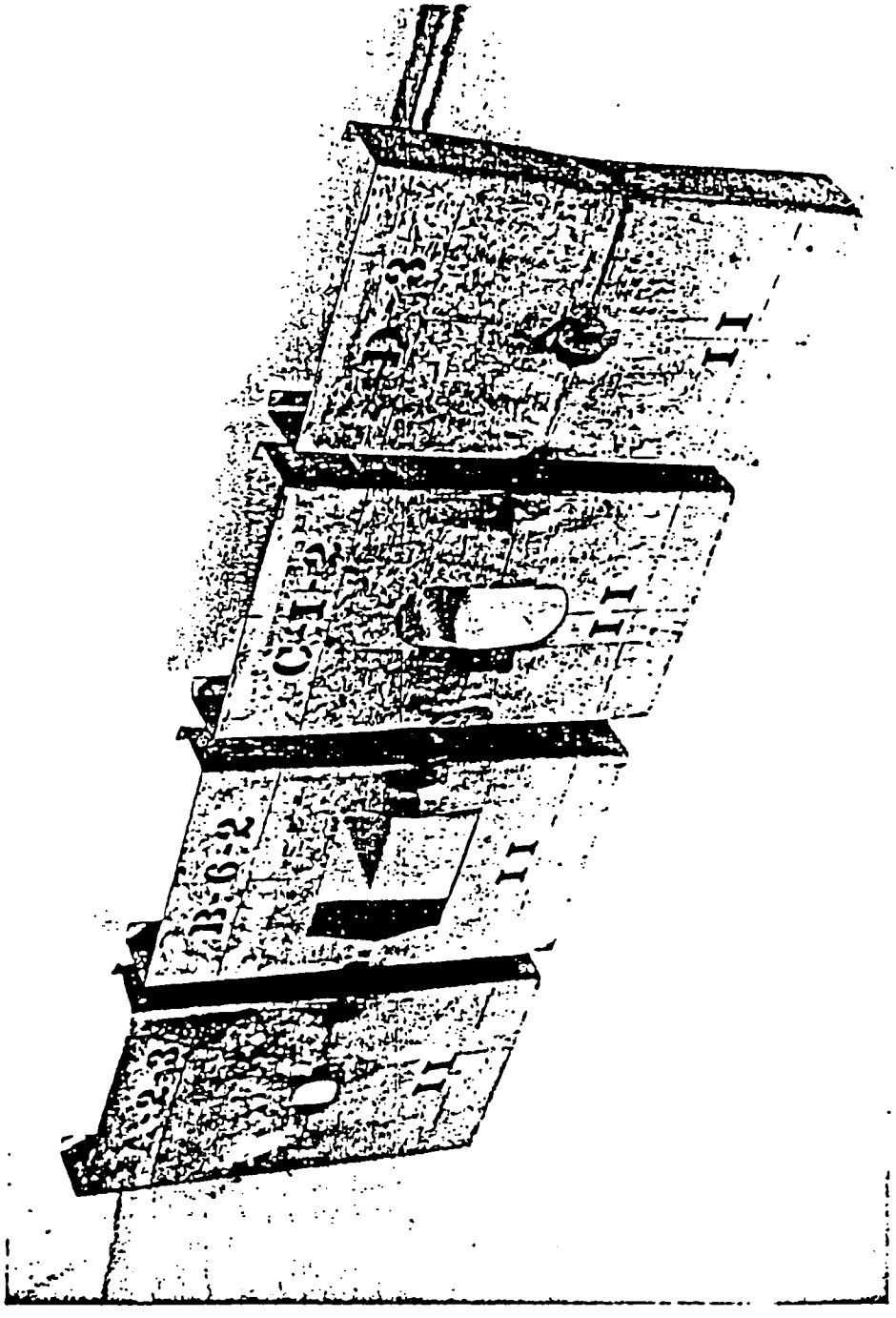

Fig. 2.3 Test Specimens of Set II (after failure) showing typical openings

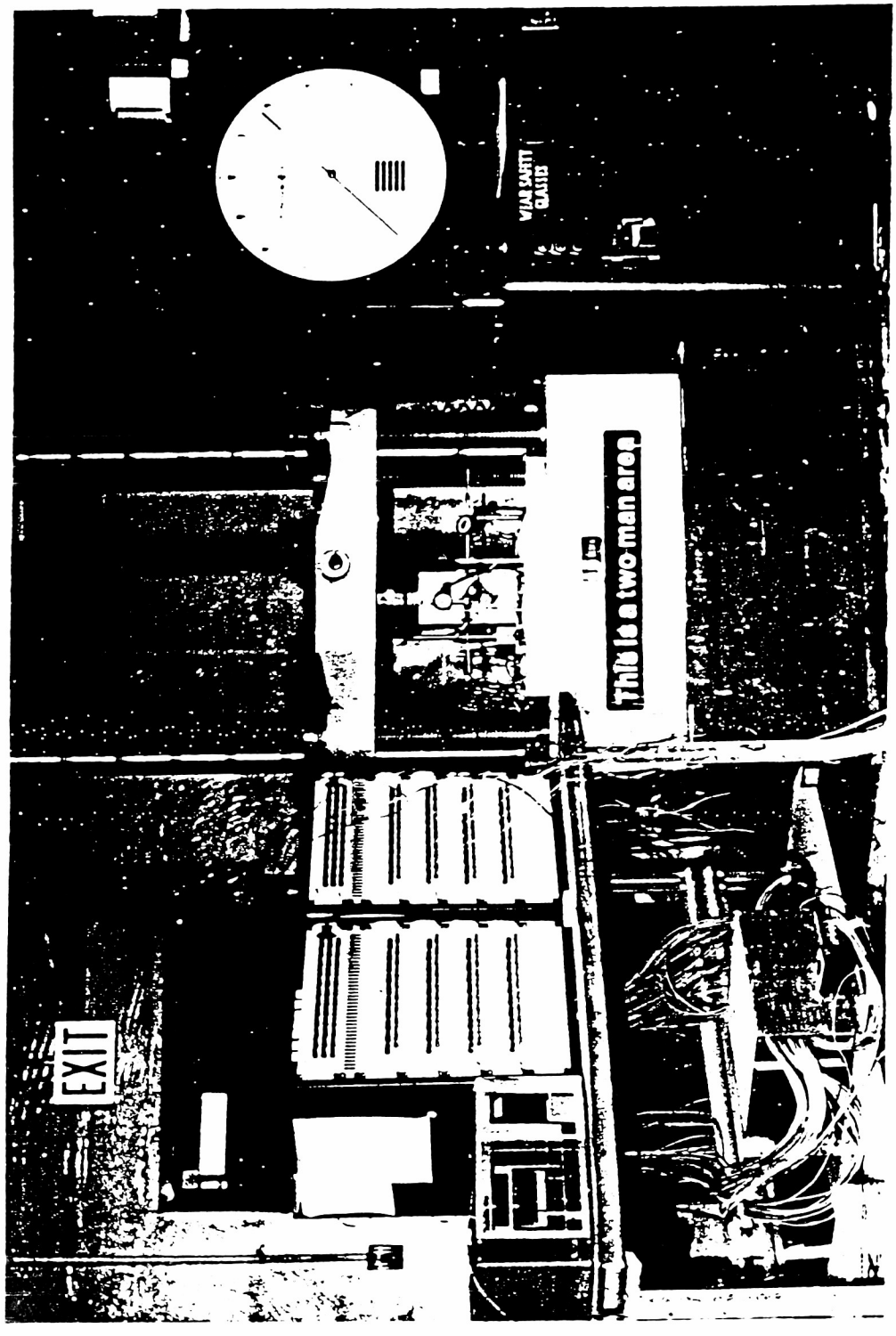

Fig. 2.4 Experimental Set-up: Overall View

Fig. 2.5 Experimental Set-Up: Instrumentation on Web

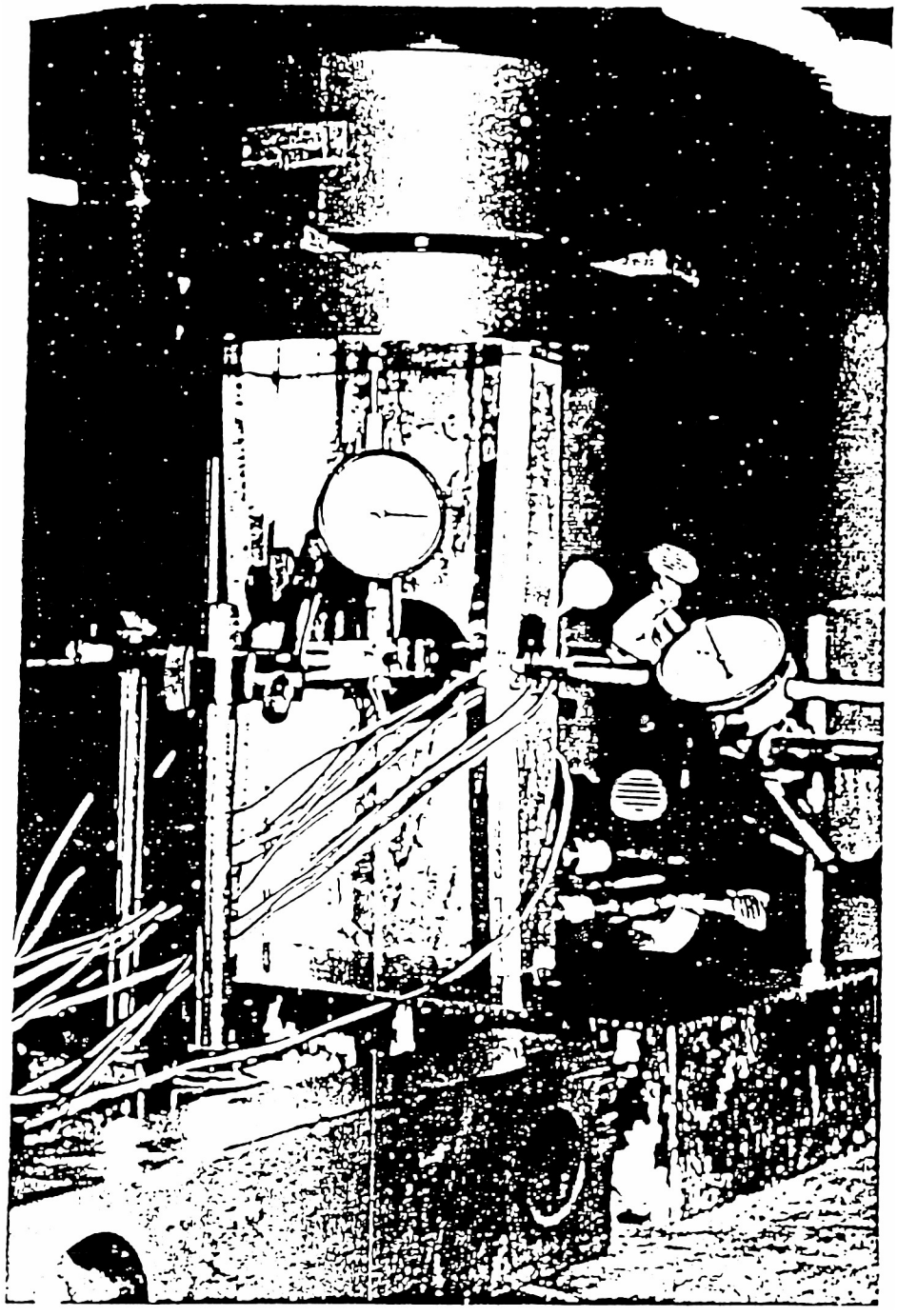

Fig. 2.6 Experimental Set-up: Instrumentation on Flanges
and inner side of the specimen

CHAPTER 3

EXPERIMENTAL RESULTS

In the previous chapter, detailed information on the stub column tests performed on the cold formed lipped channel steel sections was given. In this chapter, the results obtained from the stub columns tests are reported. Load vs axial shortening and load vs lateral deflection behaviour of the specimens, which form an important part of the experimental data, is presented in the form of graphs. The ultimate strengths of the specimens are also reported. A detailed analysis for determination of buckling loads and ultimate loads is given in chapters 4 and 5.

3.1 ULTIMATE LOADS OF TEST SPECIMENS

The ultimate loads of all specimens, corresponding to the maximum load reading obtained during a test, are given in Table 3.1. The maximum variation noted in the ultimate loads for identical specimens, having the same size and shape of hole, is less than 3% of their mean value (usually about 1%). This shows that ultimate load readings were very consistent.

In the case of specimens with circular holes (type 'A'). it can be seen that there is no significant decrease in ultimate load up to a hole diameter of 20% of the flat width of the web. For the specimens with a greater hole

diameter, there is an evident decrease in ultimate load with the increase in hole diameter. This is due to the loss in stiffness of the specimen, indicating that the central part of a plate does contribute to the resistance of loads.

The ultimate loads of specimens with square holes follow the same pattern as specimens with circular holes. However, for the same hole size (diameter of a circle or side of a square), the ultimate loads for specimens with square holes are slightly less than those with the circular holes. This indicates there is only a small effect due to the shape of the hole on ultimate loads.

The effect of the size of the hole in the longitudinal direction is clearly evident from the ultimate loads obtained from specimens having slotted (type 'C') holes (Table 2.2. and Fig. 2.1). The ultimate loads of specimens with slotted holes, having hole widths of 46% and 26% of the web flat widths for Set I and Set II, respectively, are less than the ultimate loads of the specimens with circular or square holes, which have greater hole widths. A maximum drop of about 14% in ultimate load for slotted holes from the unperforated section was obtained for Set I.

3.2 LOAD VS AXIAL SHORTENING BEHAVIOUR

The graphs illustrated in Figures 3.1 to 3.8 and 3.9 to 3.16 show the load vs axial shortening behaviour for specimens of Sets I and II, respectively. The hexagon,

square, and triangular indicators in these figures represent the data points of the first, second, and third specimen, of a group of identical specimens, respectively. In all these figures, the solid line denotes the mean curve obtained from the data points of the identical specimens. A computer program was written (with the aid of IMSL Subroutines ICSFKU and ICSEVU of university library programs) to obtain the data for the mean curves. The mean curves are obtained to see the dispersion of the experimental data for one type of specimens and to compare its mean curve with those of specimens having different sizes or shapes of openings.

It is clear from Figures 3.1 to 3.16 that the load versis axial shortening behaviour of identical specimens is quite consistent. To see the effect of the size and shape of the hole on the load vs axial shortening behaviour, the mean curves are drawn in two groups(Figures 3.17 to 3.20), consisting of four curves each, for a set of specimens.

The first group consisting of Figures 3.17 and 3.19 for Set I and II, respectively, shows the mean curves of specimens with circular and slotted holes. The mean curves of specimens with square holes and unperforated specimens are shown in Figures 3.18 and 3.20 for Set I and Set II, respectively. As expected, these figures indicate the reduction in stiffness of the specimen with the increase in hole size. This reduction in stiffness becomes more apparent as failure loads of the specimens approaches. The effect of

the size of a hole in the longitudinal direction, on the behaviour of the specimens in axial compression is clearly evident from Figures 3.17 and 3.19. The specimens with slotted holes made by the manufacturers show the least stiffness.

3.3 LOAD VS LATERAL DEFLECTION BEHAVIOUR

Load versis lateral deflection graphs were also plotted in the same fashion as those of load vs axial shortening. These are shown in Figures 3.21 to 3.28 and 3.29 to 3.36 for Set I and Set II, respectively. It is evident in some of the figures that the mean curve is the average of data for only two of the three specimens. This is because the deviation of data for the third specimen is more than 10% of the mean value. This may be due to variations in initial imperfections, some local weakness, or experimental error. In the case of load vs lateral deflection, deviation may also be because the failure has taken place at a position along the length of the member other than that of the dial gauge location.

Figures 3.37 and 3.39 show the mean load versis out-of-plane deflection curves of specimens with circular and slotted perforations, for Sets I and II respectively. Similarly, Figures 3.38 and 3.40 show the mean curves drawn together for unperforated specimens and specimens with square holes for Sets I and II. In these figures, the effect

of hole size and shape on the behaviour of the specimens is clear, as is in the case of load vs axial shortening curves. The load vs lateral deflection curves cross each other because the deflection was taken at the point adjacent to the hole, which is not the same point for every section. For the unperforated specimens, the lateral deflection shown is at the centre of the web.

The out-of-plane deflections were small up to failure. However, after failure, the deflections increased at a faster rate, more so in the case of the specimens with slotted holes, because the long cut reduced the stiffness.

3.4 MODE OF FAILURE OF SPECIMENS

It was stated in the second chapter that the length of the specimens was based on the reasoning that the half buckle wave length lies between the dimensions of the web and the flange in unperforated sections (Allen and Bulson, 1980). The length was calculated by multiplying the average of the flat widths of web and flange by three, so that at failure the specimen may form three half buckle waves.

In order to confirm this, two horizontal additional transducers (position indicated by points S and B in Figure 2.1) were mounted on the centre vertical line of web, during the tests of the the specimens of Set II. Point S is at a height equal to one sixth of the length of the specimens from the bottom, and point B was located as near the bottom edge of specimen as possible. Point C (Figure 2.1)is at the

centre of the web or adjoining the hole at mid-height.

It was found that the deflections at point B and S are in the opposite direction to the deflections at point C. As expected, the lateral deflections at point B were very small, with a maximum value of 0.35 mm. The deflections at point S were about one half of the deflection at point C at failure. The deflections of points C, S and B in the load versis web out-of-plane deflection graphs (shown in Fig. 3.41 to 3.64) are of the same sign. The deflections of points S and B for those figures were obtained by multiplying the actual deflection by minus one to show these in the same direction as were the deflections of point C.

It can be seen from these figures that prior to failure, the deflection at point S is increasing at a considerable rate as compared to the deflection at point C. However, after failure, the lateral deflection at C increased at a greater rate than at S or B. In fact, in some of the specimens the after failure deflections at points B and S decreased to zero and then started increasing in the same direction as those of point C.

Figures 3.65 and 3.66 show the buckled shape of the specimens, while the specimens were still under compressive loads. The mode of failure (or buckling pattern) of the web of specimen (Fig.3.65) is much clearer than that for the flanges (Fig 3.66). The above observations confirm that the specimens failed in the form of three half buckle waves.

Table 3.1 Experimental ultimate loads of specimens

Set No.	Specimen Designation	Experimental ultimate load (kN)	Mean value of ultimate load (kN)	variation of loads from mean value (%)	Drop in strength (mean value) (%)
I	A-2-1	85.50	85.75	(-)0.29	(-)00.05
	A-2-2	85.65		(-)0.12	
	A-2-3	86.10		0.41	
I	A-4-1	81.45	81.70	(-)0.31	4.25
	A-4-2	81.90		0.24	
	A-4-3	81.75		0.06	
I	A-6-1	78.35	78.13	0.27	8.43
	A-6-2	77.35		(-)1.00	
	A-6-3	78.70		0.73	
I	B-2-1	84.20	84.70	(-)0.59	0.73
	B-2-2	84.40		(-)0.35	
	B-2-3	85.50		0.94	
I	B-4-1	81.35	81.55	(-)0.25	4.42
	B-4-2	81.40		(-)0.18	
	B-4-3	81.90		0.43	
	B-4-4	81.55		0.00	
	B-6-1	76.35	77.70	(-)1.74	8.94
	B-6-2	77.80		0.13	
	B-6-3	78.50		1.03	
	B-6-4	78.85		1.48	
	B-6-5	77.00		(-)0.90	
I	C-I-1	72.50	73.24	(-)1.01	14.17
	C-I-2	72.65		(-)0.81	
	C-I-3	72.60		(-)0.87	
	C-I-4	75.20		2.70	
I	D-0-1	84.55	85.33	(-)0.91	0.00
	D-0-2	84.70		(-)0.74	
	D-0-3	86.75		1.66	

Table 3.1 continued-------

Set No.	Specimen designation	Experimental ultimate load (kN)	Mean value of ultimate load (kN)	variation of loads from mean value (%)	Drop in strength (mean value) (%)
II	A-2-1	54.00	53.95	0.09	0.05
	A-2-2	54.00		0.09	
	A-2-3	53.85		(-)0.18	
II	A-4-1	54.00	53.37	1.18	1.13
	A-4-2	53.00		(-)0.69	
	A-4-3	53.10		(-)0.50	
II	A-6-1	48.30	47.1	2.55	12.75
	A-6-2	45.70		(-)2.97	
	A-6-3	47.30		0.42	
II	B-2-1	52.75	53.22	(-)0.88	1.4
	B-2-2	52.70		(-)0.97	
	B-2-3	54.20		1.84	
II	B-4-1	52.00	50.97	2.02	5.58
	B-4-2	51.30		0.64	
	B-4-3	49.60		(-)2.68	
II	B-6-1	47.70	47.00	1.49	12.9
	B-6-2	46.70		(-)0.64	
	B-6-3	46.60		(-)0.85	
II	C-I-1	52.30	51.57	1.42	4.22
	C-I-2	51.70		0.26	
	C-I-3	50.70		(-)1.68	
II	D-0-1	54.30	53.98	0.59	0.00
	D-0-2	54.40		0.78	
	D-0-3	53.25		(-)1.35	
P	A-3-1	213.00	-	-	3.46
P	A-6-1	203.13	-	-	7.93
P	D-0-1	220.63	-	-	0.00

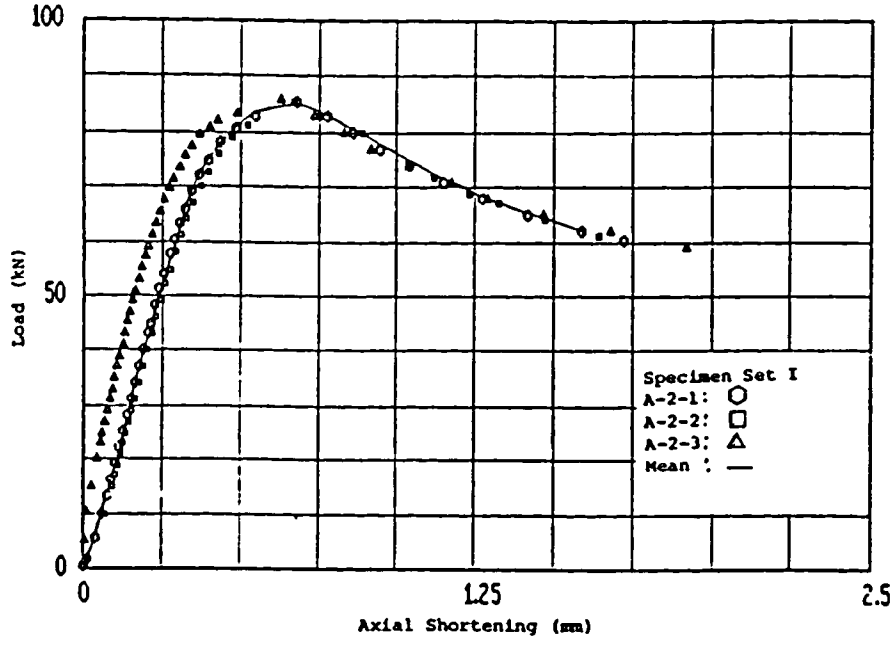

Fig. 3.1 Load Vs Axial Shortening Behaviour of Specimen Set I Type A-2

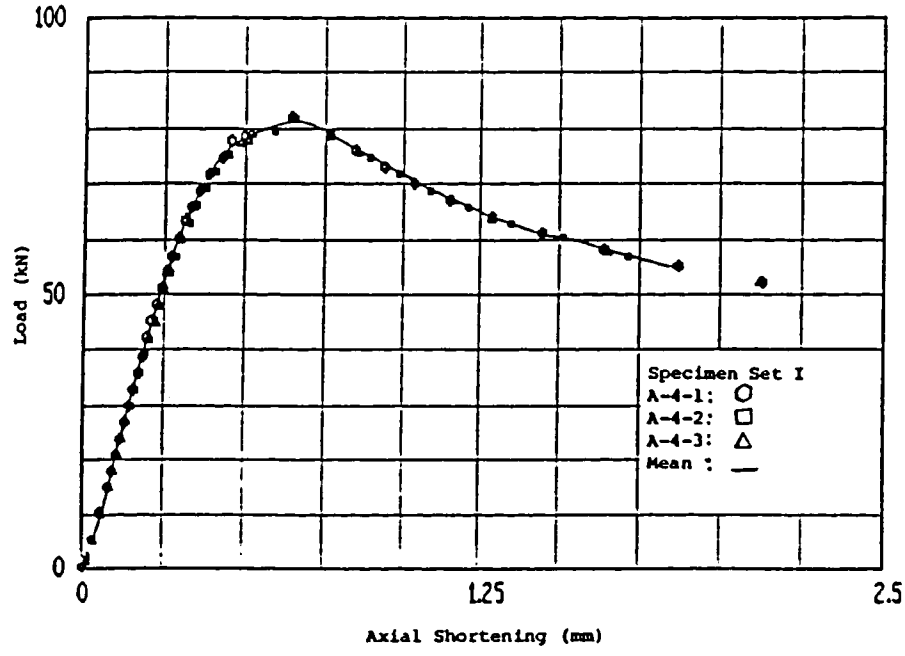

Fig. 3.2 Load Vs Axial Shortening Behaviour of Specimen Set I Type A-4

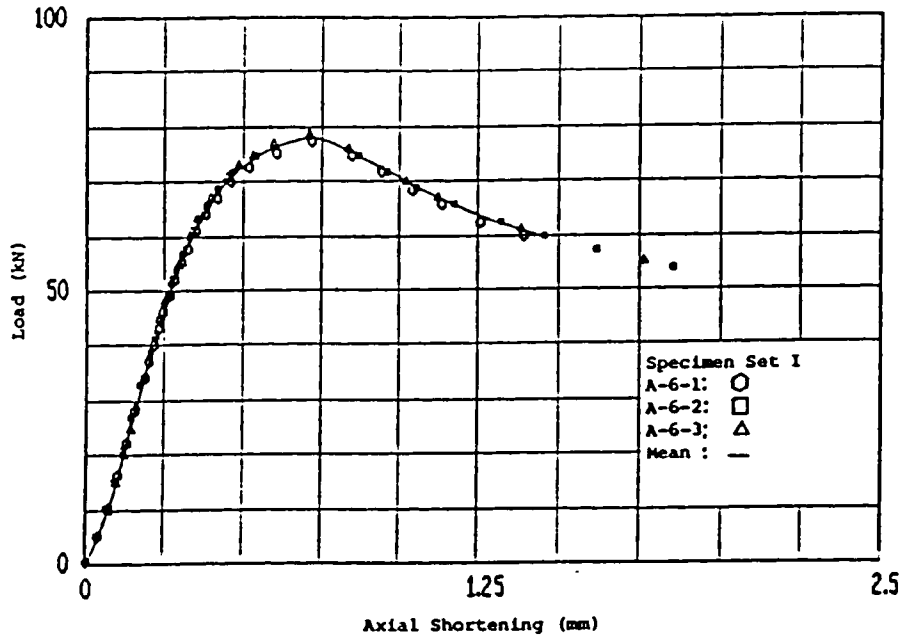

Fig. 3.3 Load Vs Axial Shortening Behaviour of Specimen Set I Type A-6

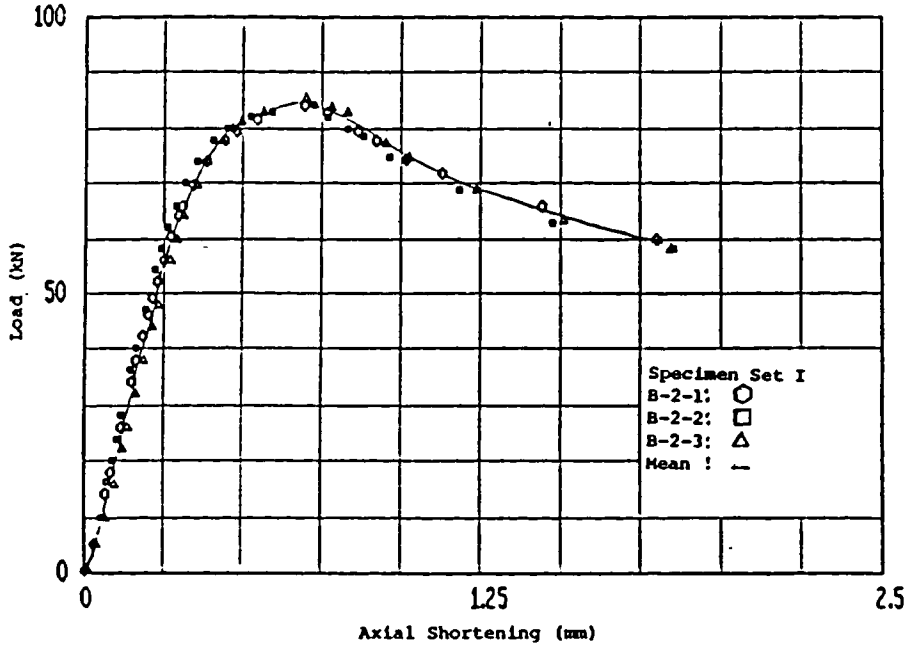

Fig. 3.4 Load Vs Axial Shortening Behaviour of Specimen Set I Type B-2

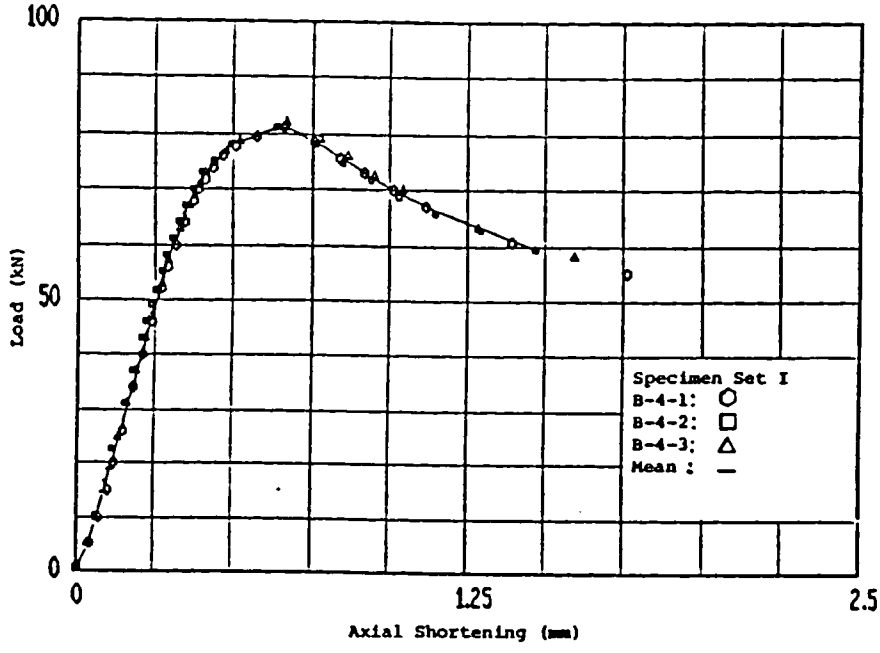

Fig. 3.5 Load Vs Axial Shortening Behaviour of Specimen Set I Type B-4

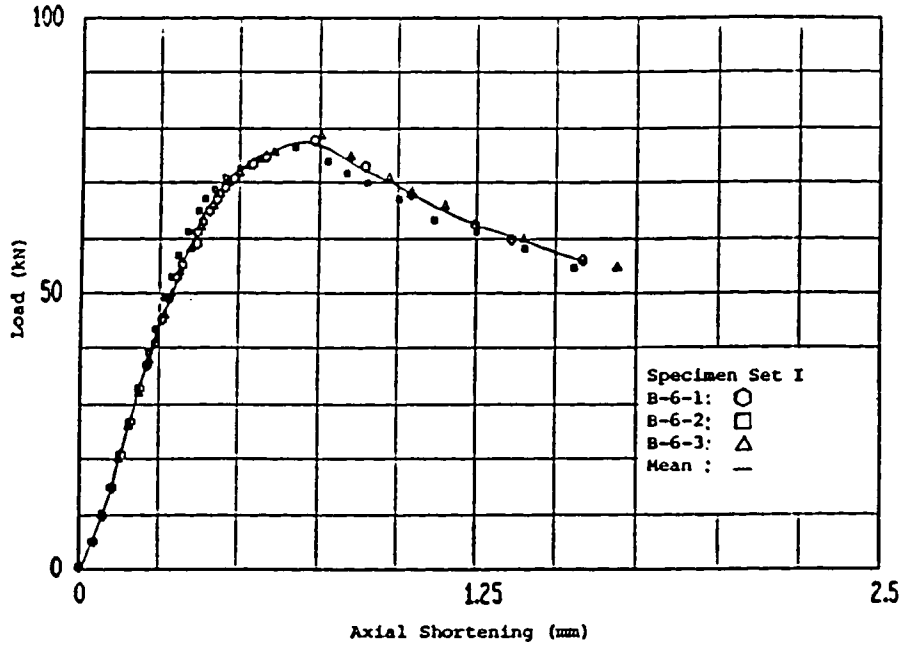

Fig. 3.6 Load Vs Axial Shortening Behaviour of Specimen Set I Type B-6

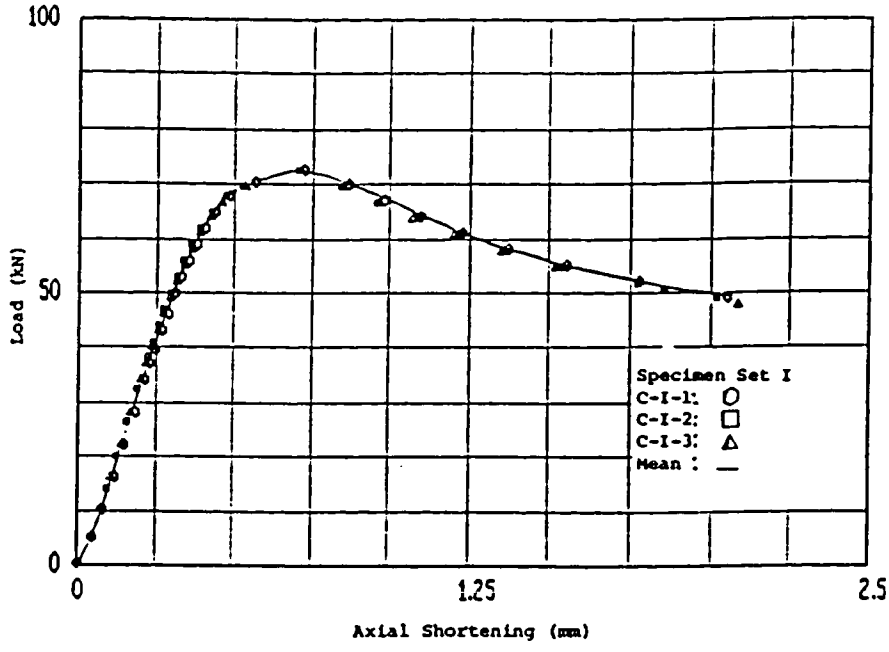

Fig. 3.7 Load Vs Axial Shortening Behaviour of Specimen Set I Type C-I

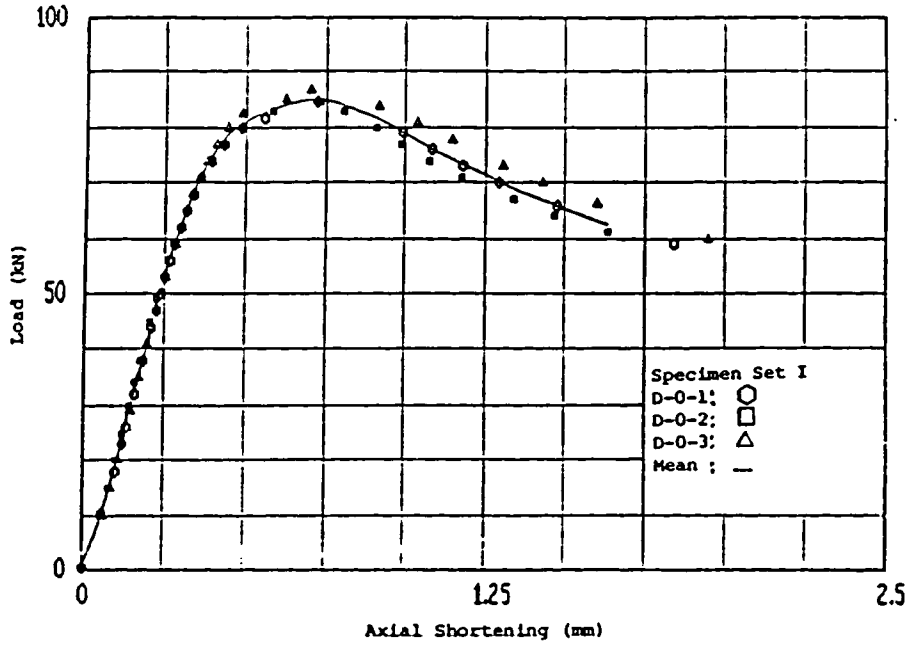

Fig. 3.8 Load Vs Axial Shortening Behaviour of Specimen Set I Type D-0

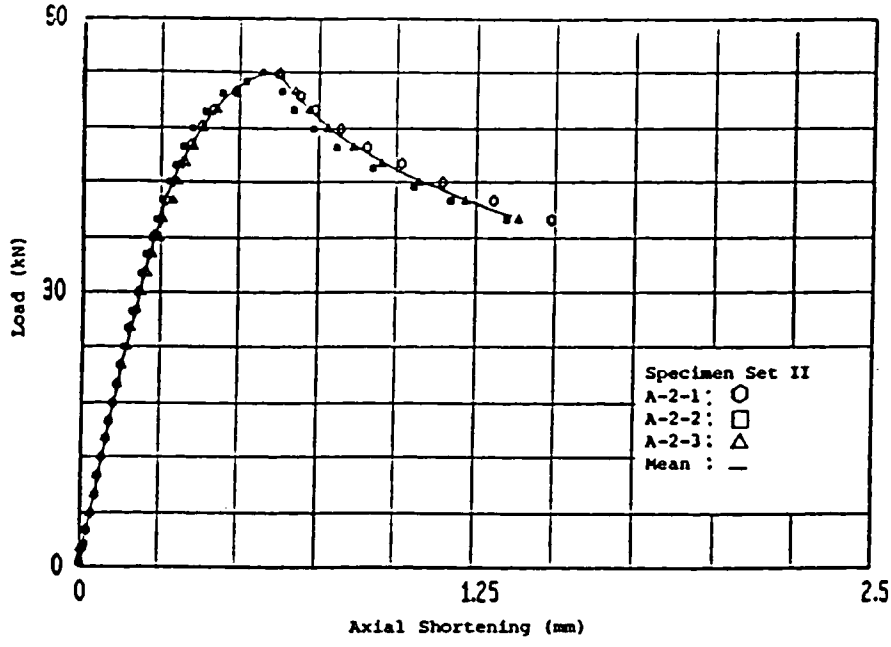

Fig. 3.9 Load Vs Axial Shortening Behaviour of Specimen Set II Type A-2

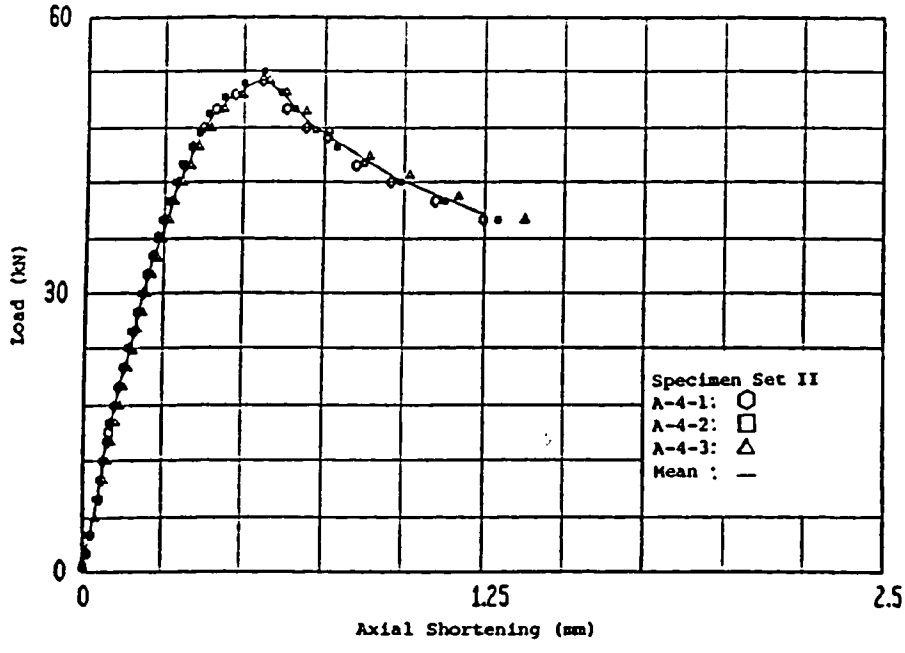

Fig. 3.10 Load Vs Axial Shortening Behaviour of Specimen Set II Type A-4

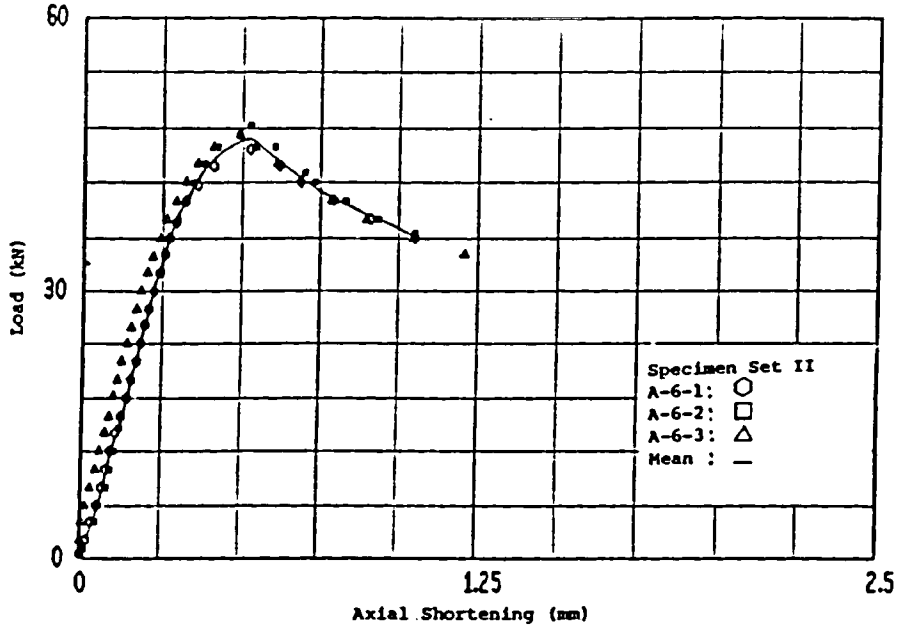

Fig. 3.11 Load Vs Axial Shortening Behaviour of Specimen Set II Type A-6

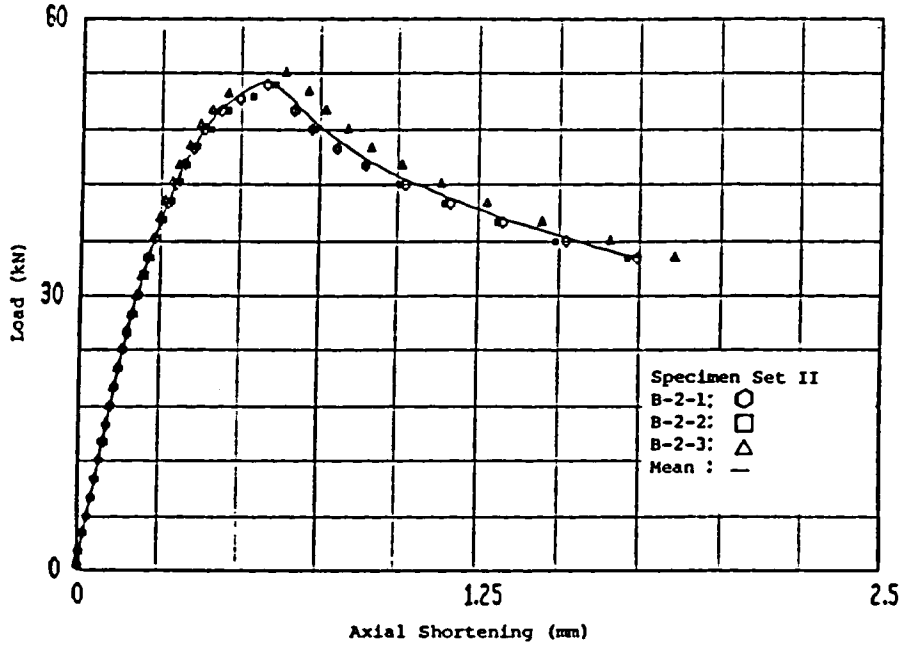

Fig. 3.12 Load Vs Axial Shortening Behaviour of Specimen Set II Type B-2

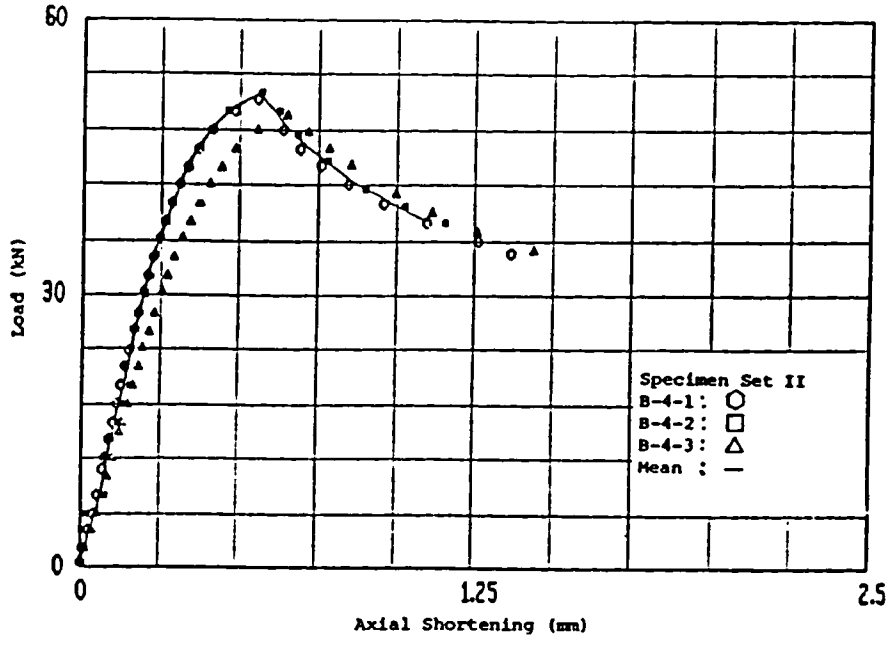

Fig. 3.13 Load Vs Axial Shortening Behaviour of Specimen Set II Type B-4

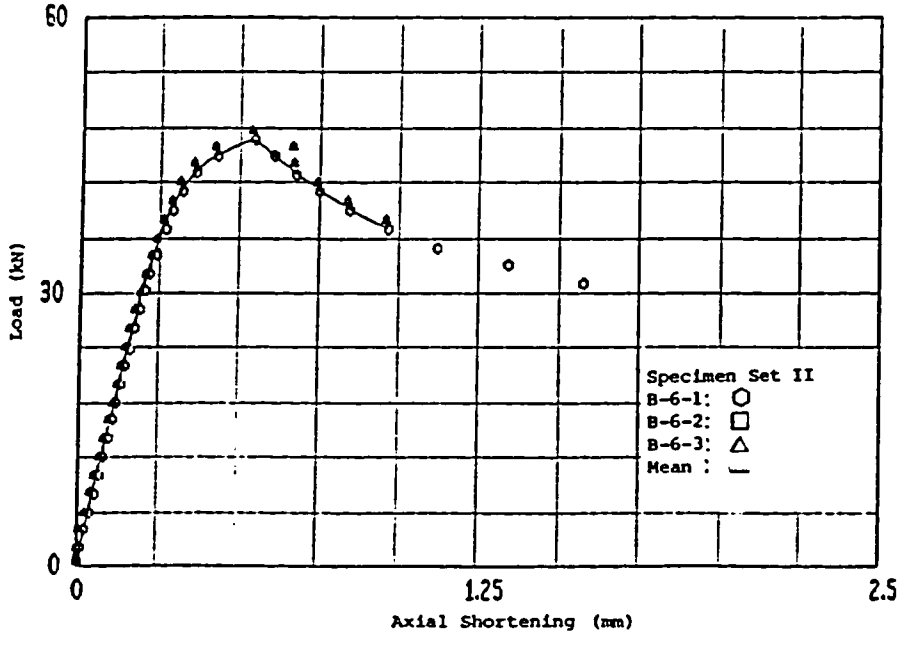

Fig. 3.14 Load Vs Axial Shortening Behaviour of Specimen Set II Type B-6

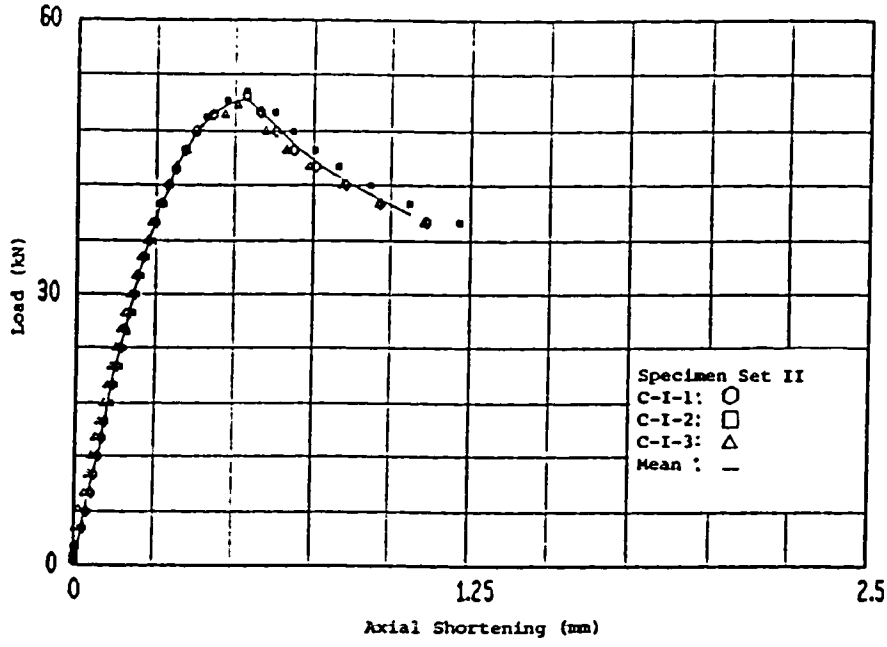

Fig. 3.15 Load Vs Axial Shortening Behaviour of Specimen Set II Type C-I

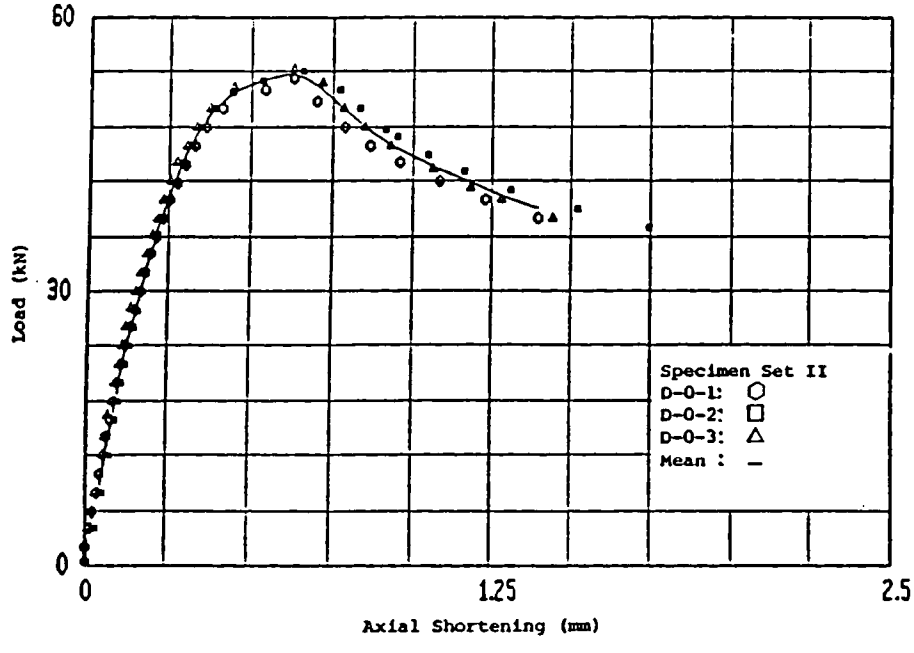

Fig. 3.16 Load Vs Axial Shortening Behaviour of Specimen Set II Type D-0

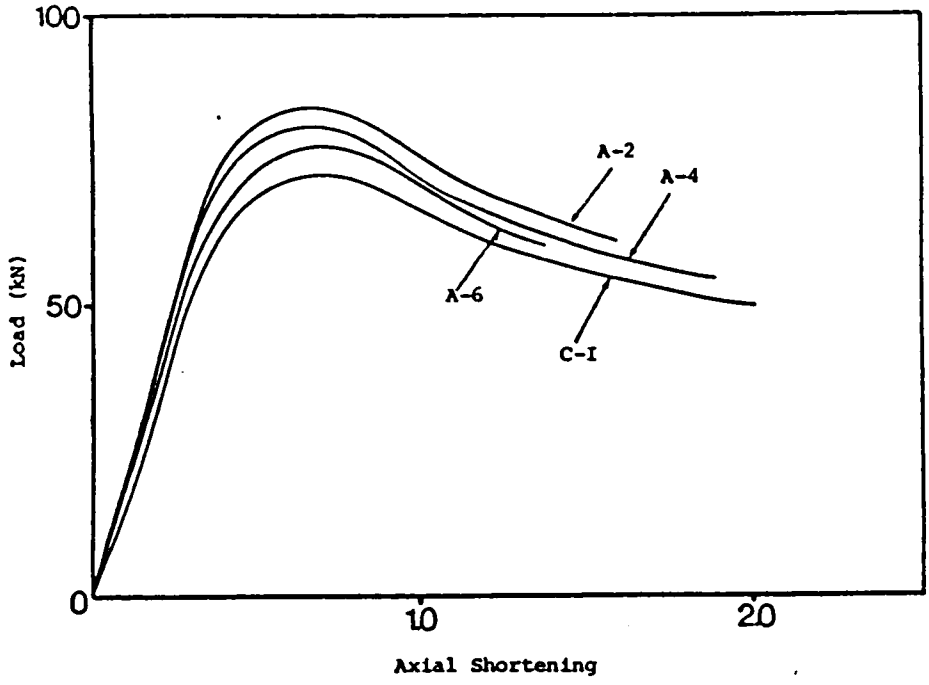

Fig. 3.17 Load Vs Axial Shortening mean Curves of Set I Specimens With Circular and Slotted Perforations

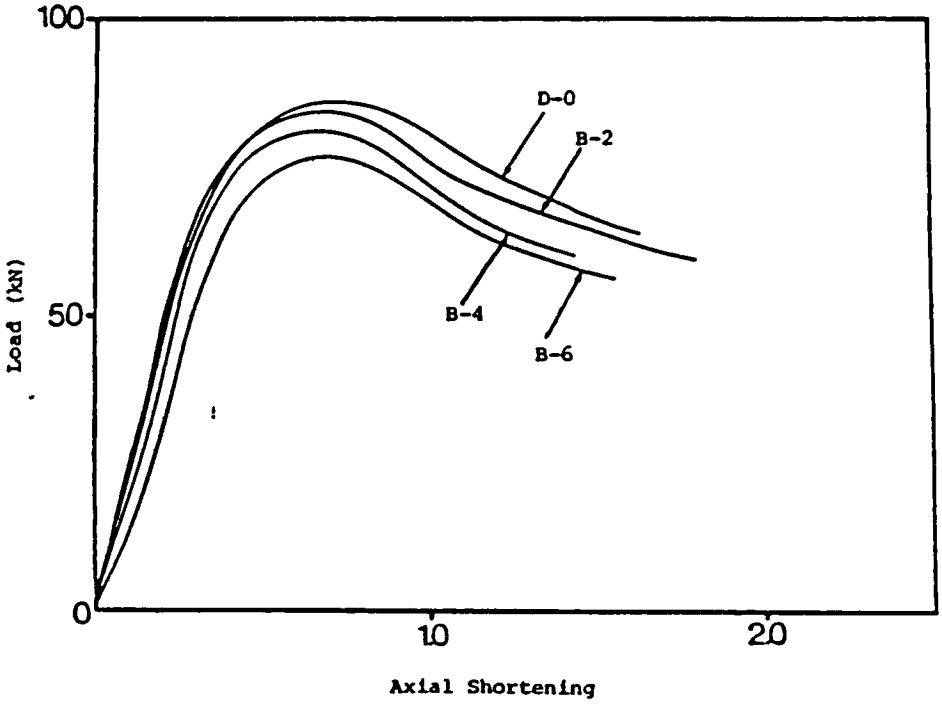

Fig. 3.18 Load Vs Axial Shortening mean Curves of Set I Specimens With Square Perforations and No Perforations

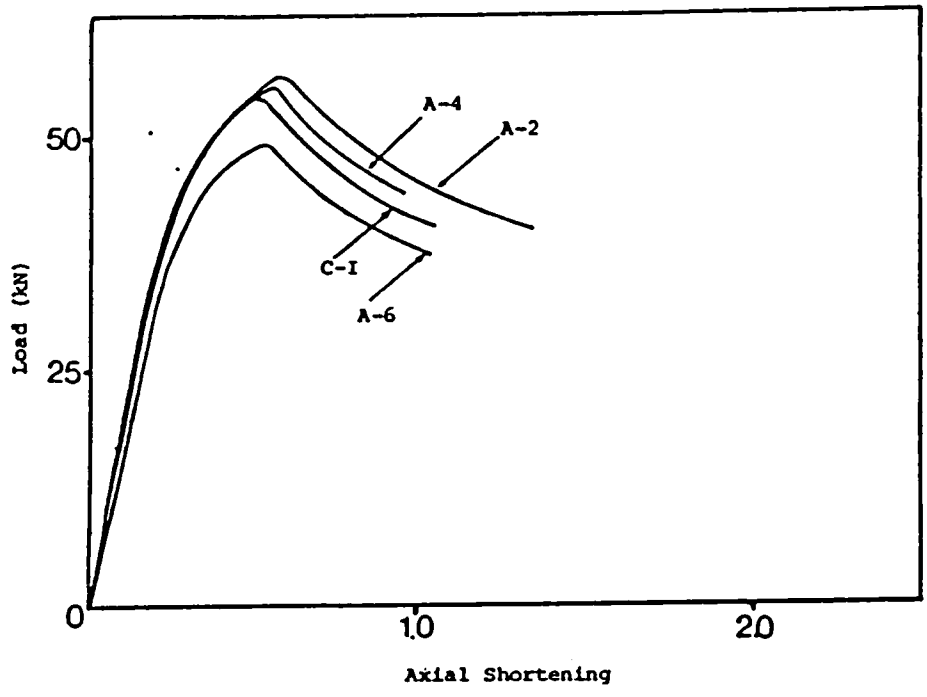

Fig. 3.19 Load Vs Axial Shortening mean Curves of Set II Specimens With Circular and Slotted Perforations

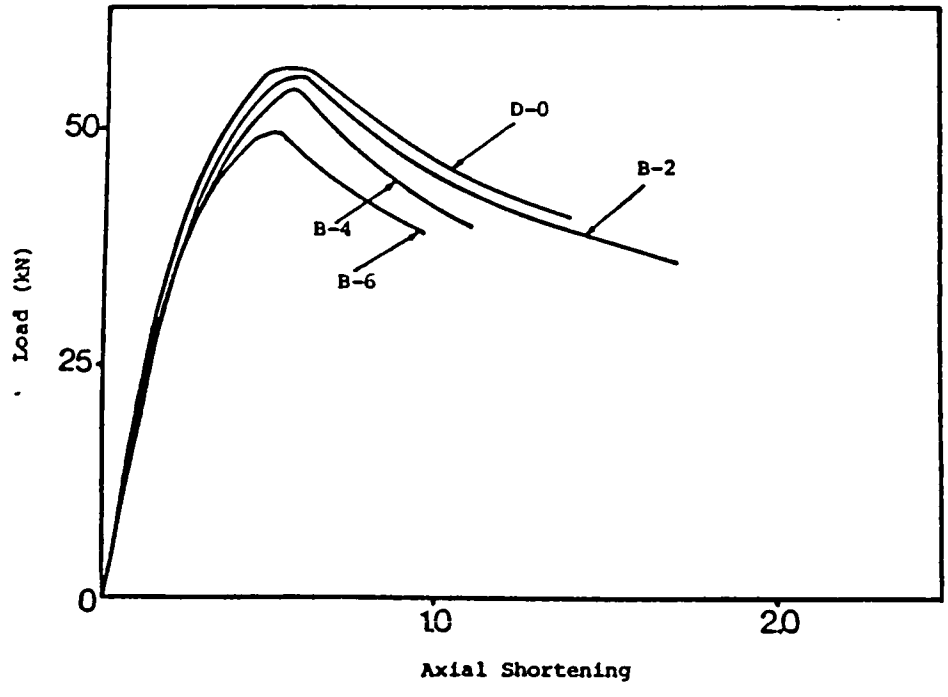

Fig. 3.20 Load Vs Axial Shortening mean Curves of Set II Specimens With Square Perforations and No Perforations

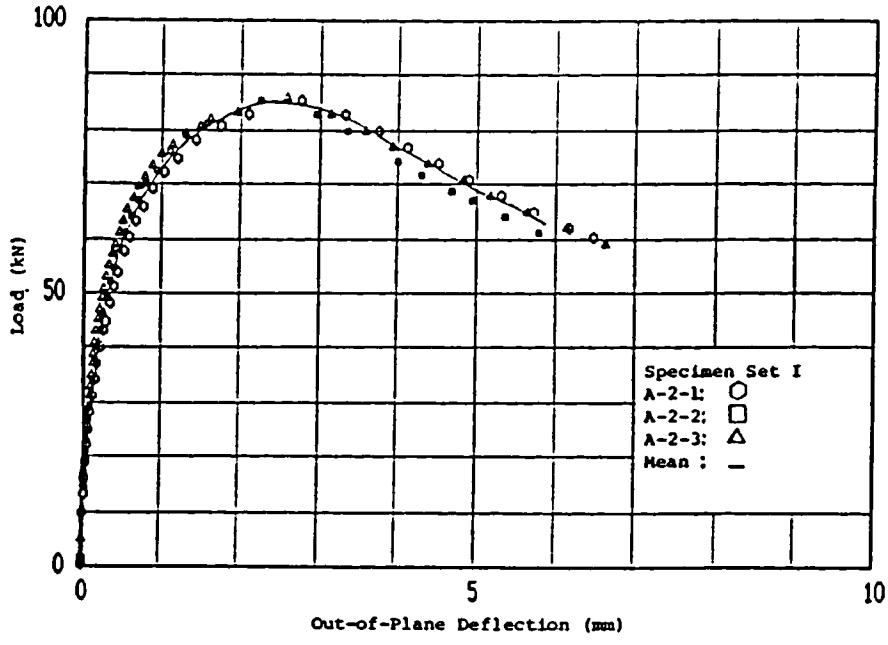

Fig. 3.21 Load Vs Web Out-of-Plane Deflection Behaviour of Specimen Set I Type A-2

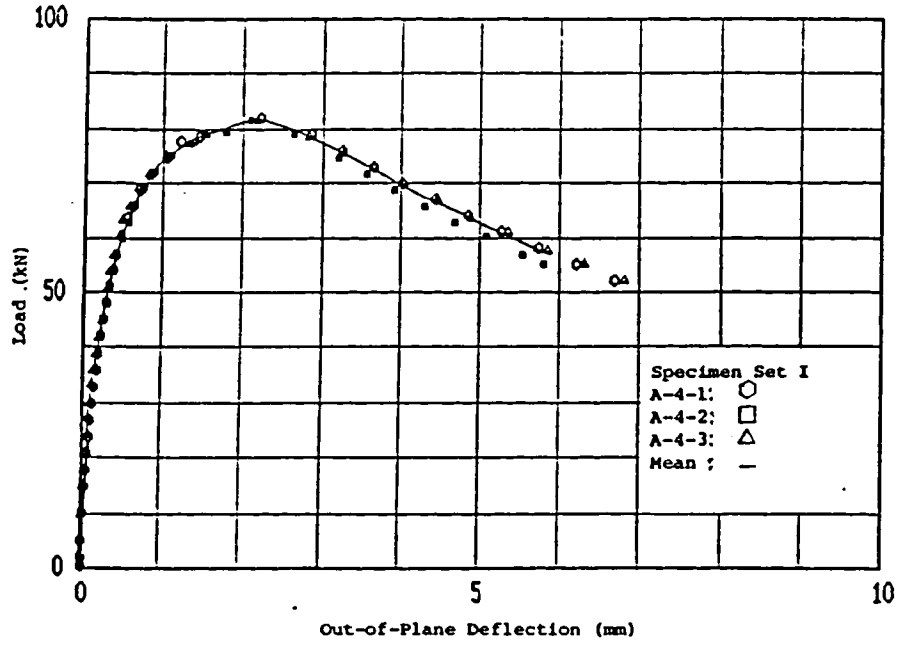

Fig. 3.22 Load Vs Web Out-of-Plane Deflection Behaviour of Specimen Set I Type A-4

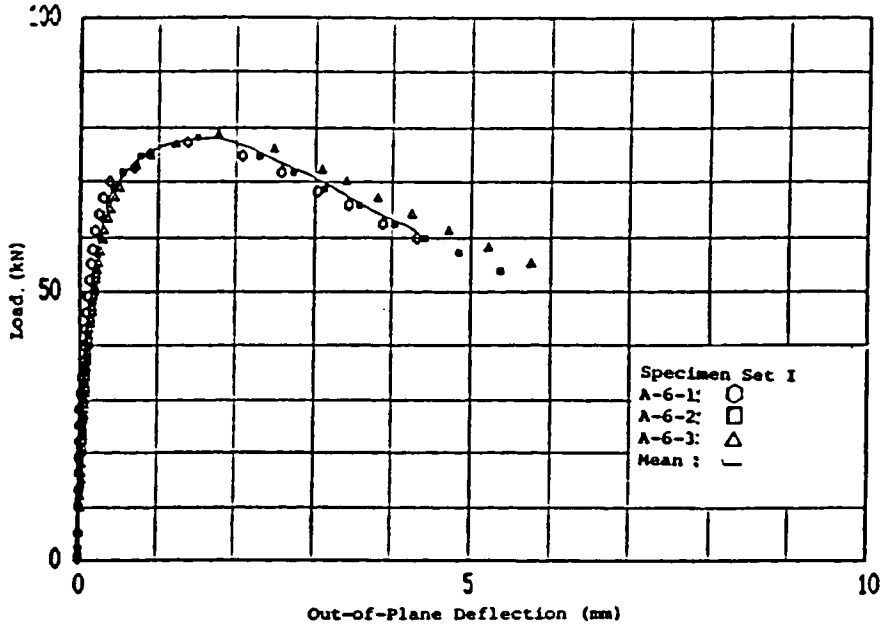

Fig. 3.23 Load Vs Web Out-of-Plane Deflection Behaviour of Specimen Set I Type A-6

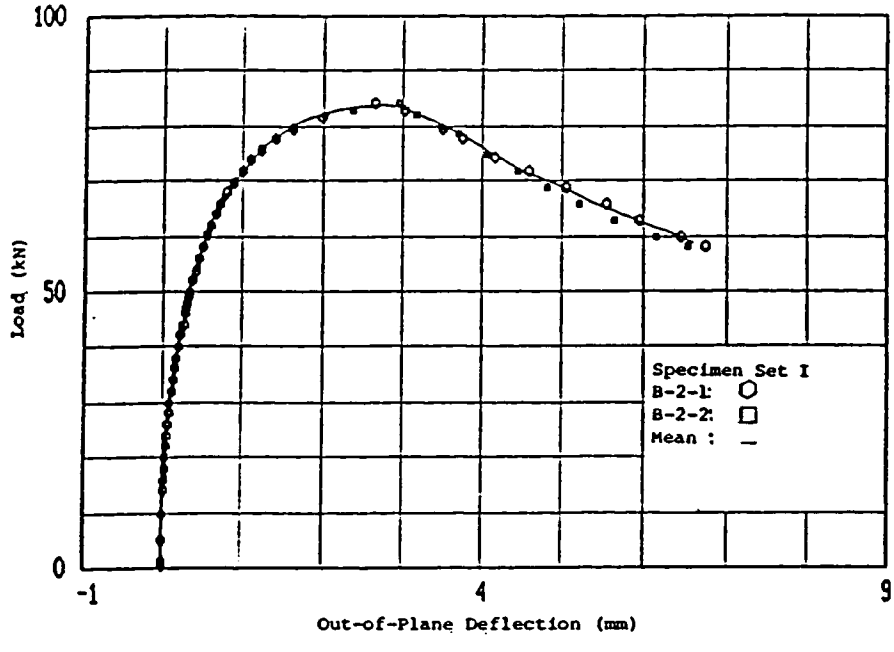

Fig. 3.24 Load Vs Web Out-of-Plane Deflection Behaviour of Specimen Set I Type B-2

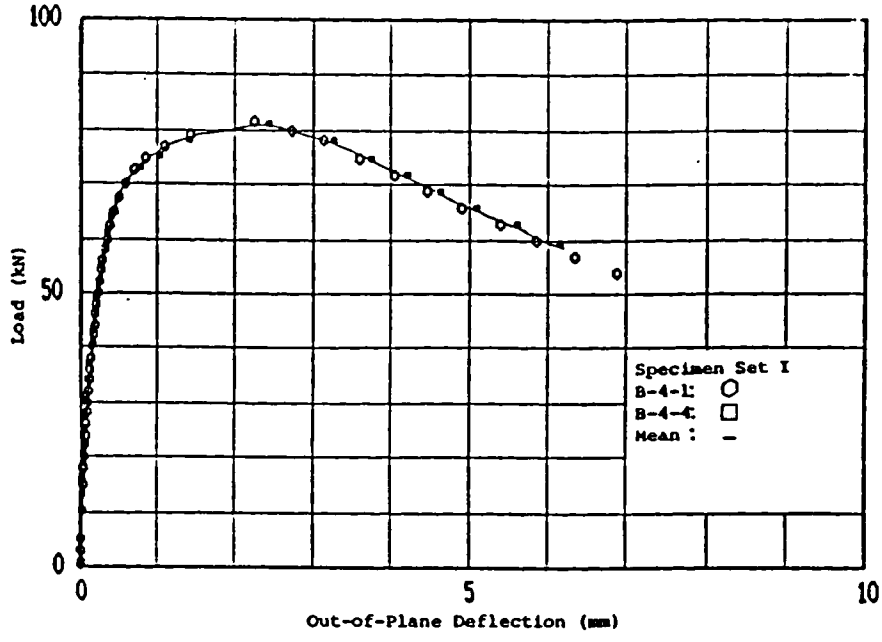

Fig. 3.25 Load Vs Web Out-of-Plane Deflection Behaviour of Specimen Set I Type B-4

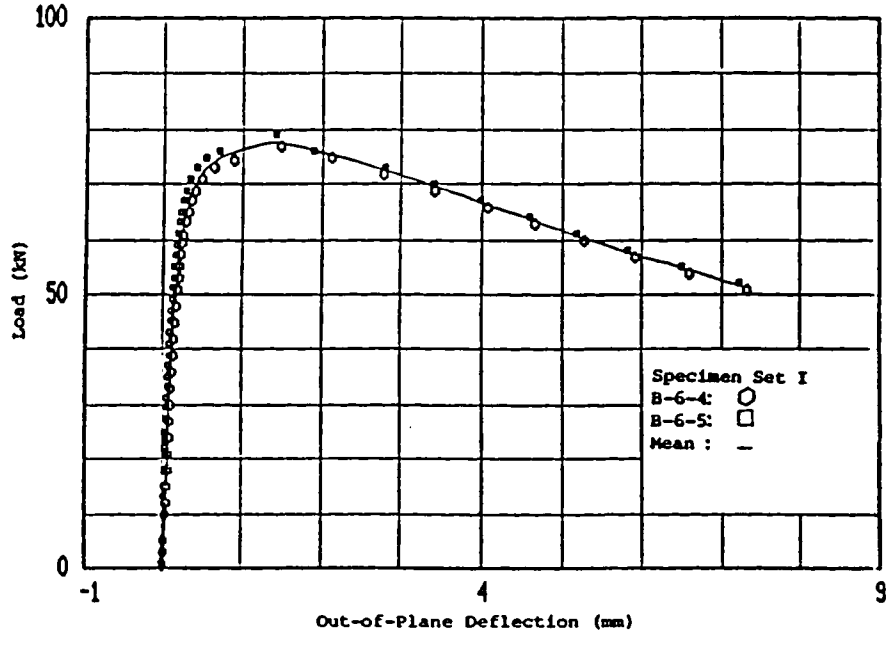

Fig. 3.26 Load Vs Web Out-of-Plane Deflection Behaviour of Specimen Set I Type B-6

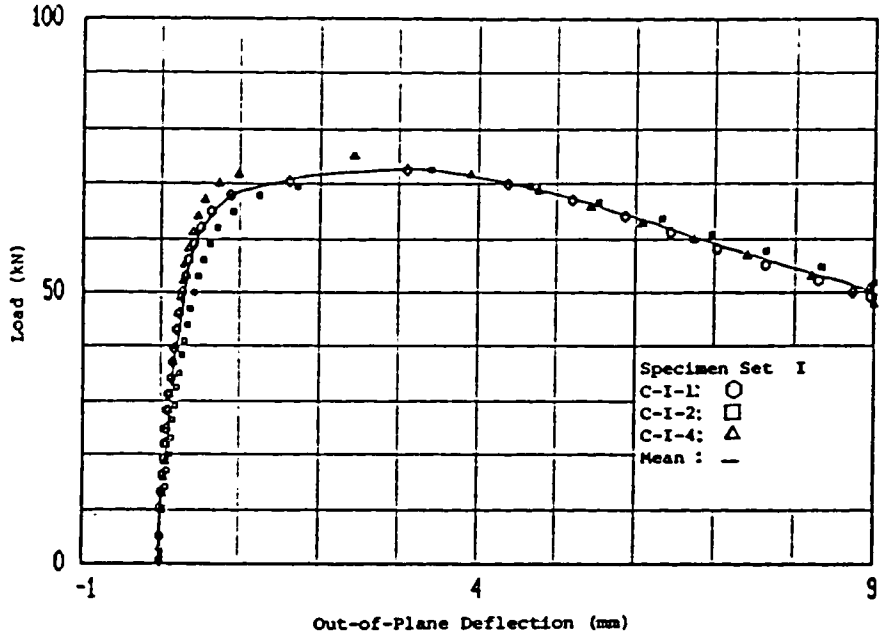

Fig. 3.27 Load Vs Web Out-of-Plane Deflection Behaviour of Specimen Set I Type C-I

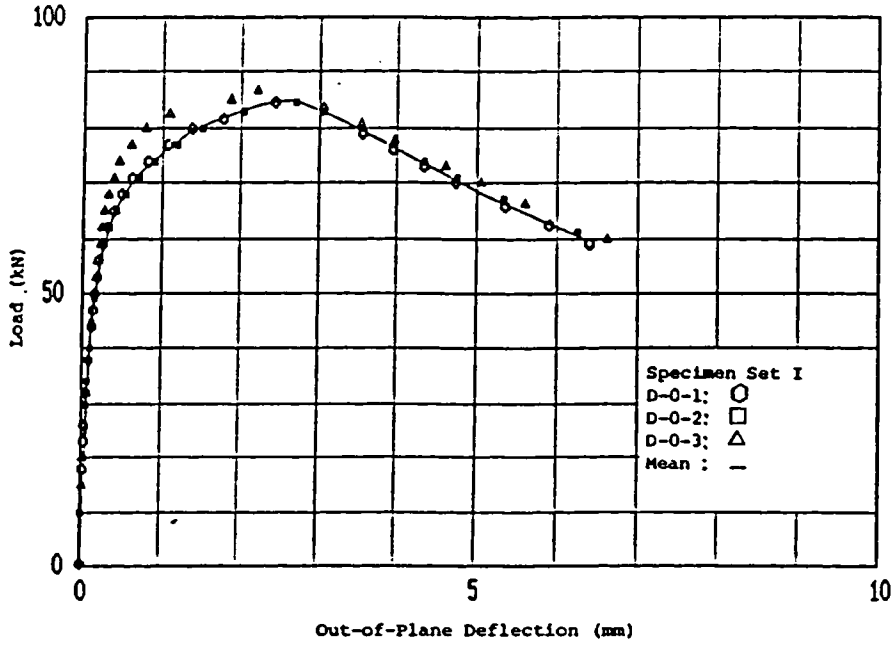

Fig. 3.28 Load Vs Web Out-of-Plane Deflection Behaviour of Specimen Set I Type D-0

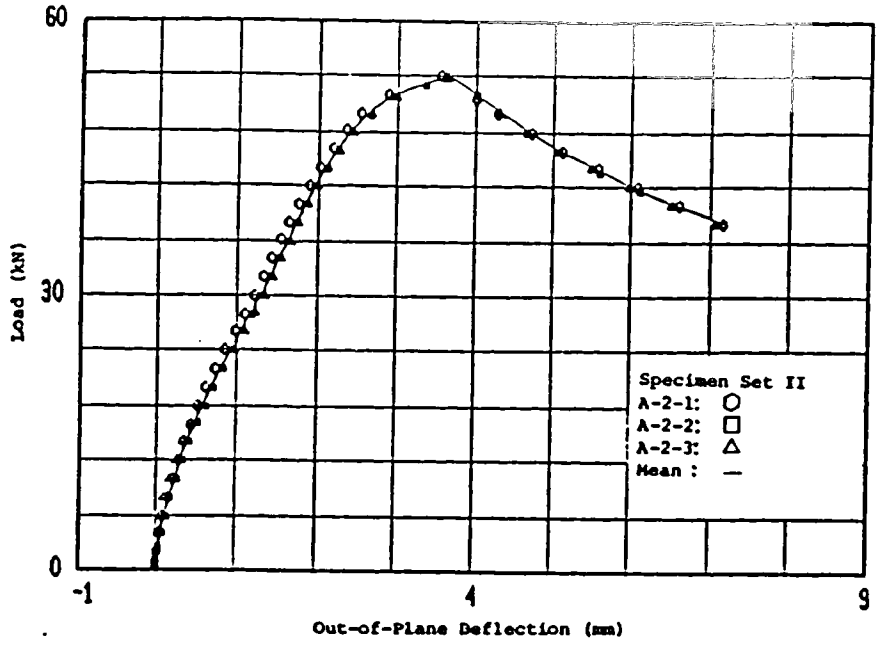

Fig. 3.29 Load Vs Web Out-of-Plane Deflection Behaviour of Specimen Set II Type A-2

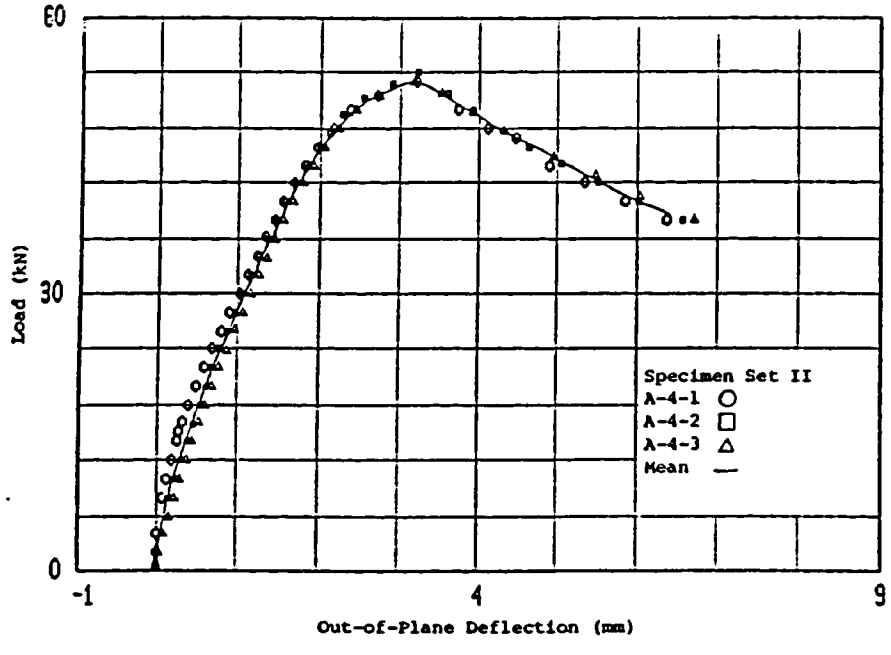

Fig. 3.30 Load Vs Web Out-of-Plane Deflection Behaviour of Specimen Set II Type A-4

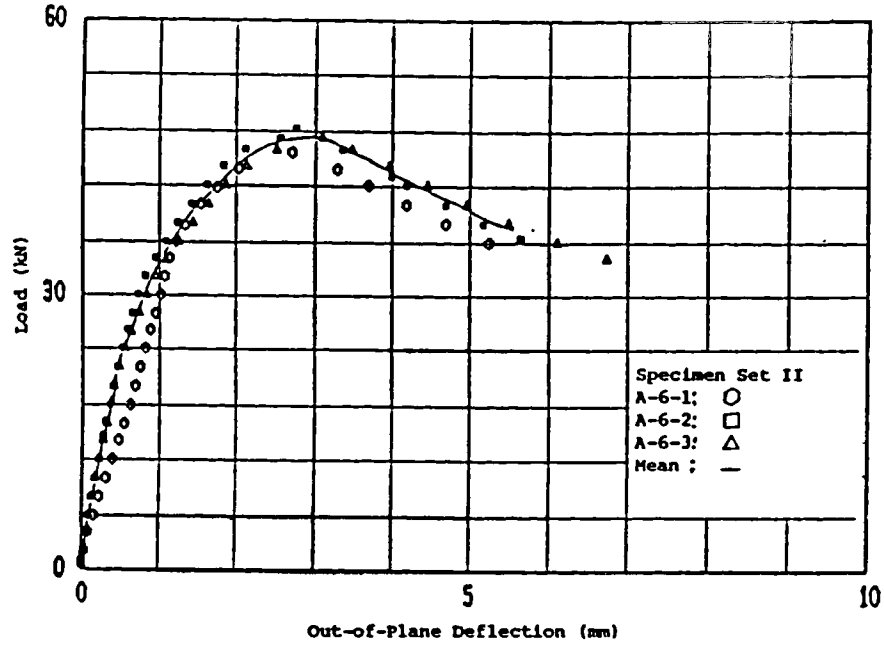

Fig. 3.31 Load Vs Web Out-of-Plane Deflection Behaviour of Specimen Set II Type A-6

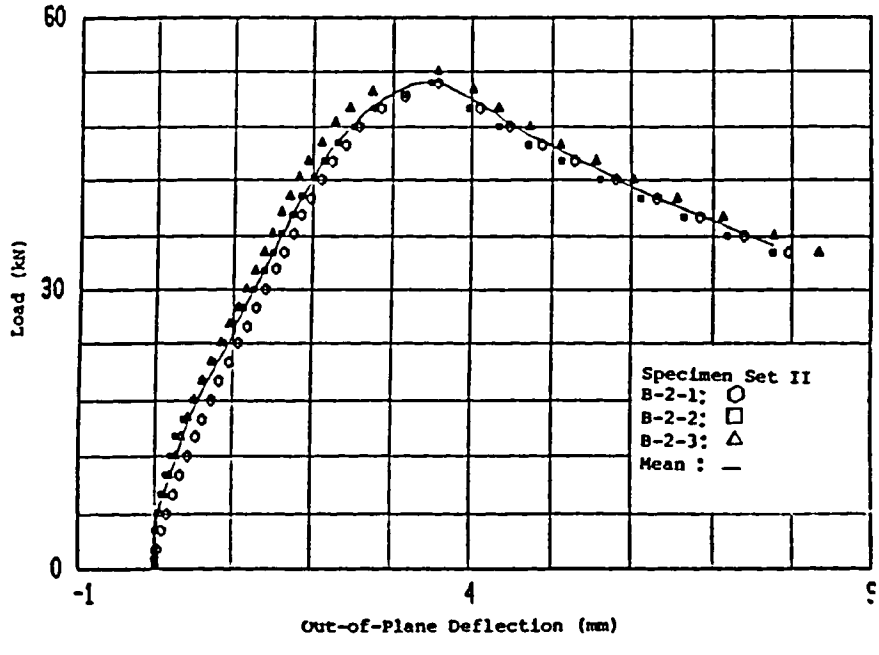

Fig. 3.32 Load Vs Web Out-of-Plane Deflection Behaviour of Specimen Set II Type B-2

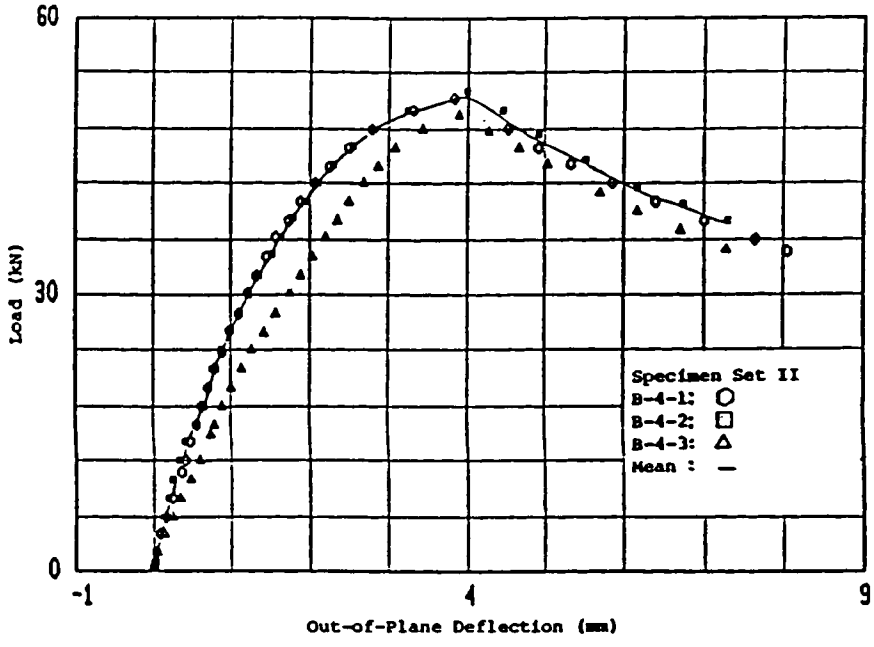

Fig. 3.33 Load Vs Web Out-of-Plane Deflection Behaviour of Specimen Set II Type B-4

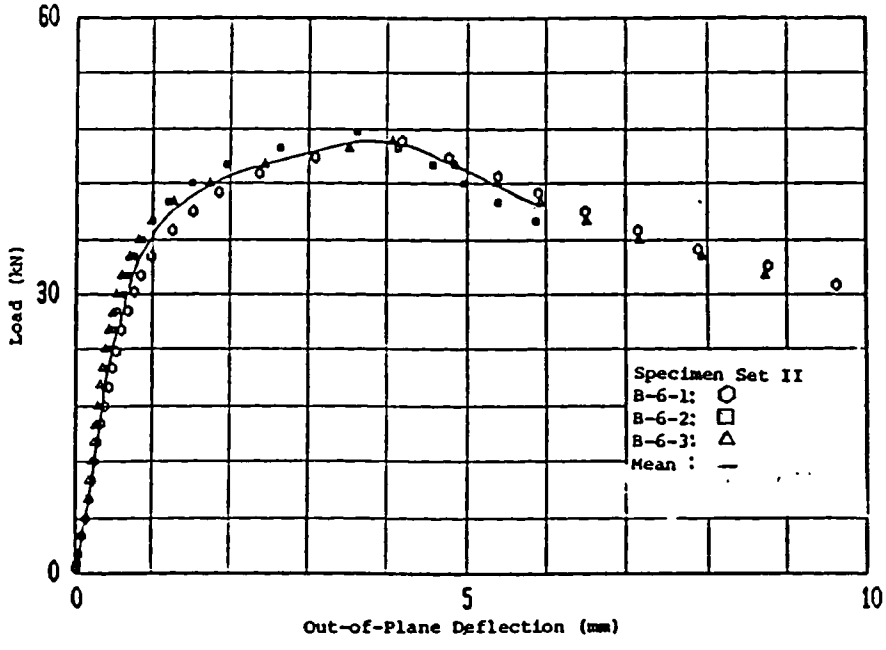

Fig. 3.34 Load Vs Web Out-of-Plane Deflection Behaviour of Specimen Set II Type B-6

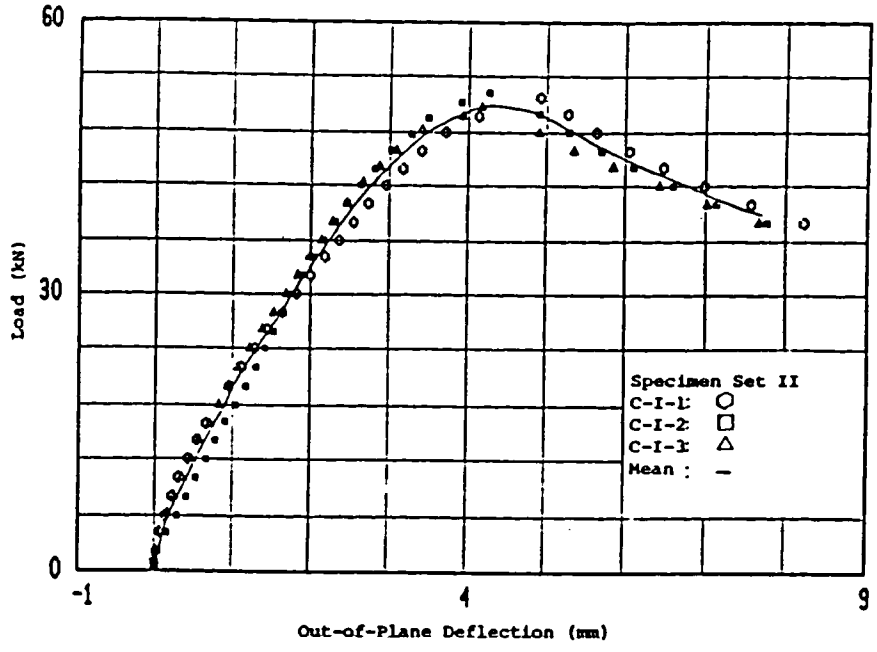

Fig. 3.35 Load Vs Web Out-of-Plane Deflection Behaviour of Specimen Set II Type C-I

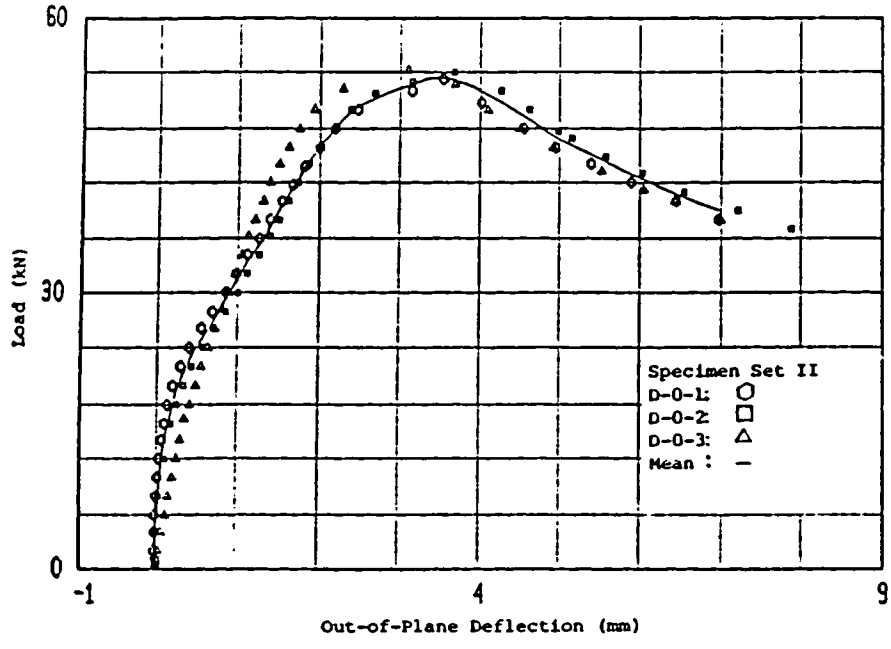

Fig. 3.36 Load Vs Web Out-of-Plane Deflection Behaviour of Specimen Set II Type D-0

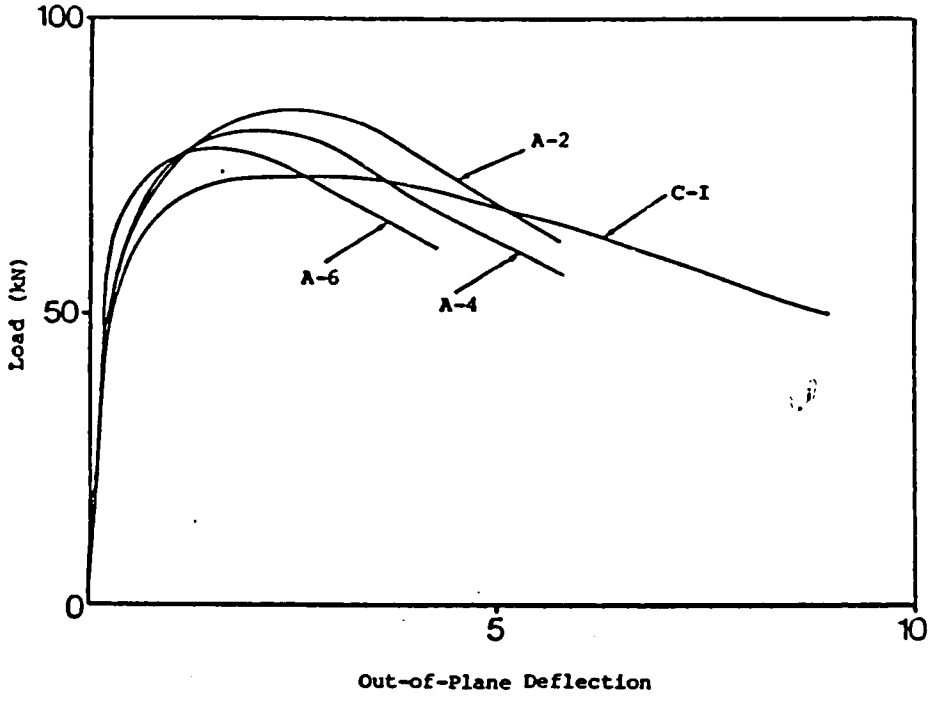

Fig. 3.37 Load Vs Web Out-of-Plane Deflection mean Curves of Set I Specimens With Circular and Slotted Perforations

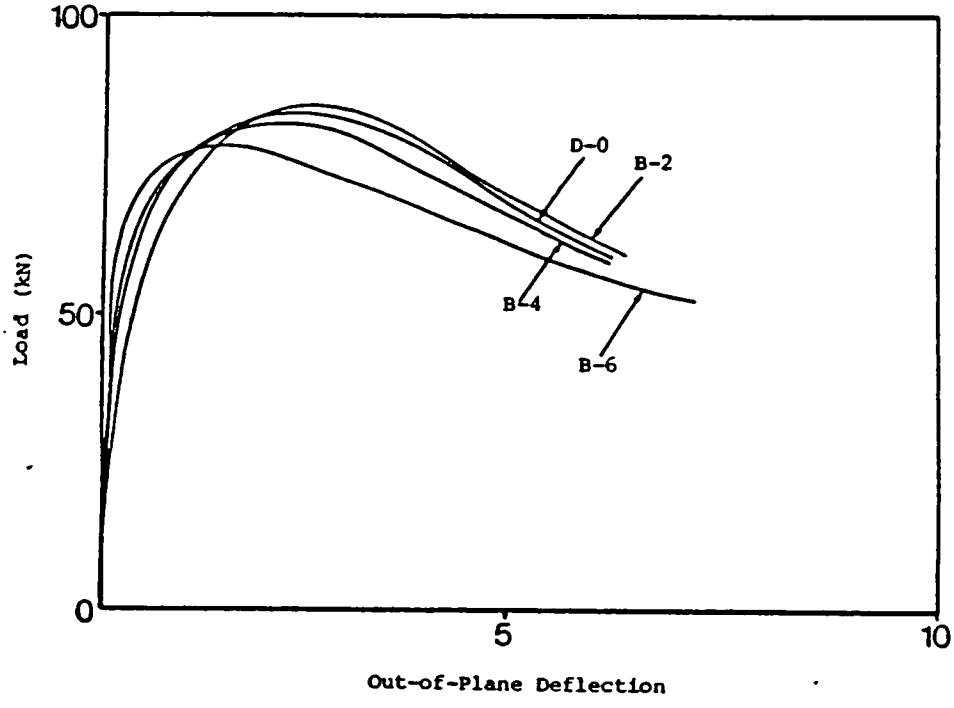

Fig. 3.38 Load Vs Web Out-of-Plane Deflection mean Curves of Set I Specimens with Square Perforations and No Perforations

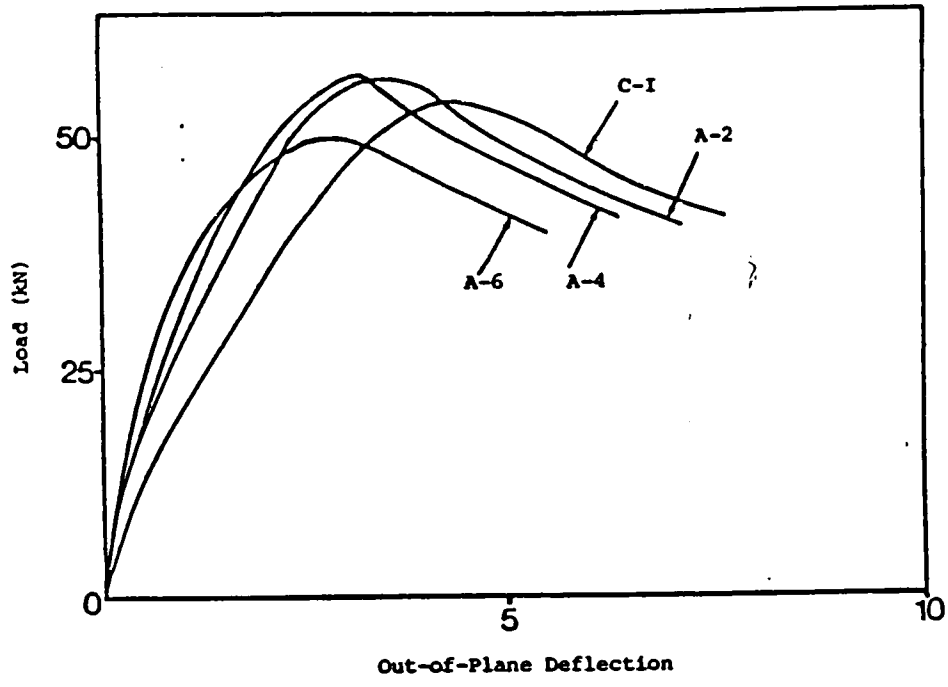

Fig. 3.39 Load Vs Web Out-of-Plane Deflection mean Curves of Set II Specimens With Circular and Slotted Perforations

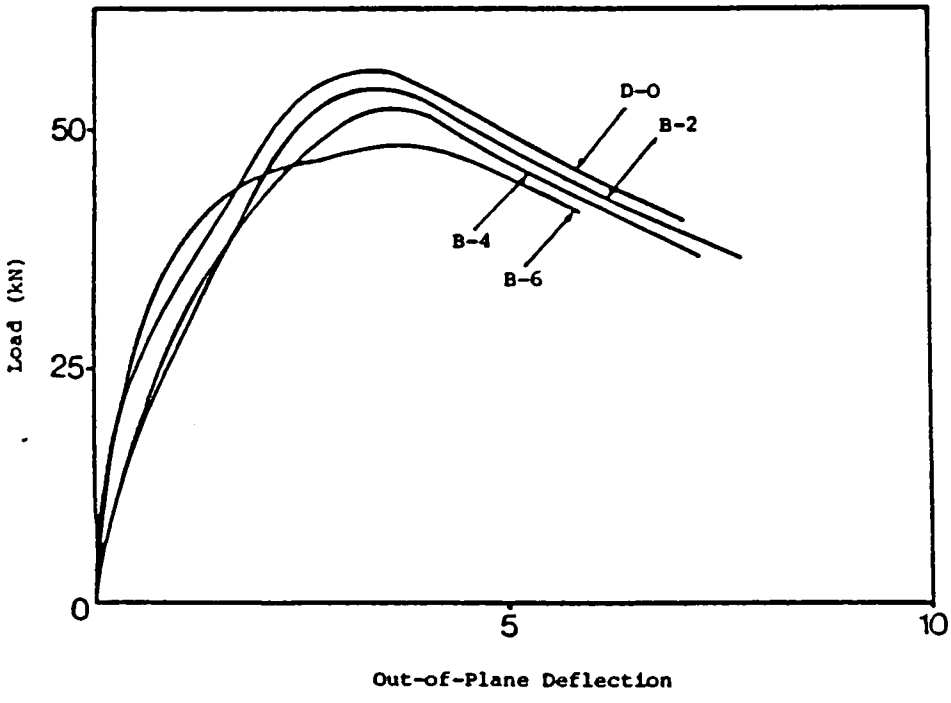

Fig. 3.40 Load Vs Web Out-of-Plane Deflection mean Curves of Set II Specimens With Square Perforations and No Perforations

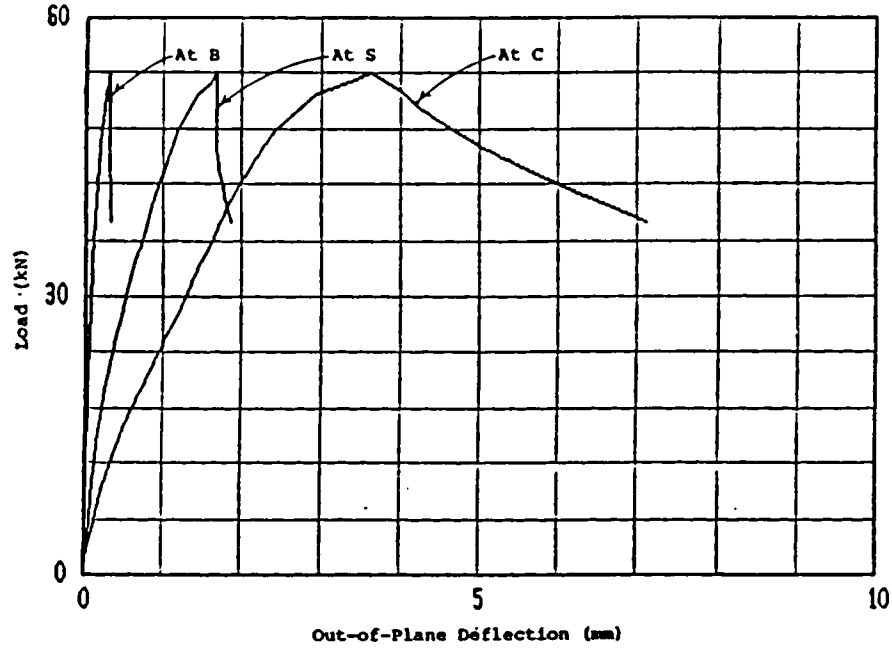

Fig. 3.41 Load Vs Web Out-of-Plane Deflection Behaviour of Specimen A-2-1 of Set II

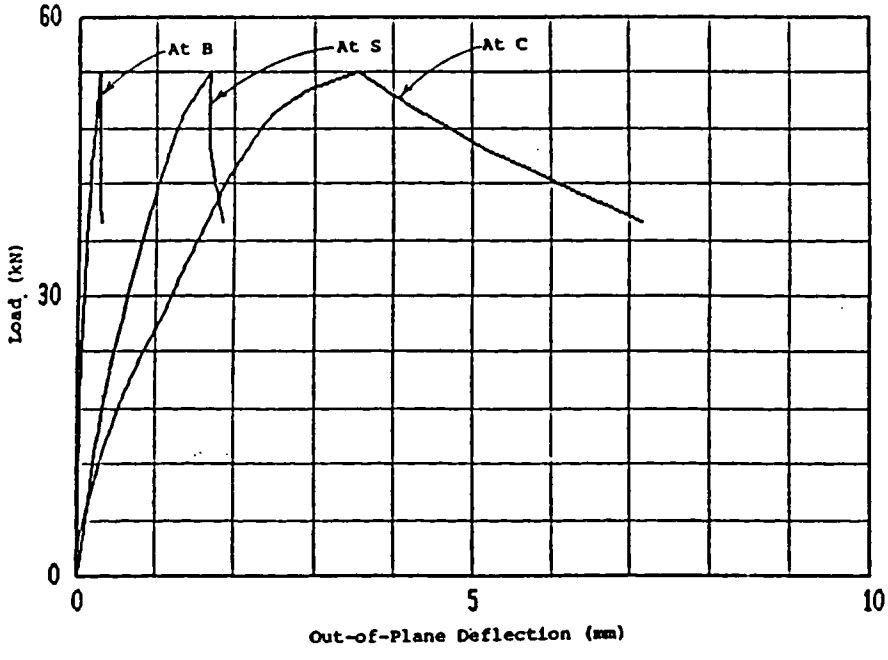

Fig. 3.42 Load Vs Web Out-of-Plane Deflection Behaviour of Specimen A-2-2 of Set II

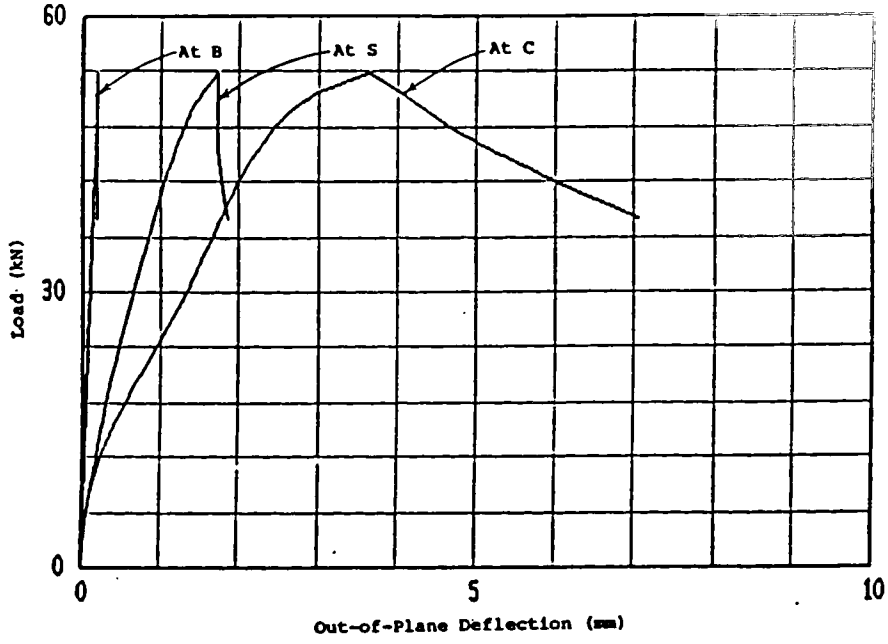

Fig. 3.43 Load Vs Web Out-of-Plane Deflection Behaviour of Specimen A-2-3 of Set II

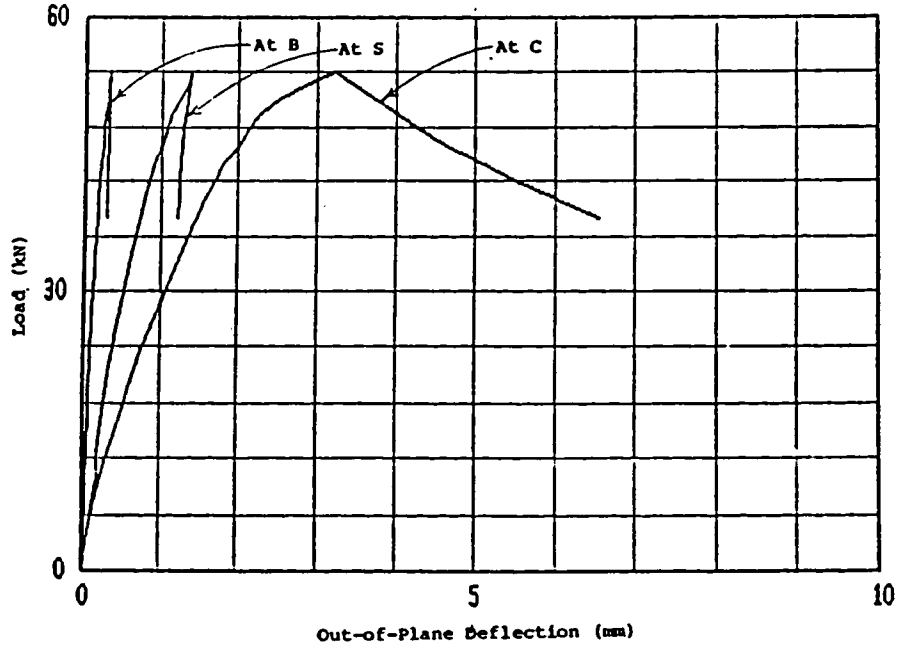

Fig. 3.44 Load Vs Web Out-of-Plane Deflection Behaviour of Specimen A-4-1 Set II

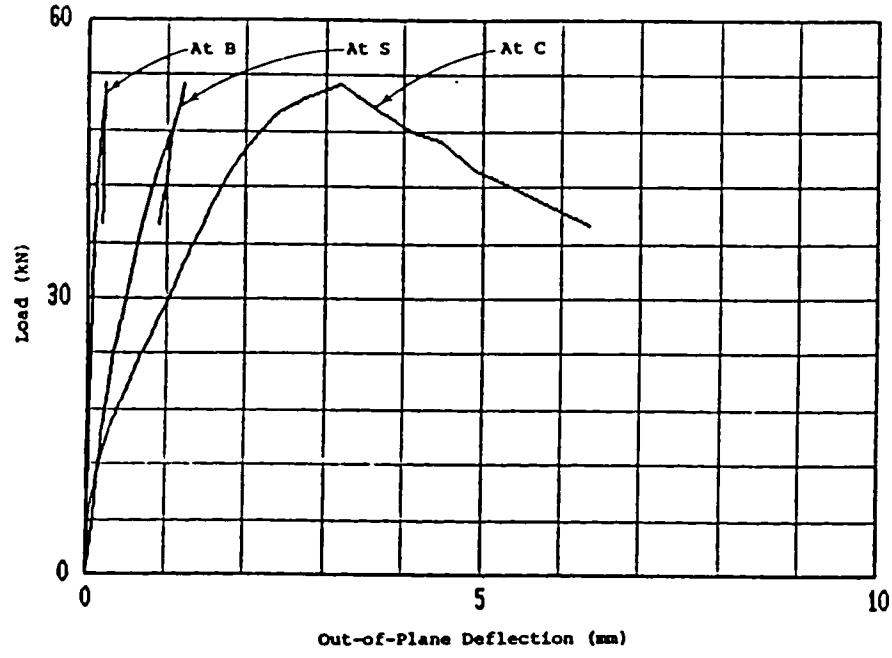

Fig. 3.45 Load Vs Web Out-of-Plane Deflection Behaviour of Specimen A-4-2 Set II

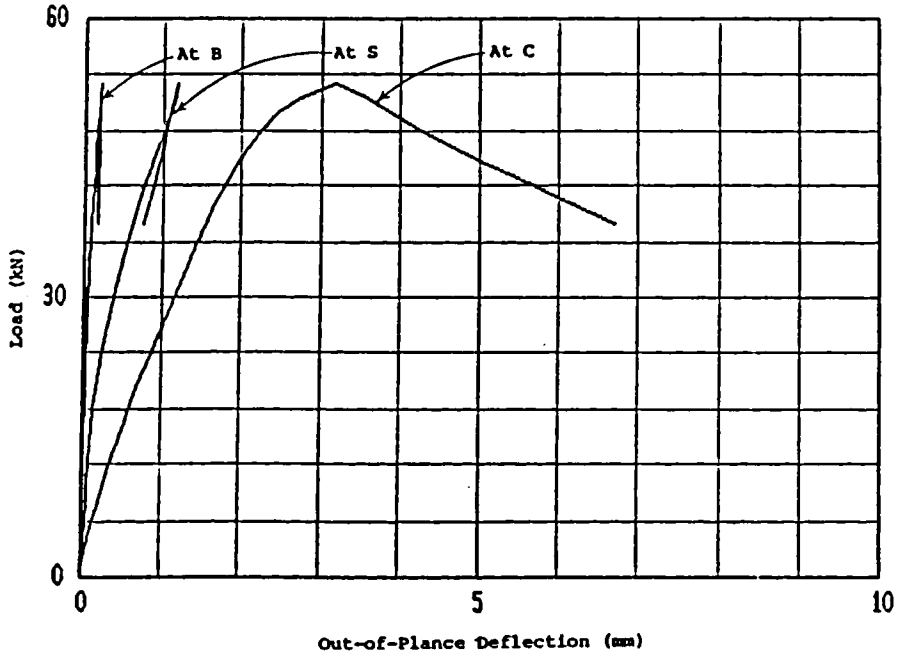

Fig. 3.46 Load Vs Web Out-of-Plane Deflection Behaviour of Specimen A-4-3 Set II

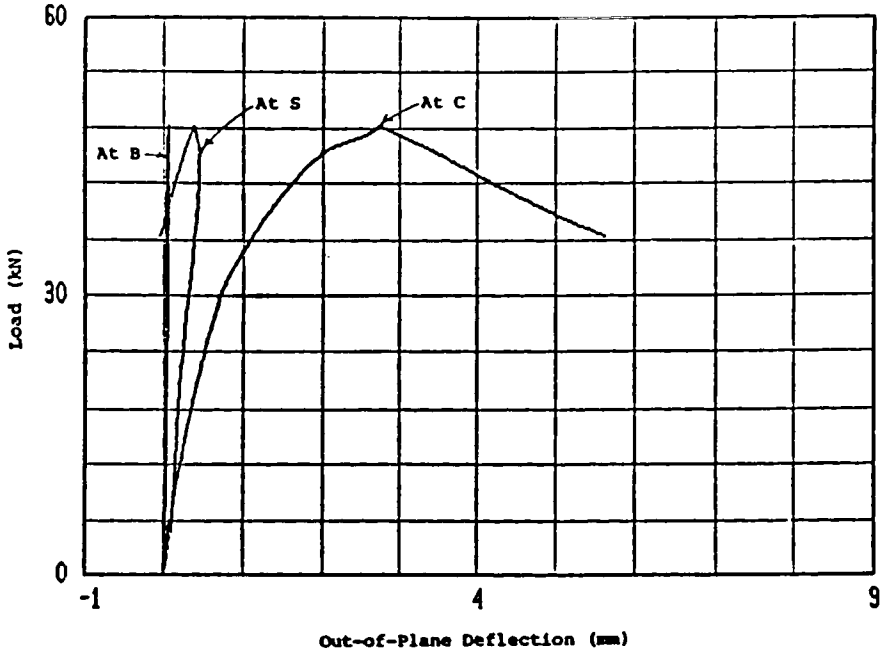

Fig. 3.47 Load Vs Web Out-of-Plane Deflection Behaviour of Specimen A-6-1 Set II

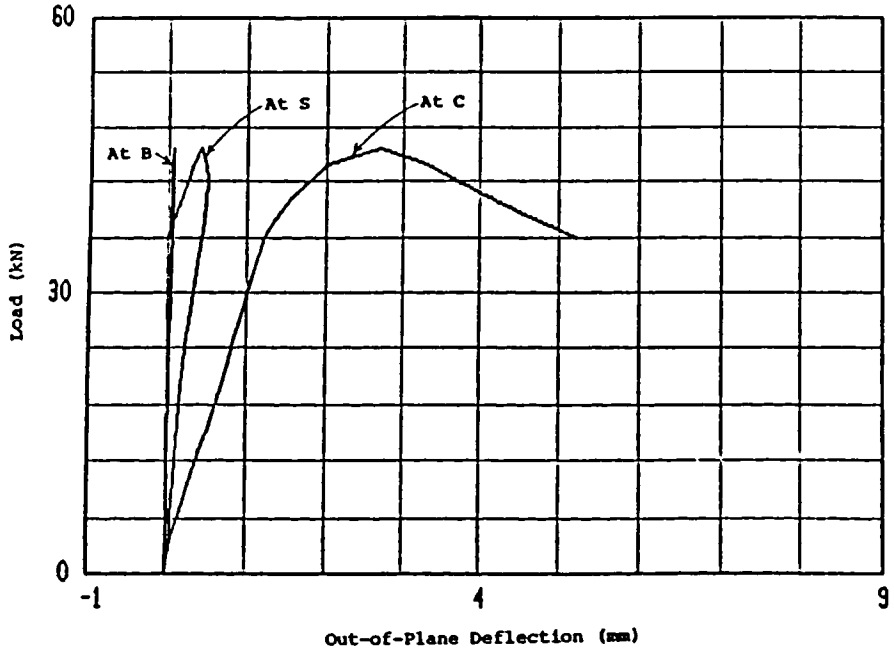

Fig. 3.48 Load Vs Web Out-of-Plane Deflection Behaviour of Specimen A-6-2 Set II

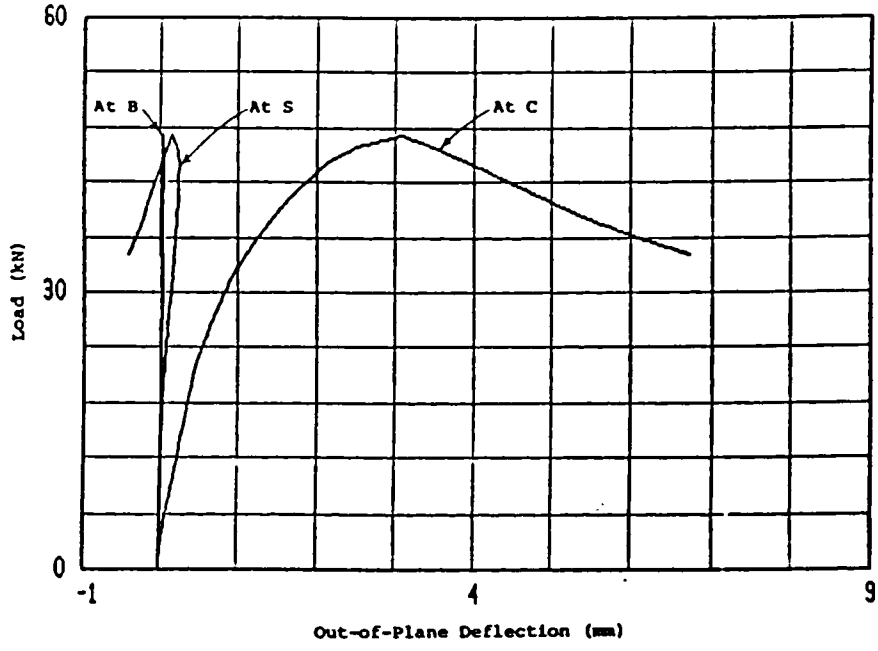

Fig. 3.49 Load Vs Web Out-of-Plane Deflection Behaviour of Specimen A-6-3 Set II

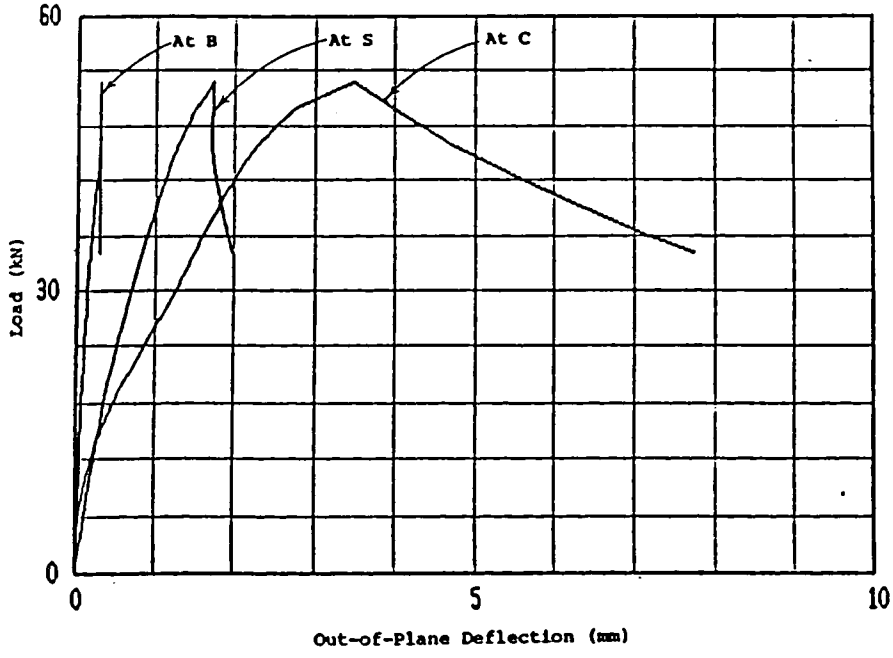

Fig. 3.50 Load Vs Web Out-of-Plane Deflection Behaviour of Specimen B-2-1 Set II

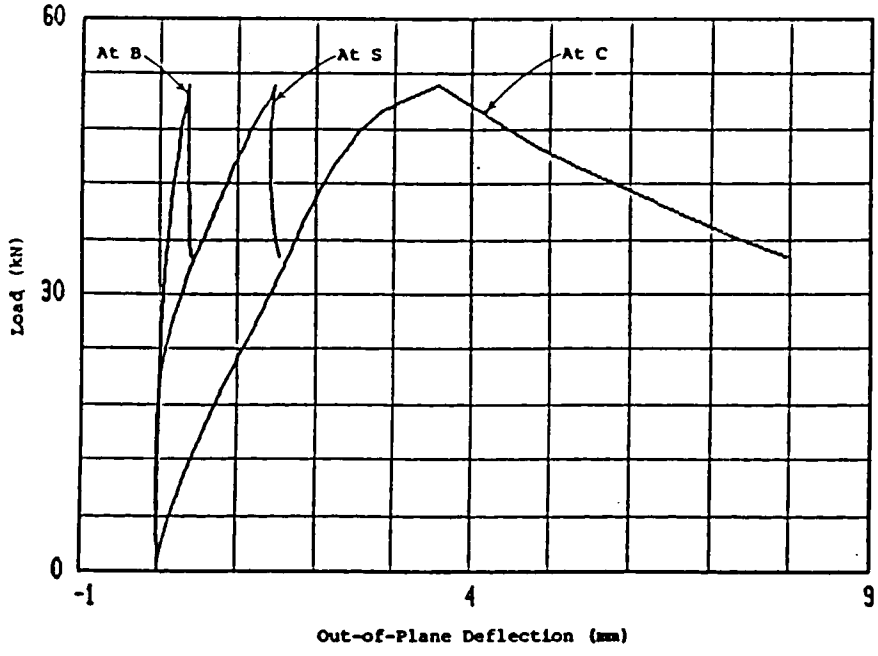

Fig. 3.51 Load Vs Web Out-of-Plane Deflection Behaviour of Specimen B-2-2 Set II

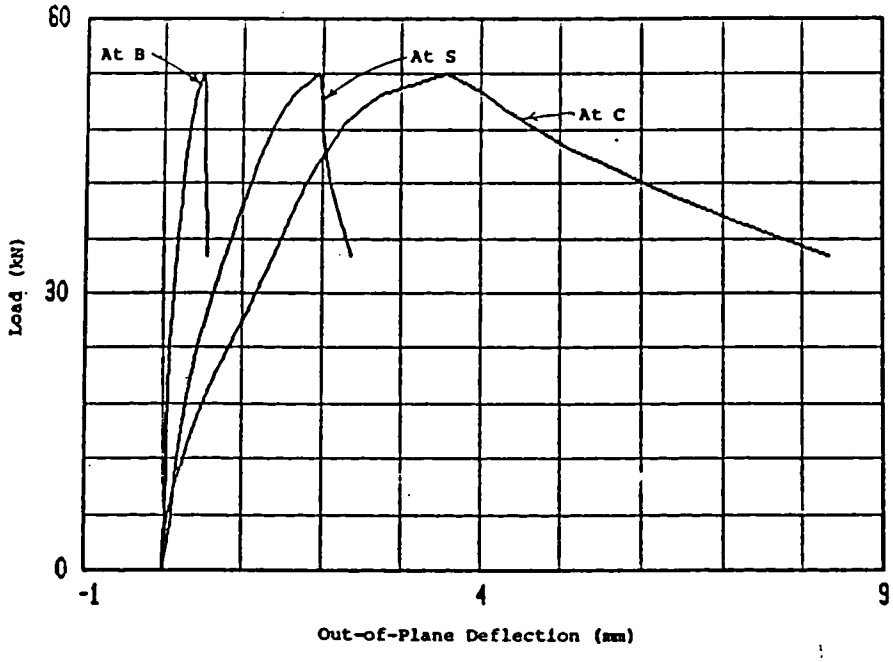

Fig. 3.52 Load Vs Web Out-of-Plane Deflection Behaviour of Specimen B-2-3 Set II

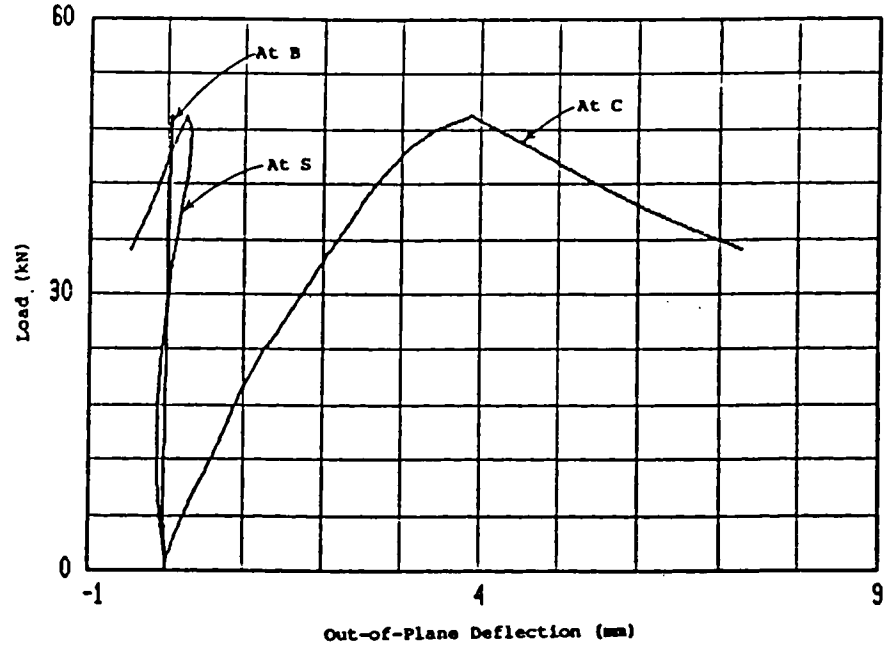

Fig. 3.53 Load Vs Web Out-of-Plane Deflection Behaviour of Specimen B-4-1 Set II

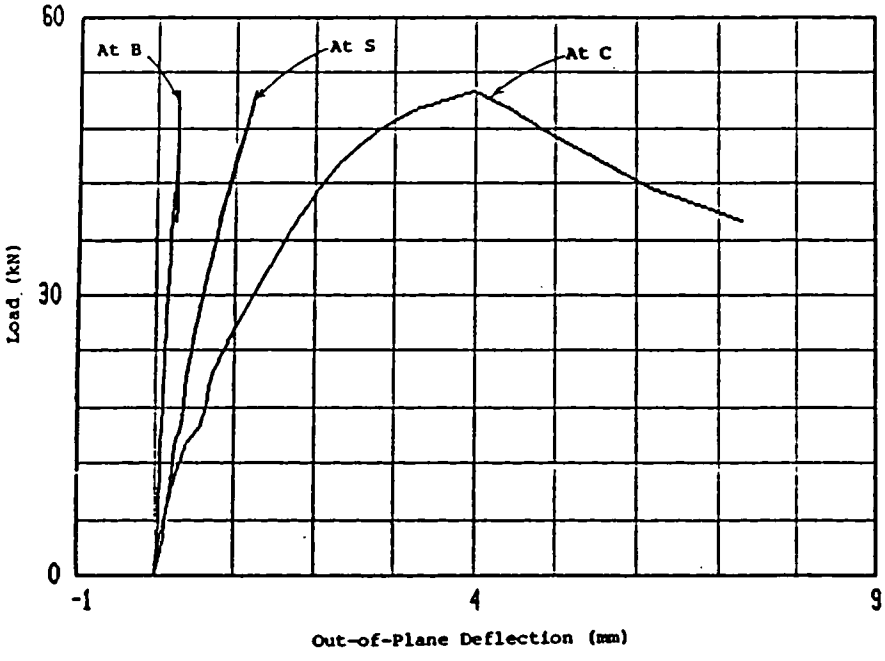

Fig. 3.54 Load Vs Web Out-of-Plane Deflection Behaviour of Specimen B-4-2 Set II

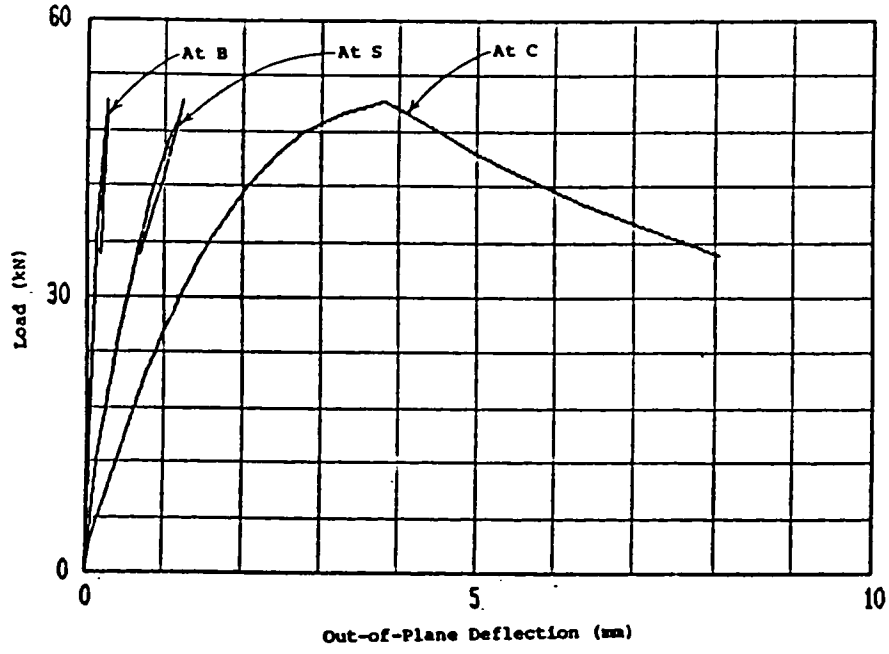

Fig. 3.55 Load Vs Web Out-of-Plane Deflection Behaviour of Specimen B-4-3 Set II

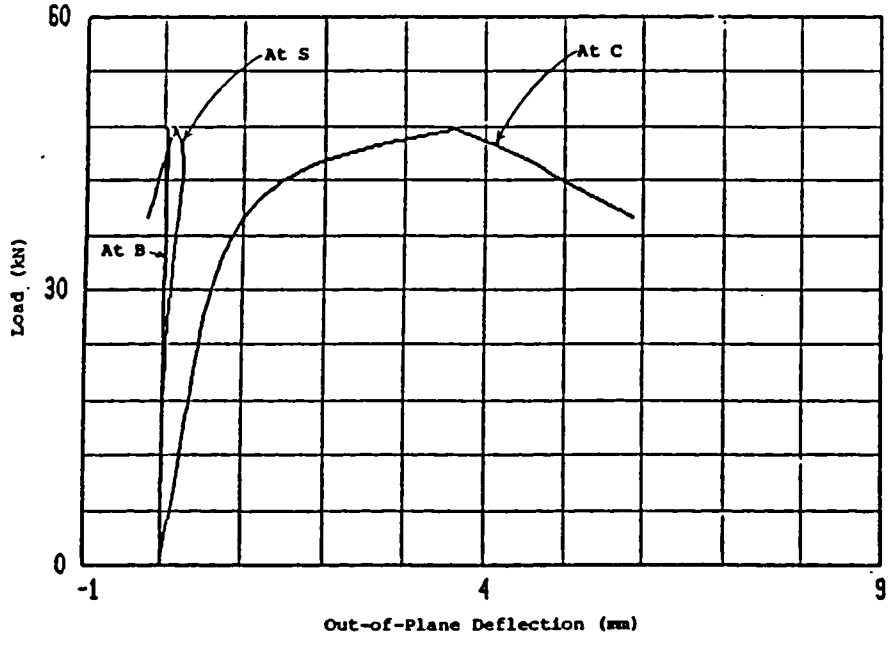

Fig. 3.56 Load Vs Web Out-of-Plane Deflection Behaviour of Specimen B-6-1 Set II

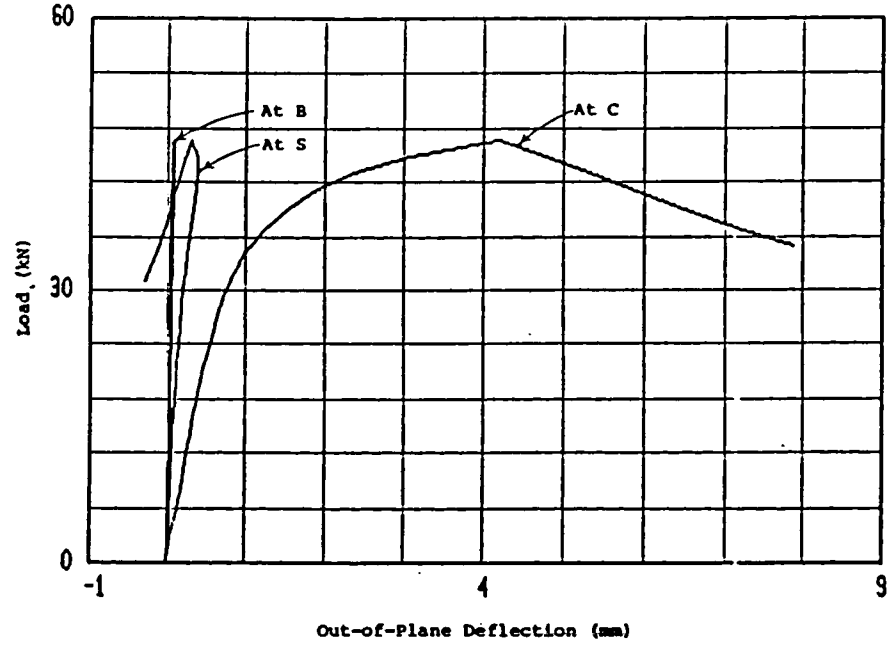

Fig. 3.57 Load Vs Web Out-of-Plane Deflection Behaviour of Specimen B-6-2 Set II

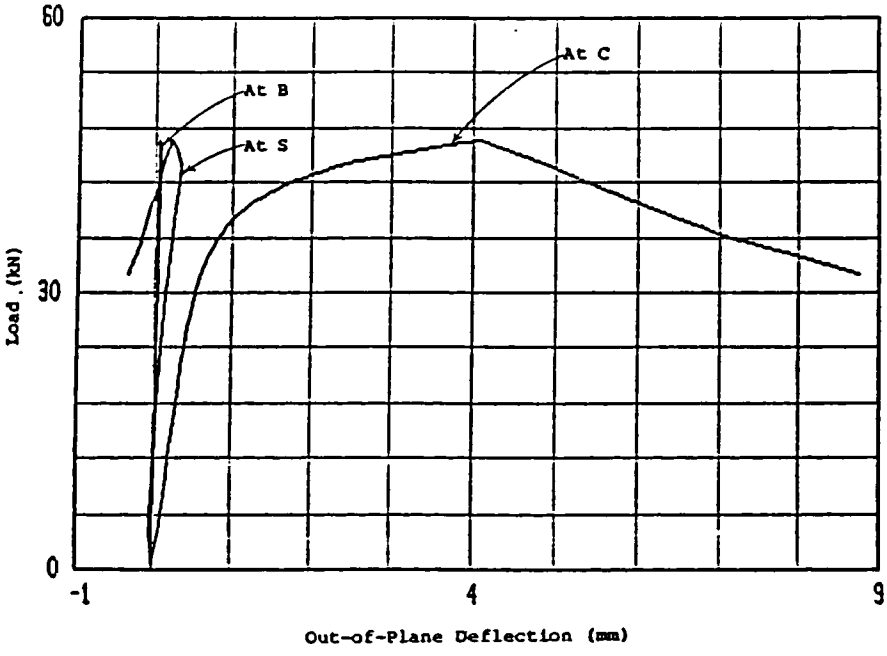

Fig. 3.58 Load Vs Web Out-of-Plane Deflection Behaviour of Specimen B-6-3 Set II

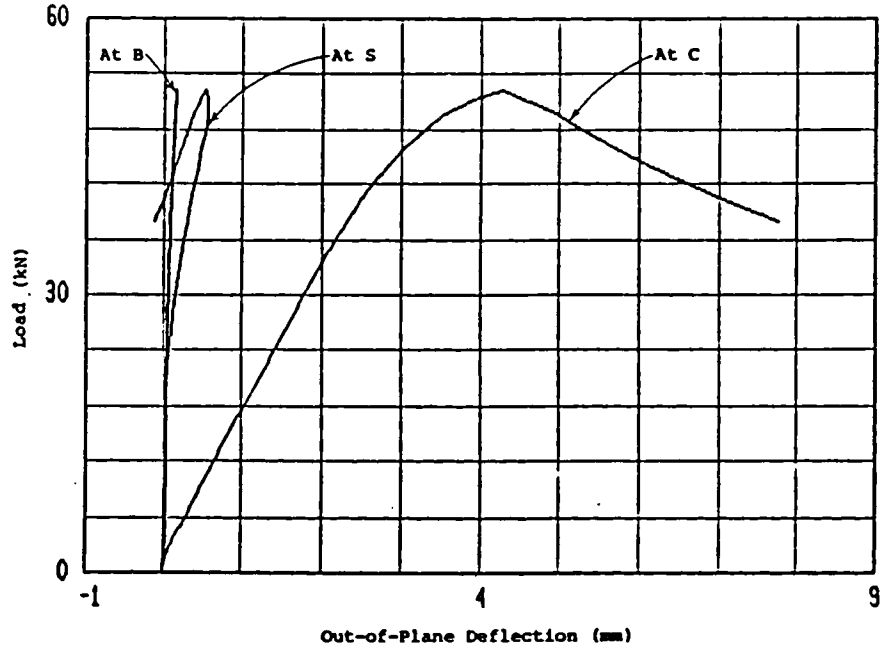

Fig. 3.59 Load Vs Web Out-of-Plane Deflection Behaviour of Specimen C-I-1 Set II

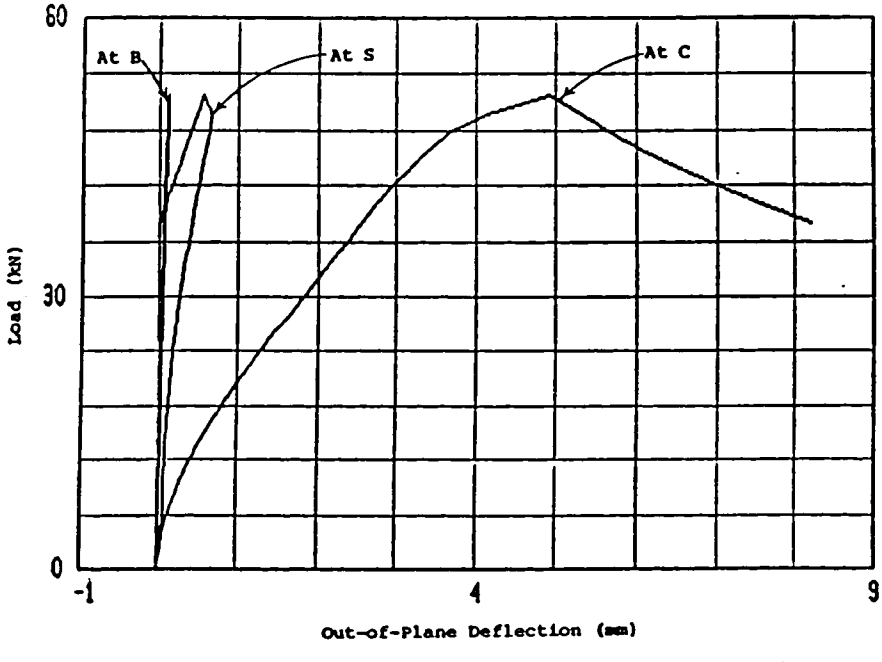

Fig. 3.60 Load Vs Web Out-of-Plane Deflection Behaviour of Specimen C-I-2 Set II

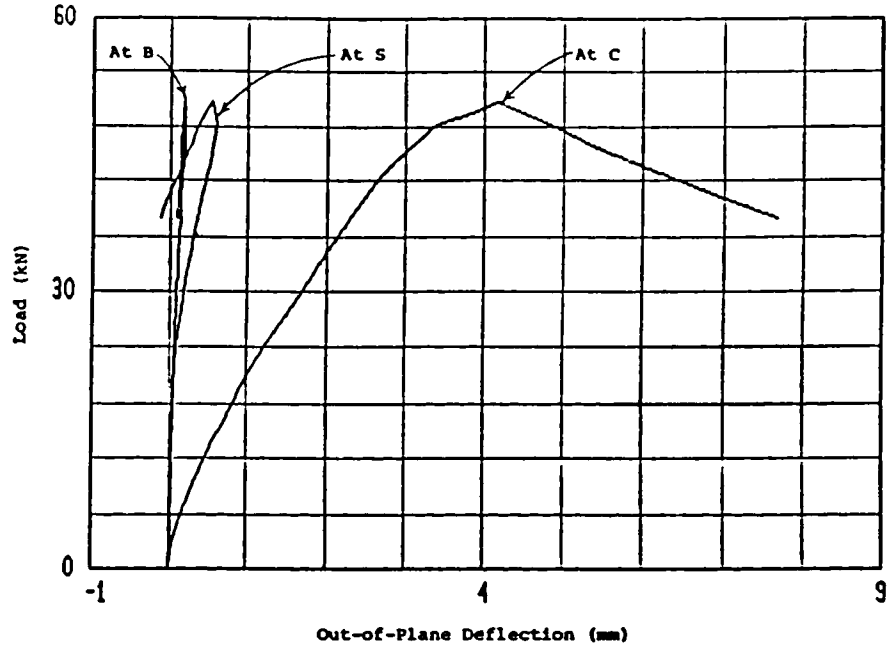

Fig. 3.61 Load Vs Web Out-of-Plane Deflection Behaviour of Specimen C-I-3 Set II

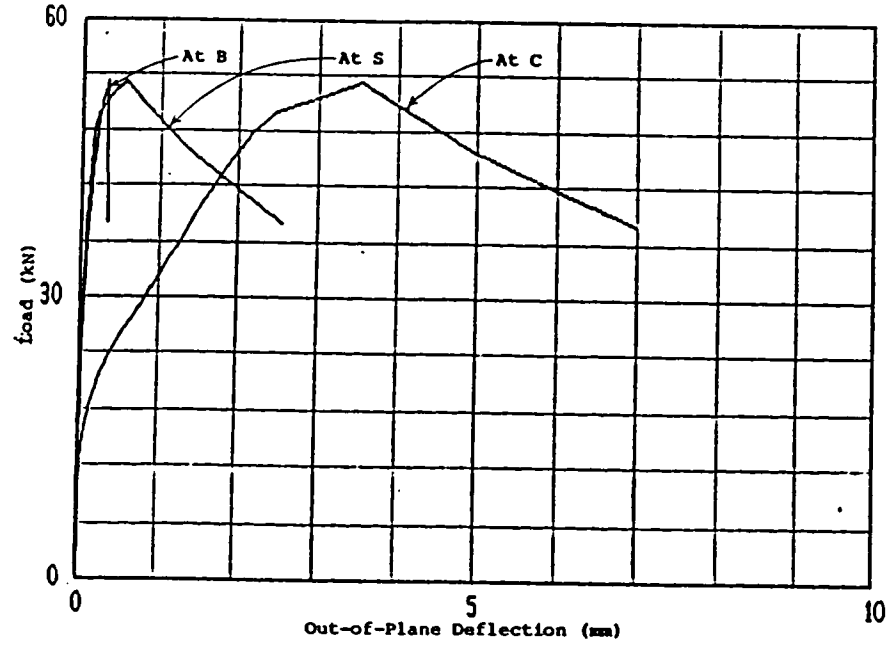

Fig. 3.62 Load Vs Web Out-of-Plane Deflection Behaviour of Specimen D-0-1 Set II

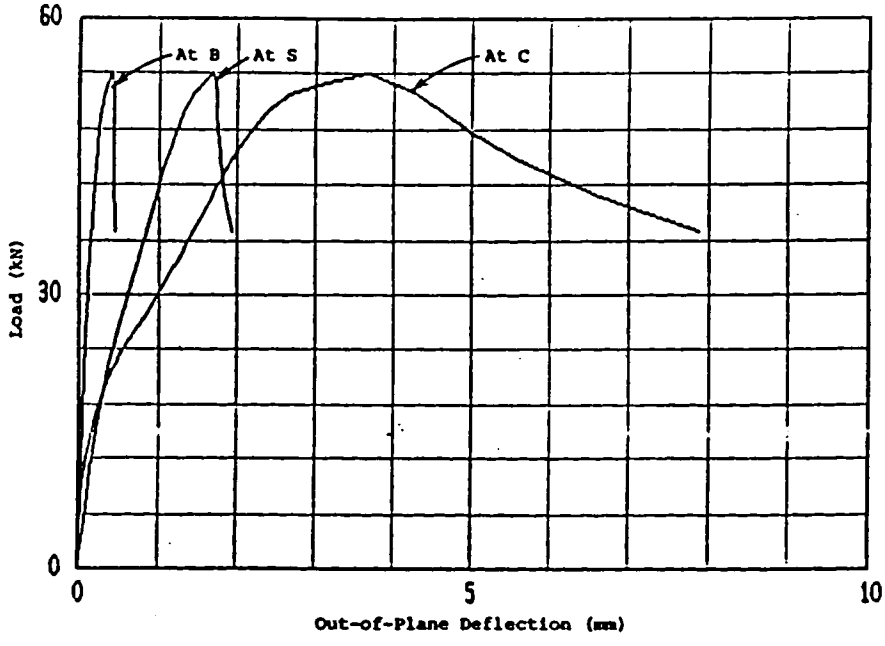

Fig. 3.63 Load Vs Web Out-of-Plane Deflection Behaviour of Specimen D-0-2 Set II

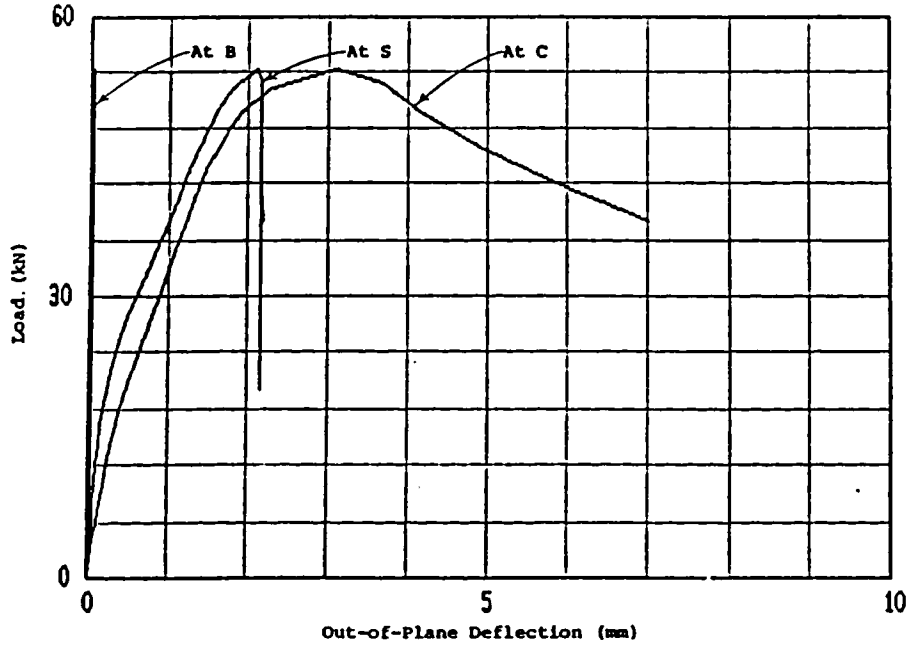

Fig. 3.64 Load Vs Web Out-of-Plane Deflection Behaviour of Specimen D-0-3 Set II

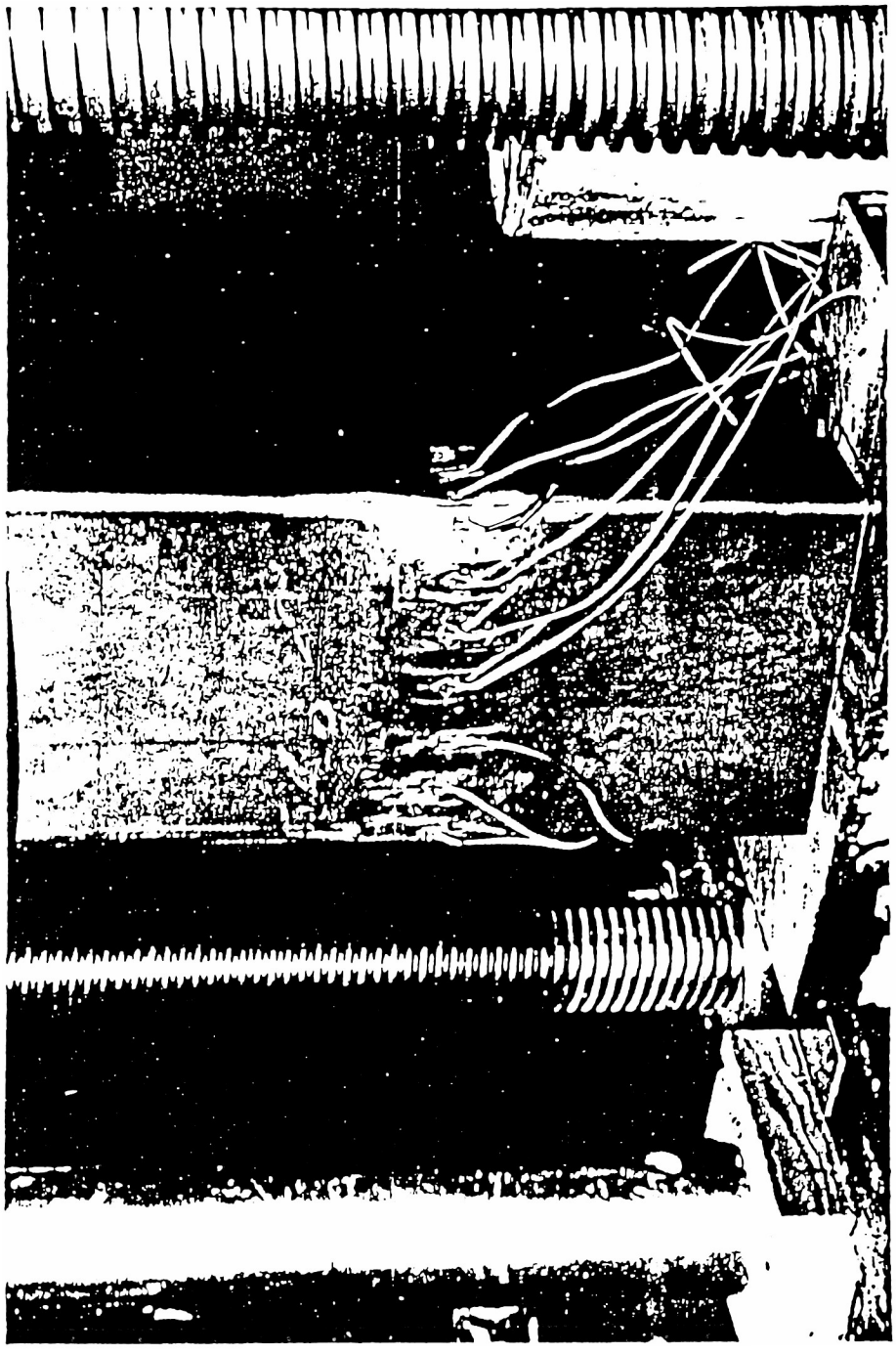

Fig. 3.65 A Specimen Showing Failure of Web

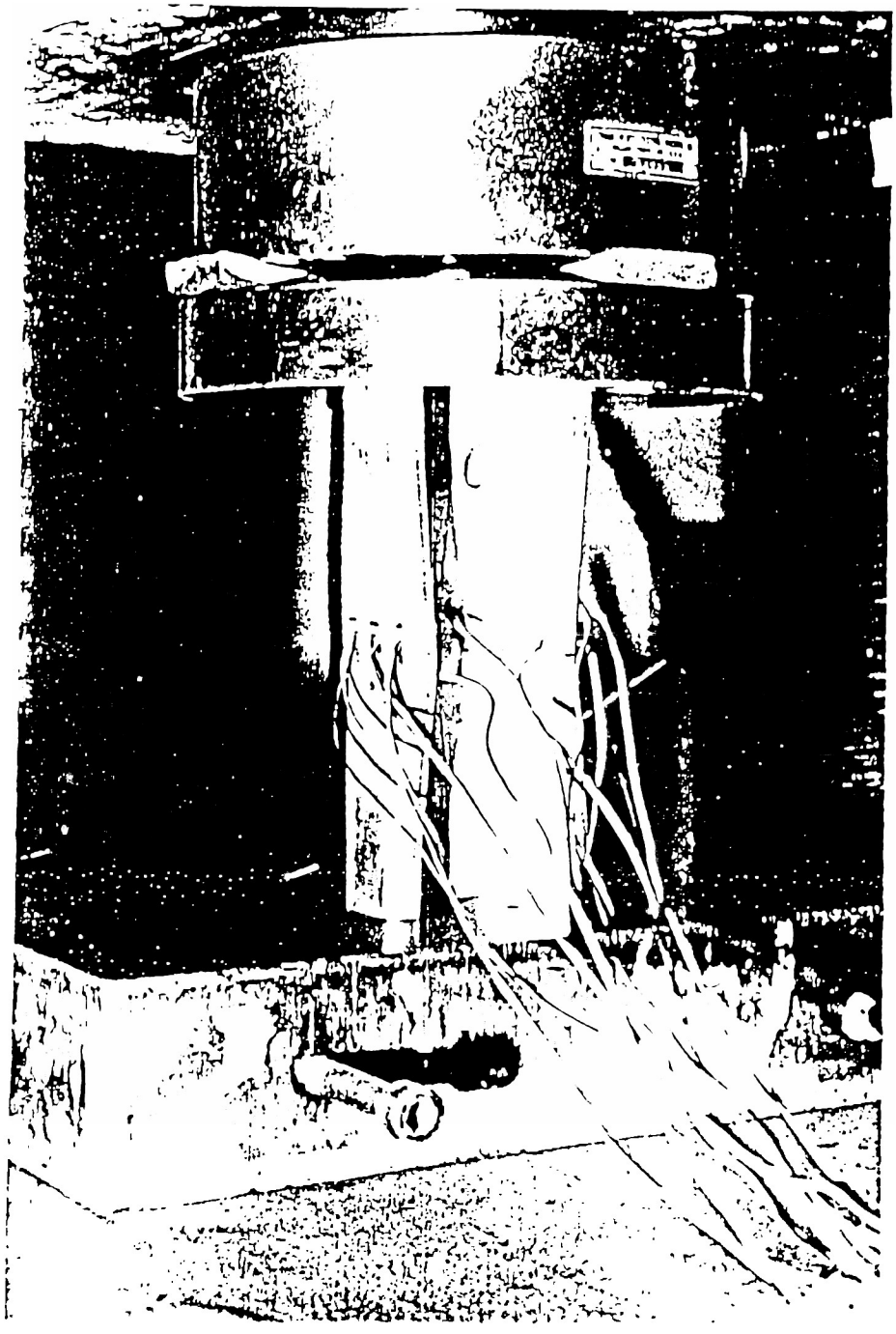

Fig. 3.66 A Specimen Showing Failure of Flanges

CHAPTER 4

ANALYSIS OF RESULTS: BUCKLING LOADS

4.1 INTRODUCTION

A brief introduction to local buckling and post local buckling phenomena was given in Chapter 1. In this chapter, various techniques that are generally applied to determine the experimental buckling loads are discussed, and some are used to determine buckling loads of the tested specimens. Buckling loads of the members are useful in estimating the limiting values of the width of the plate elements of cold formed members. The calculation of limiting values is discussed in Chapter 5. The knowledge of buckling loads also gives the sense of deformations of the plate elements at the design load level.

4.2 EXPERIMENTAL DETERMINATION OF BUCKLING LOADS

Based on analytical studies using small deflection theories, the load vs lateral deflection plots of the perfectly flat plate elements subjected to compressive loads have a well-defined bifurcation point (point B, Curve I, Figure 1.1). Hence, the buckling load of a flat plate, under edge compression corresponds, to this bifurcation point and has a unique value. However, plate imperfections and experimental errors in centering the specimen lead to

eccentricity of loads in edge compression of the plate. This causes deviation from classical buckling theory, and therefore, the load versis deflection curve (Curve II, Figure 1.1) of an imperfect plate does not have a well-defined bifurcation point. Therefore, it is difficult to distinguish between the pre-buckling and post-buckling path of the imperfect plate, and hence, to determine its experimental buckling load. To determine the experimental buckling loads of the thin plates, analysis of the following two types of data is usually done.

(a) load vs lateral deflection of the plate

(b) load vs strain in the plate elements.

A few common methods for determining buckling loads are discussed below.

4.2.1 METHODS BASED ON LOAD VS LATERAL DEFLECTION MEASUREMENTS

I - INFLECTION POINT METHOD

In this method, the buckling load is defined as the load corresponding to a point with minimum slope (point A, Curve II, Figure 1.1) on the load vs lateral deflection curve. The important physical significance of this method is that the inflection point is a point of maximum rate of increase of lateral deflection with respect to load (Schlack 1964,1968). If the initial imperfection is not excessive this method gives satisfactory results. However, the

selection of the point of contraflexure depends on the individual choice (Coan 1951, Fok and Yeun 1981).

II - THREE POINTS METHOD

In this method, the buckling load P_{cr} can be determined using a modified relationship, originally proposed by William and Walker (1975), for large deflection analysis of plates. This relationship, between load and lateral deflection of a plate, can be used to obtain P_{cr}, if any three sets of data points in the post buckling range are known. The original relationship was developed by using a perturbation method in which the intrinsic problem parameters are expanded in a power series. The orignal relationship is given as:

$$(\Delta^2 + 2\Delta\Delta_0)^{1/2} = A\Psi + B\Psi^3 \qquad [4.1]$$

where

$$\Psi = \sqrt{\frac{P}{P_{cr}} - 1 + \frac{\Delta_0}{\Delta + \Delta_0}}$$

P_{cr} is the buckling load, Δ_0 and Δ are the magnitudes of the initial imperfection and the measured deflection (corresponding to the applied load P) at the centre of the plate, respectively. A and B are constants depending upon boundary conditions. For small Δ_0, and for a data point in the post buckling range, the second term on the right hand side of equation [4.1] can be dropped, and the equation may be rewritten as (Fok and Yuen 1981)

$$\Delta^2 + 2\Delta\Delta_0 = A^2 \left[\frac{P}{P_{cr}} - 1 + \frac{\Delta_0}{\Delta + \Delta_0} \right] \qquad [4.2]$$

Equation [4.2] is the modified relationship used in the three points method. To evaluate P_{cr}, along with two other unknowns A and Δ_0, the values of load P and corresponding lateral deflection Δ for three sets of data from a test are substituted in equation [4.2] to form a set of non-linear simultaneous equations. P_{cr} is obtained from these equations. To avoid experimental errors, care should be taken not to select three points too close to each other. There are small fluctuations in the calculated results by this method when different sets(deflections corresponding to respective loads) of data points from a test are substituted in equation [4.2].

III - PIVOTAL PLOT METHOD

In plates, the effect of the initial imperfection on load vs lateral deflection behaviour is most prominent in the region around, and below the buckling load. However, for large deflections in the post buckling range, its effect is less, and the load deflection behaviour of even an imperfect plate is akin to a perfect plate. Based on this fact, Spencer and Walker (1974) first modified equation [4.2], and Fok and Yuen (1981) gave the final form. Deleting the terms containing Δ_0 in equation [4.2] it has the form:

$$\Delta^2 \simeq A \left[\frac{P}{P_{cr}} - 1 \right] \qquad [4.3]$$

If $\bar{P}$ and $\bar{\Delta}$ are the values of load and corresponding deflection of a selected point (pivotal point) from a set of experimental data in the post buckling range, then the unknown A can be calculated as:

$$A \simeq \frac{\bar{\Delta}^2}{\left[\frac{P}{P_{cr}} - 1 \right]} \qquad [4.4]$$

Substituting for A in equation [4.2], the final form of the equation, as given by Fok et al(1981) is

$$P_{cr} = \Delta_0 \left[\frac{H_2 H_3 - 1}{H_1} \right] - \frac{H_2}{H_1} \qquad [4.5]$$

where

$$H_1 = \frac{(\bar{\Delta}^2 - \Delta^2)}{\phi}$$

$$H_2 = \frac{P\bar{\Delta}^2 - \bar{P}\Delta^2}{\phi}$$

$$H_3 = \frac{3}{\bar{\Delta} + \Delta}$$

$$\phi = P\bar{\Delta} \left[3 + \frac{\bar{\Delta}}{\Delta} \right] - \bar{P}\Delta \left[3 + \frac{\Delta}{\bar{\Delta}} \right]$$

Thus, the $(H_2H_3-1)/H_1$ versus H_2/H_1 plot results in a straight line. The intercept of this line with the H_2/H_1 axis gives the buckling load P_{cr}, and the slope of the line gives the initial imperfection. The functions ϕ and H_1 may have zero values. Hence, there is a risk of instabilty in calculations (Fok and Yuen, 1981, Souza et al, 1983).

IV - METHOD OF LEAST SQUARES

In this method, the unknowns A, B, P_{cr} and Δ_0 of equation [4.1] are evaluated based on the best fit of the load vs lateral deflection curve obtained from a test. This is done by the least square curve fitting technique. Fok (1984) first applied this method to determine the buckling load of plates with large deformations.

The evaluation of unknowns of equation [4.1] is done in two steps. First, the trial values of buckling load and initial imperfection are assumed and substituted in equation [4.1] which becomes linear in A and B, and is expressed as

$$R^2 \equiv \left[f(\Delta) - A\Psi - B\Psi^3\right]^2 \qquad [4.6]$$

where

$$f(\Delta) = (\Delta^2 + 2\Delta\Delta_0)^{1/2}$$

R^2 = the square of the difference between the measured and calculated values of P.

The optimum values of A and B are then found as:

$$\begin{bmatrix} \Sigma\Delta^2 & \Sigma\Delta^4 \\ \Sigma\Delta^4 & \Sigma\Delta^6 \end{bmatrix} \begin{bmatrix} A \\ B \end{bmatrix} = \begin{bmatrix} \Sigma\Psi f(\Delta) \\ \Sigma\Psi^3 f(\Delta) \end{bmatrix} \qquad [4.7]$$

In the second step, the optimum values of P_{cr} and Δ_0 are found using A and B of equation 4.7. The optimum values of buckling load and initial deformation are those which satisfy equation [4.1] and minimize R^2. These are found by means of the Newton-Raphson iteration technique (Fok, 1984).

4.2.2 METHODS BASED ON LOAD VS STRAIN MEASUREMENTS

In these methods, normally two strain gauges are mounted opposite to each other at the probable buckling location on the flat surfaces of a plate element. Experimental buckling loads are determined by analysing the strain readings of and the corresponding loads. Some of the methods based on the above technique are given below.

V - STRAIN DEVIATION METHOD

In this method, the strain corresponding to the buckling load is defined at a point, where the strain increments, for successive readings for either of two strain gauges, mounted opposite to each other on either side of a plate, begin to decrease. The strain determined from this criterion represents the situation, in which the stress distribution across the thickness of the plate element is beginning to change from uniform compressive stress to a state of combined compression and bending. This gives an

indication of the initiation of out-of-plane deformation (Johnson and Winter, 1966, Wang and Winter, 1969).

VI - STRAIN REVERSAL METHOD (MAXIMUM SURFACE STRAIN METHOD)

In this method, buckling load is defined as the load, corresponding to the critical strain, which is taken as the maximum compressive strain on the convex side of the plate element. Beyond this point, the compressive strain on the convex side starts to decrease and ultimately changes into tensile strain. Critical strain, and hence the buckling load, obtained from this method is usually higher than the buckling load obtained by the strain deviation method (Johnson and Winter 1966, Wang and Winter 1969). The difficulties faced in this method include inability to predict accurately the location of the buckle crest on the plate element prior to the experiment, and the absence of strain reversal (Stowel et al 1951, Souza et al 1983).

VII- MAXIMUM MEMBRANE STRAIN METHOD (AVERAGE STRAIN METHOD)

In this method, the critical strain is taken as the maximum average of the strains recorded by a pair of strain gauges mounted at the probable buckle crest location. It indicates the point where the increment of the membrane strain is zero, and the membrane strain has reached its maximum value. At this point, bending and waving of the plate is involved, and the direct stretching of the thin plate due to excessive deformation is beginning to take

place. The buckling load is usually obtained by extending the pre-buckling and post-buckling segments of the load-average strain relationship. The load corresponding to the point of intersection of these two segments is the buckling load. The buckling loads determined from this method are usually higher than those obtained by Strain Deviation and Strain Reversal Methods. (Johnson and Winter 1966, Wang and Winter 1969). This method can be very successful if the post buckling path of a plate is clearly defined. If the test has to be terminated prematurely due to early failure of the specimen, the resulting buckling load may be inaccurate (Souza et al, 1983).

VIII- STRAIN DIFFERENCE METHOD

In this method the load is plotted against the difference in axial strains of a pair of strain gauges mounted at the centre of the plate element. The buckling load is determined by locating the inflection point (point of minimum slope) of load vs strain difference curve. The strain difference depends only on the deflection, and not on the mean axial stress. The reasoning employed in this method to locate the buckling load is analogous to that employed in connection with the inflection point method (Coan, 1951).

4.2.3 DETERMINATION OF EXPERIMENTAL BUCKLING LOADS OF PERFORATED PLATES

Most studies on the analysis of buckling loads of perforated plates are restricted to flat square plates with a central circular hole (Levy et al 1947, Kumai 1952, Schlak 1967, 1968, Yoshiki et al 1967, Kawai et al 1968, Ritchie and Rhodes 1975, Narayanan and Chow 1984, and Roberts and Azizian 1984). Except for Levy et al and Roberts and Azizian, who performed theoretical studies only, all the other studies are theoretical, as well as experimental. Narayanan and Chow also studied the behaviour of a flat square plate with a central or eccentric square hole. Ritchie and Rhodes performed a study on the behaviour of rectangular plates(aspect ratio 2:1) with a central hole.

The only experimental study for determination of buckling loads of cold formed sections is by Yu and Davis (1973). They formed rectangular box section by bolting two cold formed lipped channel steel sections. They studied the effect of a centrally cut circular or square hole on the buckling loads and ultimate strengths of these sections. The flat width to thickness ratio of the perforated elements varied from 36.6 to 73.8 and d/W_1 ratio varied from 0 to 0.722.

Experimental methods used by these investigators to determine buckling loads are essentially the same as those used in unperforated plates listed in section 4.2. The

inflection point method has been employed for determination of buckling loads of perforated square plates by Schlak and Narayanan and Chow while the strain reversal method was prefered by Yu and Davis for buckling loads of perforated cold-formed sections. The maximum membrane strain method was used by Ritchie and Rhodes for square and rectangular plates. Later, Fok applied the three point method and the least square technique to perforated square plates.

Of the various methods used to experimentally determine buckling loads, it can be said that the inflection point method and the strain difference method, which are based on a curve fitting technique and the location of the inflection point are tedious particularly for imperfect plates. This is due to the absence of any distinction between pre-buckling and post-buckling paths. The three points method, the pivotal plot method and the method of least squares are essentially based on equation 4.1 and may give accurate results. The three points method and the pivotal plot method are reliable for plates with imperfections up to half the plate thickness, while the method of least squares may be used for larger imperfections (Fok 1984, Souza et al 1983). There exists a variation in results depending on the choice of the three data points (three points method), or the pivotal point (pivotal plot method).

The strain deviation method, strain reversal method

and the maximum membrane strain method are experimental, and determination of buckling loads are less dependent on the judgement of the individual. The lowest buckling loads are obtained by using the strain deviation method, but this method has rarely been used. The strain reversal method has been used by many investigators because of its ease for determining buckling loads. The difficulty in this procedure is that strain reversal may occur at lower loads than the actual critical loads due to imperfections. If the post-buckling path of the plate is clearly defined, the maximum strain method is very reliable but will give a buckling load of higher value than the actual. The selection of methods used in this study to determine buckling loads is discussed in section 4.3.

From the experimental and theoretical studies, Yu and Davis (1973) and Narayanan and Chow (1984) observed that the buckling loads of perforated plates decrease with formation of a small opening in the centre of a plate. However, Azizian and Roberts(1984) found that buckling loads are independent of hole size, varying from zero to half the width of the plate element. Buckling loads may increase with an increase in hole size above this. Buckling loads also decrease with the increase in the eccentricity of the hole (Narayanan and Chow 1984).

4.3 BUCKLING LOADS OF COLD FORMED STEEL SECTIONS WITH OPENINGS

A detailed description of the various methods that may be used to determine the buckling loads of the plates has been given in the preceding sections. Initially in this study, an effort was made to obtain the buckling loads using the three point method and the pivotal plot method using data from some of the specimens. As stated earlier, the buckling load obtained using these methods depends largely on the choice of data points used. Using the pivotal point method no well defined straight line graph was obtained for some of the tests. The three point method gave a wide range of values of the buckling load for data of the same test when different sets of points were used. Therefore, these methods were not used for the remaining specimens and the results are not documented here. Moreover, the analysis of ultimate loads, given in the next chapter, is emphasized because of their importance in the design of thin walled sections. Keeping this in view, buckling loads of various specimens are determined using the strain reversal method and the maximum membrane strain method only, which are easy to apply and depend less on individual judgement. The results are given in Table 4.1.

In the case of the strain reversal method, the buckling loads are obtained by scanning through load vs strain readings. Therefore, buckling loads here correspond

to maximum compressive strain on the convex side of the strain gauge. Similarly, in the case of the maximum membrane strain method the buckling loads correspond to a maximum of the average strain in a pair of strain gauges located adjoining the hole at mid-height of the specimen.

It is evident from Table 4.1 that predicted buckling loads by the strain reversal method is more uniform in set I than in Set II. This may be because of the effect of larger initial imperfections in the case of Set II due to the higher flat width-to-thickness ratio of the web. To predict the buckling loads correctly using the strain reversal method, the strain gauge should be at the crest of the buckle. Sometimes the crest of buckle formed at a slightly different location than that of the strain gauge, causing some error in prediction of buckling loads.

As shown by the dash marks in Table 4.1, the buckling loads could not be obtained in many tests using the maximum membrane strain method. One reason may be because for stiffened edges of the web, there is less lateral deflection resulting in no reduction in average strain upto failure. However, wherever possible to obtain, the buckling loads using the maximum membrane strain method are higher than those obtained using the strain reversal method, but these are unduly high. This is because of the poorly defined post-buckling path of the sections. Therefore, in the case of the sections used in practice, the maximum membrane

strain method does not seem to work since the buckling loads could not be determined using this method.

In the case of buckling loads obtained using the strain reversal method on specimens of Set I, it can be seen that the buckling load of specimens with an opening size of 20% is less than the buckling loads of unperforated specimens. However, as the hole size is increased, the buckling load also increases. This is because with formation of an opening in the web, each surrounding plate element of the web becomes almost akin to an unstiffened element. The elements of web with its smaller opening have a larger width-to-thickness ratios and therefore more flexible than the elements of the web with larger opening. Therefore, the specimen with larger hole size has a higher buckling stress than the specimen with a smaller opening. Accordingly, the buckling loads of the former may be higher than the latter.

Table 4.1 Buckling loads of test specimens

Specimen	Buckling load of specimens of Set I: strain reversal method (VI)	Set I: maximum membrane strain method (VII)	Set II: strain reversal method (VI)	Set II: maximum membrane strain method (VII)
A-2-1	46.0	-	10.0	40.0
A-2-2	48.1	-	8.1	44.1
A-2-3	55.1	-	10.0	44.0
A-4-1	59.9	-	12.0	-
A-4-2	60.3	-	8.0	-
A-4-3	63.1	-	10.0	-
A-6-1	72.0	74.7	12.0	-
A-6-2	72.9	-	6.0	-
A-6-3	72.0	-	16.0	-
B-2-1	50.0	-	8.0	42.2
B-2-2	38.2	81.5	8.1	42.1
B-2-3	52.2	83.5	10.0	42.3
B-4-1	60.9	-	10.0	-
B-4-2	62.0	-	10.7	-
B-4-3	67.0	-	8.0	-
B-4-4	58.0	-		
B-6-1	72.7	-	30.1	44.0
B-6-2	73.7	74.9	34.1	43.0
B-6-3	74.5	-	30.0	43.0
B-6-4	76.2	-		
B-6-5	74.2	-		
C-I-1	65.0	-	3.0	-
C-I-2	61.8	67.9	10.0	-
C-I-3	64.2	66.8	6.1	40.0
C-I-4	61.2	-		
D-0-1	62.0	79.9	10.0	-
D-0-2	74.0	79.8	16.0	-
D-0-3	73.8	82.5	16.0	48.0

CHAPTER 5

ANALYSIS OF RESULTS: ULTIMATE LOADS

5.1 INTRODUCTION

In the previous chapter the methods used in the determination of buckling loads were reviewed. The buckling loads of the specimens were also calculated. A brief description of the general behaviour of the stub columns, including the variation of their ultimate loads, was given in chapter 3. In this chapter, various techniques usually applied to determine ultimate strength, are reviewed. The effective width approach is discussed in detail. Strength of stub columns is calculated using provisions given in CAN3-S136-M84 and AISI (1986). The calculated strength values using these provisions are compared with the experimental values of this study. An empirical relationship is derived to predict the ultimate loads of stub columns with openings, and is verified by comparison with some of the available test results of other reported studies.

5.2 DETERMINATION OF ULTIMATE LOADS OF UNPERFORATED SECTIONS

As stated earlier, plates have significant reserve strength after buckling. The ultimate strength of a plate element essentially depends on its edge conditions, width-to-thickness ratio, and material properties. Many theoretical and experimental investigations have been

carried out to utilize this strength in thin walled structural members. In the theoretical analysis of post-buckling of plates, material and geometric non-linearities of the specimen are involved. Procedures involved to correctly account for these presents a formidable task. However, many methods have been used, which include the Ritz energy method, numerical methods such as the Finite Element Method, and studies based on the deformation theory of plasticity. Among these, the Finite Element Method has been extensively used in plate analysis during the last few years. Many reviews are available and one of these is by Little (1977).

An approximate method, relatively simple and more economical to apply was proposed by Korol and Sherbourne (1972). By this method, one can predict the ultimate capacity of thin walled structural members which corresponds to the point of intersection of the elastic loading line and rigid plastic unloading (mechanism) line of the load vs lateral deflection plot. The ultimate load obtained by this method will be an upper bound to the experimental load (Korol and Sherbourne, 1972).

The methods previously discussed for analysis of thin walled structural members may not be suitable for design office use because of the time, money, and skill required. Therefore, for post buckling analysis, and to predict the ultimate capacity of these thin walled

structural members, two semi-empirical approaches are used. The first approach, proposed by Gerard(1957), has been widely used in European codes of practice (Lee and Harris, 1978 and Allen and Bulson, 1980). In this approach a simplified formula is proposed where the ultimate strength of the member is expressed as a function of buckling stress and yield stress. In North America, however, the effective width approach, first proposed by Von Karman et al (1932). is the most popular. This approach will be discussed in detail in section 5.4.

5.3 ULTIMATE LOADS OF PERFORATED SECTIONS

Few studies have been performed on the post-buckling behaviour (including ultimate capacity) of perforated plates and sections in axial compression. Ritchie et al (1975) studied both theoretical and experimental post buckling behaviour of perforated square and rectangular flat plates. In the theoretical analysis, they employed an approximate approach using a combination of the Ritz energy method and Finite Element Method. Their theoretical predictions were not accurate for small size holes in the post buckling range. However, Azizian and Roberts (1984) refined the theoretical analysis by employing a Finite Element formulation in large deflection elasto-plastic analysis of perforated square plates in axial compression, extending up to collapse. Narayanan and Chow (1984) conducted experimental and theoretical studies on the

ultimate capacity of uniaxially compressed perforated flat square plates. In their theoretical analysis, they used the approximate method proposed by Korol and Sherbourne (1972) to find the ultimate capacity by finding the point of intersection of the elastic loading line and the rigid plastic unloading line. The method compares well with experimental results, and reduces the cost of computation (Narayanan and Chow 1984).

The above investigations were done on perforated individual plates. For practical cold formed sections, Yu and Davis (1973) tested 28 rectangular stub columns. The rectangular shape was formed by bolting the lips of two lipped channels. Circular or square perforations were made in the centre of each web. They proposed a reduced effective design width based on their results. Loov (1984) also proposed an effective width equation based on his test results of perforated lipped channel sections. These tests were done as performance tests as per requirements of CAN3-S136-M84 for some special application. As a result, there was no systematic change of parameters such as size, shape, number, and distribution of holes. Recently. Pekoz (1986) proposed an effective width equation based on his stub column tests of perforated lipped channel sections with circular holes in their webs. His equation has been incorporated in AISI-1986, for the design of perforated cold formed sections. This will be discussed in section 5.4.1.

Azizian and Roberts (1984) found that, though the buckling load of plates may increase with increase in size of hole, there will always be a decrease in ultimate load. Narayanan and Chow (1984) confirmed these findings regarding the decrease in ultimate strength of plate, with corresponding increase in hole size.

5.4 EFFECTIVE WIDTH APPROACH

This approach was proposed by Von Karmen et al (1932). According to this approach, the axial stress of a flat plate element under compression is uniform across the width of the plate before buckling. After buckling, stress redistribution takes place with minimum stress in the central part and maximum stress at the edges. The resultant of this stress distribution, however, is equal to the axial compression load. In order to reduce the computation involved and to simplify design, the actual non-uniform stress distribution across the width of the plate element in the post buckling range may be replaced by a uniformly distributed stress equal to the edge stress acting on the effective part of the plate (Von Karmen et al 1932 and Wang and Winter 1969)

$$Bf_{max} = \int_0^W f dW \qquad [5.1]$$

where B is the width of the effective part (effective width), f_{max} is maximum compressive stress (stress at edges), f is the compressive membrane stress anywhere across the width, W, of the plate element. Therefore, according to the effective width approach the central part of the plate is considered ineffective, with the part along the restrained edges considered fully effective.

The compressive stress distribution in the post buckling range, and therefore effective width as well, depends on the edge conditions of a plate. Depending on the type of edge conditions, a plate element may be identified as stiffened or unstiffened. A stiffened compression element is a flat plate element in which both edges parallel to the direction of loading are stiffened by another plate element such as a web, a flange or a lip. The stiffening elements should however, satisfy certain stiffness requirements. These requirements, provided in North American codes, are discussed in section 5.4.1. A plate element is called unstiffened when one of its edge is free and the other is stiffened.

The effective width relationship first proposed by Von Karmen et al (1932), for effective width of a stiffened plate element is

$$B = \frac{\Pi}{\sqrt{3\ (1 - \nu^2)}} \sqrt{\frac{E}{f_{max}}}\ t \qquad [5.2]$$

The above equation was derived based on an assumption of the wave shape of a buckle and, through minimization of f/E with respect to the wave length of the buckle. Von Karman et al (1932) also postulated that a plate in local buckling reaches its ultimate load carrying capacity when its edge stress equals the yield stress. The minimum effective width of a stiffened plate element which occurs at failure load level is given by

$$B_{min} = 1.9\ t \sqrt{\frac{E}{f_y}} \qquad [5.3]$$

Equation 5.3 results from the substitution of ν = 0.3 and $f_{max} = f_y$ in equation 5.2. However, in order to improve equation 5.3 for the effective width, a great deal of experimental work was done on flat plates and on cold formed sections. Winter (1947) took a leading role and an exhaustive review of his experimental work and other relevent studies is given by Roorda and Venkataramaiah (1978). From these experimental studies, it was found that equation (5.3) was good for plates with large width to thickness ratios, whereas for small ratios, it was found to be unsafe (Winter 1947, Johnson and Winter 1968, Wang and Winter 1969, and Roorda et al 1978). For stiffened plates, the modification proposed by Winter based on his tests of steel beams and columns can be written as:

$$B = 1.9t \sqrt{\frac{E}{f_{max}}} \left[1 - 0.475 \frac{t}{W} \sqrt{\frac{E}{f_{max}}} \right] \qquad [5.4]$$

Based on their analysis of the available experimental data, Roorda and Venkataramahiah (1978) gave a very simple form for the effective width equation of stiffened plates which is a slightly upward modification of equation 5.4.and is given as:

$$B = 2.0t \sqrt{\frac{E}{f_{max}}} \left[1 - 0.5 \frac{t}{W} \sqrt{\frac{E}{f_{max}}} \right] \qquad [5.5]$$

The effective width equations given by the codes for perforated and unperforated sections are given in the following section.

5.4.1 EFFECTIVE WIDTH OF PLATES AS PER CODE PROVISIONS

In the design of plate elements in compression, the present North American codes contain effective width equations that are similar to equation 5.4. and also contain values for the limiting width. It is necessary to apply the effec-ive width equation for elements having (w/t) ratios greater than the limiting widths. As per the provisions of the Canadian Code of practice (CAN3-S136-M84) an unperforated compressive plate element of a cold formed section is fully effective (B = W), until the flat width is less than W_{lim} given by

$$W_{lim} = 0.644\ t \sqrt{\frac{kE}{f_{max}}} \qquad [5.6]$$

The effective width, B, of a plate element of cold formed compression member having flat width, W, greater than the limiting width value given by equation 5.6, is given as

$$\frac{B}{t} = 0.950 \sqrt{\frac{kE}{f_{max}}} \left[1 - 0.208 \frac{t}{W} \sqrt{\frac{kE}{f_{max}}}\right] - R \qquad [5.7]$$

where k is a coefficient based on the edge conditions. The values of k are 4.0 and 0.5 for stiffened and unstiffened compression elements, respectively. Here, a compression element is considered stiffened when both its edges are restrained by a stiffener. However, a stiffener must have a minimum moment of inertia, I_{min}, about its own centroidal axis parallel to the stiffened element, given as:

$$I_{min} = \left[\frac{2W}{t} - 13\right] t^4, \text{ but not less than } 9t^4 \qquad [5.8]$$

In equation 5.7, R is a reduction factor having zero value for a plate element with W/t ratio less than 60 or when it is stiffened on both edges in the direction of the compressive force. For W/t ratios greater than, or equal to 60, R given as

$$R = \frac{0.1W}{t} - 6.0 \qquad [5.9]$$

The AISI (1986) also provides similar guidelines for the design of compression elements, except that the value of k is 0.43 for unstiffened elements. Also, reduction factor, R, is not applied to higher ratios of W/t.

The above discussion and the equations are applicable for sections without any openings. Chapter 1 noted that there are no provisions for the design of perforated elements in the Canadian code of practice (CAN3-S136-M84). However, AISI (1986), has provided guidelines for the design of a stiffened plate element with a circular opening by modifying guidelines for unperforated plates. Accordingly, the effective width of an element is taken as the smaller of the two values as given by the following equations:

$$B = W-d \qquad [5.10]$$

$$\frac{B}{t} = 0.950\sqrt{\frac{kE}{f_{max}}}\left[1 - 0.208\,\frac{t}{W}\sqrt{\frac{kE}{f_{max}}} - 0.8\,\frac{d}{W}\right] \qquad [5.11]$$

These equations are applicable for plate elements of flat width-to-thickness ratios up to 70 with circular openings in their center. These guidelines are based on limited data (Pekoz, 1984).

5.5 CALCULATION OF ULTIMATE LOADS

In this section the ultimate loads of the sections tested for this study are determined using above discussed guidelines. Later on a new equation is proposed for the design of stiffened plate elements with a circular or square hole in their center.

Ultimate load of a section is obtained by multiplication of effective area of section and stress at ultimate loads (yield stress). The effective area of a section is determined by multiplying plate thickness of section with the sum of the effective widths of its plate elements. Effective width of a plate depends on its edge conditions. Equation 5.8 is used to determine the edge condition of plate elements of sections. Table 5.1 shows the actual values of moments of inertia, I, and minimum required by Canadian code(equation 5.8), of the plate elements of specimens of all sets. The actual value of I for a particular element for all the sets is greater than that required by equation 5.8. Therefore, for all the specimens the flanges act as stiffeners to the webs, and the lips act as stiffeners to the flanges. However, the lips are considered unstiffened since they are stiffened on one side only.

The limiting width values of webs, flanges and lips of various specimens corresponding to the respective thicknesses of plates were calculated using equation 5.6.

These values and the actual widths of plate elements are given in Table 5.2. From comparison of calculated and actual values, it is evident that the lips and flanges are fully effective. Here, the rounded edges of the specimens are also considered fully effective. This has been treated as such for calculating ulimate loads using various methods. Since actual widths of webs are greater than the respective limiting widths, therefore, the effective widths of webs must be calculated. This is done using various approaches.

The unfactored ultimate loads, P_{csa} and P_{aisi} shown in Table 5.3, of the tested sections are calculated by modifying guidelines of Canadian code and using AISI (1986) guidelines, respectively. These are shown in columns 3 and 4 of Tables 5.3-(I) and 5.3-(II) for sets I and II, respectively. To calculate ultimate loads, P_{csa}, equation 5.7 was used for finding the effective widths of webs. For sections with different types of openings the plate elements of webs on both sides of the opening were considered unstiffened. P_{aisi} were calculated using equations 5.10 and 5.11 for finding the effective width of perforated webs. Although the AISI (1986) guidelines apply for circular holes, the same are applied in this study for square and slotted holes. For comparison with the experimental results of this study, the ratios P_t/P_{csa} and P_t/P_{aisi} are calculated and shown in column 5 and 6 of Table 5.3.

For perforated sections, it was found that the

loads P_{csa} are conservative for smaller sized circular and square holes and are more accurate for larger sized holes. However, by applying provisions of AISI 1986, we obtain more accurate results for circular and square perforations, up to 20% of the flat width of the web. However, for larger hole sizes the results are conservative and will give uneconomical results. These provisions, therefore, appear inadequate because they do not give uniform results.

It is important to note from Table 5.3 that the calculated loads for unperforated sections are higher than the corresponding experimental loads. This may be due to the experimental scatter. The guidelines provided in North American codes, in the form of equation 5.7, are the best fit of the previous test results. In this study, however, the calculated values of ultimate loads, obtained by provisions of North American codes, are consistently higher than the experimental values. Therefore, there may be a need for a re-evaluation of the present code guidelines.

No attempt is made to re-evaluate the equation to determine the effective width of plates provided by North American codes. However, it seems that the discrepancy of code guidelines to correctly predict the ultimate loads, is due to the use of limiting width value (equation 5.6) of plate elements of the specimen. This is the width, below which the plate element acts as a totally effective element. It has been pointed out by Roorda and Venkataramaiah (1978)

that at this limiting point, the plot of effective width given by equations 5.6 and 5.7 with respect to actual width makes a kink which is unnatural. Winter (1947) performed tests on plates in the so-called total effective width range and found that the effective width is, in fact, dependent on the actual width in the range below W_{lim} (given by equation 5.6.) where the plate should be fully effective according to the code guidelines (Roorda and Venkataramaiah 1978). Therefore, Winter's orginal equation 5.4 seems more relevant for determination of effective widths of plates.

For the above reasons, ultimate loads of the sections are also calculated using Winter's equation (equation 5.4). Since the AISI guidelines do not give uniform results for perforated specimens, a new equation for calculation of ultimate loads for sections with circular or square openings in the centre of the stiffened plate element will be obtained for values of flat width-to-thickness ratios up to 112. Most of the cold formed sections used in practice fall into this range.

5.5.1 PREDICTION OF ULTIMATE LOADS OF PERFORATED PLATES BY PROPOSED EQUATION

The effect of a circular or square opening in the centre of a plate element is accounted for by considering an empirical relation between the effective widths of perforated and unperforated webs. A selected function should be such that :

a) $B_p = B_{un}$, when d = 0

Here, B_p and B_{un} are effective widths of the perforated and unperforated web of the section and d is the diameter of a circular opening or the side of a square opening.

b) $B_p = 0$, when d = W

c) For intermediate values of hole diameter,it should predict correctly the effective widths of the web.

Many functions were tried, but the best suited and most simple function is found to be

$$\frac{B_p}{B_{un}} = C R_w^n \qquad [5.12]$$

Here, C and n are constants and R_w is a non-dimensional parameter that reflects the size of the opening, given as

$$R_w = \frac{W - d}{W} \qquad [5.13]$$

The effective width of a perforated web of a section can be obtained from experimental results as:

$$B_p = \frac{A_e}{t} - 2B_2 - 2B_3 - 5\pi t \qquad [5.14]$$

where B_2 and B_3 are the effective widths of unperforated flanges and lips and A_e is given as

$$A_e = \frac{P_t}{f_y} \qquad [5.15]$$

The unperforated effective width of web, B_{un}, is calculated the same way as B_p by substituting the value of d equal to zero. The value of B_{un} used in equation 5.12 to find the empirical relation is the average B_{un} of the three unperforated specimens each, for sets I and II. B_p is calculated for each perforated specimen with a square or circular opening only. Since the experimental data to evaluate the effect of the longitudinal dimensions of the openings on the ultimate loads of the specimens is insufficient, no attempt is made to propose any relationship for specimens for slotted openings.

The values of C and n are found by a curve fitting technique. A best fit function of the data for various sets of specimens, excluding slotted holed specimens, is found. The values of C and n are given in Table 5.4. It is found that the constant C is slightly greater than 1, and n is less than, or equal to, 0.557. Therefore, a simple and conservative equation for a specimen with a circular or square opening in the centre of its web may be given as;

$$\frac{B_p}{B_{un}} = \sqrt{R_w} \qquad [5.16]$$

For comparison, plots of the best fit equation and the proposed equation, along with data points corresponding to all 47 specimens are shown in Figure 5.1. This graph is plotted for B_p/B_{un} of web along the Y-axis and W_p/W of web along the X-axis. It is evident that the plot of the proposed equation is below the best fit curve. Therefore, the ultimate load calculated using equation 5.16 will be safe.

The ultimate loads of the sections are calculated using equation 5.16 for finding the effective width of the perforated section. Here, the effective width of the unperforated web (B_{un})to be used for relation 5.16 is calculated using equation 5.4 (Winter 1947) or equation 5.7 (CAN3-S136-M84). These ultimate loads calculated using equations 5.4 and 5.7 are denoted as P_1 and P_2, respectively. and are shown in column 2 and 3 of Table 5.5. The ratios of experimental and calculated values of ultimate loads, P_t/P_1 and P_t/P_2, are given in columns 5 and 6 of Table 5.5, respectively. It is evident that the calculated values of the ultimate loads are higher for almost all of the sections, but P_1 values are closer to the experimental values of all sections. This is because equation 5.4 predicted ultimate loads of unperforated section better than

did equation 5.7. This is evident from the rows corresponding to unperforated (D-type) sections.

Since the calculated loads, P_2, of unperforated sections using provisions of CAN3-S136-M84 (equation 5.7), are higher than the experimental ultimate loads (P_t), all P_2 values are divided by a factor, D.F.. This is done to determine the validity of equation 5.16 and for easy comparison of calculated values, P_2, with experimental values, P_t. The factor D.F. for a set of specimens is given by:

D.F. = P_2 value of unperforated section of a set divided by average value of experimental loads of the unperforated sections of the same set.

For example, for Set I the P_2 value for unperforated sections is 89.57 KN and the average value of the ultimate loads of specimens D-0-1, D-0-2, and D-0-3 is 85.33 KN. The value of D.F. for Set I is, therefore, equal to 1.05. Similarly, the D.F. values for Set II and Set P are 1.04 and 1.00, respectively.

Using the value of D.F. for a set of specimens the values P_3 are calculated for easy comparison with the experimental values of the ultimate loads. The P_3 values of specimens are shown in Table 5.5 in column 4, along with the ratios, P_t/P_3, in column 7. It is evident that the P_3 values of ultimate loads of the perforated sections are very

close to their experimental values.

For comparison of various methods, a statistical analysis of the experimental data was done by calculating the mean value and standard deviation of the ratios of experimental and calculated loads. Calculated loads were obtained using various methods for unperforated specimens, and for the specimens with circular and square holes. The results are shown in Table 5.6. The standard deviations obtained using the values of loads: P_1, P_2, and P_3 are less than the standard deviations obtained using the values of load of P_{csa} and P_{aisi}. The calculated ultimate loads for unperforated sections of a set are the same except for P_1, which was obtained using Winter's equation. In spite of this, the mean value of the ratio of the experimental ultimate load and P_{aisi} are more than the values obtained using the other methods for values of P_{csa}, P_2, and P_3. It appears that the results obtained using AISI guidelines (equations 5.10 and 5.11) are rather conservative. The values of effective widths by equation 5.16 are very reasonable.

Equation 5.16 was verified by comparing the calculated ultimate loads with test results of Pekoz (1986) and Loov (1984). The effective width, B_{un}, used in calculating B_p is determined by equation 5.7. Both experimental and calculated ultimate load values are shown in Tables 5.7 and 5.8. The values of the ratios of experimental values and calculated values, using equation

5.16, are given in column 8 of the respective tables. The values of mean and standard deviation of these ratio are also calculated. For the experiments of Pekoz (1986), given in Table 5.7, these are 1.054 and 0.062, whereas by the guidelines of AISI 1986 (equation 5.10) are 1.072 and 0.086 (Pekoz 1986).

In the case of experiments done by Loov (1984), the mean and standard deviation for the ratio of experimental results and loads calculated using equation 5.16 are 0.999 and 0.038. The mean value, 0.999, is less than one. This may be because of the presence of two small circular openings very close to the central square opening in the web. The presence of the two additional openings will affect the ultimate strength of the section. Therefore, it is concluded that equation 5.16 gives satisfactory results.

Table 5.1 Moment of inertia of flanges and lips of specimens

Set	Moment of inertia of a plate element			
	flange		lip	
	required minimum (mm^4)	actual provided (mm^4)	required minimum (mm^4)	actual provided (mm^4)
I	592.52	8336.17	174.80	182.48
II	581.20	6857.82	107.38	159.44
P	4172.10	76926.34	1137.77	2352.45

Table 5.2 Limiting values of flat widths of specimen plate elements.

Set No.	name of element	type of element	flat width symbol	limiting width as per eq. 5.6 (mm)	actual flat width (mm)
I	Web	stiffened	W1	50.62	82.46
	Flange	stiffened	W2	50.62	31.66
	Lip	unstiffened	W3	17.90	7.89
II	Web	stiffened	W1	46.91	144.68
	Flange	stiffened	W2	46.91	33.55
	Lip	unstiffened	W3	16.58	8.84
P	Web	stiffened	W1	71.42	189.48
	Flange	stiffened	W2	71.42	62.48
	Lip	unstiffened	W3	25.25	18.54

Table 5.3-I Calculation of loads as per North American Codes for Set I of specimens

Specimen Designation	Experimental Loads (P_t)	Calcuated Loads		$\frac{P_t}{P_{csa}}$	$\frac{P_t}{P_{aisi}}$
		CAN3-S136 (P_{csa})	AISI-1986 (P_{aisi})		
A-2-1	85.50			1.060	1.030
A-2-2	85.65	80.66	83.04	1.062	1.031
A-2-3	86.10			1.067	1.037
A-4-1	81.45			1.031	1.064
A-4-2	81.90	78.98	76.52	1.037	1.070
A-4-3	81.75			1.035	1.068
A-6-1	78.35			1.046	1.119
A-6-2	77.35	74.88	70.00	1.033	1.105
A-6-3	78.70			1.051	1.124
B-2-1	84.20			1.044	1.014
B-2-2	84.40	80.66	83.04	1.046	1.016
B-2-3	85.50			1.060	1.030
B-4-1	81.35			1.030	1.063
B-4-2	81.40	78.98	76.52	1.031	1.064
B-4-3	81.90			1.037	1.070
B-4-4	81.55			1.033	1.066
B-6-1	76.35			1.020	1.091
B-6-2	77.80			1.039	1.111
B-6-3	78.50	74.88	70.00	1.048	1.121
B-6-4	78.85			1.053	1.126
B-6-5	77.00			1.028	1.100
C-I-1	72.50			0.927	0.973
C-I-2	72.65	78.22	74.54	0.929	0.975
C-I-3	72.60			0.928	0.974
C-I-4	75.20			0.961	1.009
D-0-1	84.55			0.944	0.944
D-0-2	84.70	89.57	89.57	0.946	0.946
D-0-3	86.75			0.969	0.969

Table 5.3-II Calculation of loads as per North American Codes for Set II of specimens

Specimen Designation	Experimental Loads (P_t)	Calcuated Loads CAN3-S136 (P_{csa})	Calcuated Loads AISI-1986 (P_{aisi})	$\frac{P_t}{P_{csa}}$	$\frac{P_t}{P_{aisi}}$
A-2-1	54.00			1.071	1.027
A-2-2	54.00	50.42	52.59	1.071	1.027
A-2-3	53.85			1.068	1.024
A-4-1	54.00			1.082	1.105
A-4-2	53.00	49.90	48.85	1.062	1.085
A-4-3	53.10			1.064	1.087
A-6-1	48.30			0.988	1.071
A-6-2	45.70	48.88	45.11	0.935	1.013
A-6-3	47.30			0.968	1.049
B-2-1	52.75			1.046	1.003
B-2-2	52.70	50.42	52.59	1.045	1.002
B-2-3	54.20			1.075	1.031
B-4-1	52.00			1.042	1.064
B-4-2	51.30	49.90	48.85	1.028	1.050
B-4-3	49.60			0.994	1.015
B-6-1	47.70			0.976	1.058
B-6-2	46.70	48.88	45.11	0.955	1.035
B-6-3	46.60			0.953	1.033
C-I-1	52.30			1.040	1.017
C-I-2	51.70	50.29	51.43	1.028	1.005
C-I-3	50.70			1.008	0.986
D-0-1	54.30			0.964	0.964
D-0-2	54.40	56.34	56.34	0.966	0.966
D-0-3	53.25			0.945	0.945

Table 5.4 Best fit values of C and n for equation 5.12

Set no.	No. of data points	value of C	value of n	Standard deviation of data from best fit
I	23	1.049	0.371	0.038
II	21	1.096	0.557	0.093
P	3	0.999	0.342	0.002
all sets	47	1.065	0.451	0.077

Table 5.5-I Predicted ultimate loads by proposed equation 5.16 for specimens of Set I

SPECIMEN	Predicted ultimate loads			P_t/P_1	P_t/P_2	P_t/P_3
	P_1	P_2	P_3			
A-2-1	85.73	86.77	82.67	0.997	0.985	1.034
A-2-2	85.73	86.77	82.67	0.999	0.987	1.036
A-2-3	85.73	86.77	82.67	1.004	0.992	1.041
A-4-1	82.59	83.53	79.58	0.986	0.975	1.024
A-4-2	82.59	83.53	79.58	0.992	0.981	1.029
A-4-3	82.59	83.53	79.58	0.990	0.979	1.027
A-6-1	78.74	79.54	75.78	0.995	0.985	1.034
A-6-2	78.74	79.54	75.78	0.982	0.973	1.021
A-6-3	78.74	79.54	75.78	0.999	0.989	1.039
B-2-1	85.73	86.77	82.67	0.982	0.970	1.018
B-2-2	85.73	86.77	82.67	0.985	0.973	1.021
B-2-3	85.73	86.77	82.67	0.997	0.985	1.034
B-4-1	82.59	83.53	79.58	0.985	0.974	1.022
B-4-2	82.59	83.53	79.58	0.986	0.975	1.023
B-4-3	82.59	83.53	79.58	0.992	0.981	1.029
B-4-4	82.59	83.53	79.58	0.987	0.976	1.025
B-6-1	78.74	79.54	75.78	0.970	0.960	1.008
B-6-2	78.74	79.54	75.78	0.988	0.978	1.027
B-6-3	78.74	79.54	75.78	0.997	0.987	1.036
B-6-4	78.74	79.54	75.78	1.001	0.991	1.041
B-6-5	78.74	79.54	75.78	0.978	0.968	1.016
C-I-1	81.52	82.41	78.52	0.889	0.880	0.923
C-I-2	81.52	82.41	78.52	0.891	0.882	0.925
C-I-3	81.52	82.41	78.52	0.891	0.881	0.925
C-I-4	81.52	82.41	78.52	0.922	0.912	0.958
D-0-1	88.42	89.57	85.33	0.956	0.944	0.991
D-0-2	88.42	89.57	85.33	0.958	0.946	0.993
D-0-3	88.42	89.57	85.33	0.981	0.969	1.017

Table 5.5-II Predicted ultimate loads by proposed equation 5.16 for Specimens of Set II

SPECIMEN	Predicted ultimate loads			P_t/P_1	P_t/P_2	P_t/P_3
	P_1	P_2	P_3			
A-2-1	54.23	54.55	52.27	0.996	0.990	1.033
A-2-2	54.23	54.55	52.27	0.996	0.990	1.033
A-2-3	54.23	54.55	52.27	0.993	0.987	1.030
A-4-1	52.18	52.47	50.27	1.035	1.029	1.074
A-4-2	52.18	52.47	50.27	1.016	1.010	1.054
A-4-3	52.18	52.47	50.27	1.018	1.012	1.056
A-6-1	49.66	49.90	47.82	0.973	0.968	1.010
A-6-2	49.66	49.90	47.82	0.920	0.916	0.956
A-6-3	49.66	49.90	47.82	0.952	0.948	0.989
B-2-1	54.23	54.55	52.27	0.973	0.967	1.009
B-2-2	54.23	54.55	52.27	0.972	0.966	1.008
B-2-3	54.23	54.55	52.27	0.999	0.994	1.037
B-4-1	52.18	52.47	50.27	0.996	0.991	1.034
B-4-2	52.18	52.47	50.27	0.983	0.978	1.020
B-4-3	52.18	52.47	50.27	0.951	0.945	0.987
B-6-1	49.66	49.90	47.82	0.960	0.956	0.998
B-6-2	49.66	49.90	47.82	0.940	0.936	0.977
B-6-3	49.66	49.90	47.82	0.938	0.934	0.975
C-I-1	53.63	53.94	51.68	0.975	0.970	1.012
C-I-2	53.63	53.94	51.68	0.964	0.958	1.000
C-I-3	53.63	53.94	51.68	0.945	0.940	0.981
D-0-1	55.99	56.34	53.98	0.970	0.964	1.006
D-0-2	55.99	56.34	53.98	0.972	0.966	1.008
D-0-3	55.99	56.34	53.98	0.951	0.945	0.986

Table 5.6 Mean and standard deviation of the ratios of experimental loads and calculated loads

	P_t/P_{csa}	P_t/P_{aisi}	P_t/P_1	P_t/P_2	P_t/P_3
			Set I		
mean	1.030	1.058	0.987	0.976	1.024
standard deviation	0.033	0.053	0.012	0.013	0.013
			Set II		
mean	1.014	1.031	0.976	0.971	1.013
standard deviation	0.052	0.041	0.029	0.029	0.030

Table 5.7 Comparison of ultimate loads predicted by equation 5.16 with experimantal results of Pekoz(1986)

(1) Total Web (mm)	(2) Total Flange (mm)	(3) Total lip (mm)	(4) Hole size (mm)	(5) Yield Stress Fy (MPa)	(6) Test Loads P_t (kN)	(7) Calculated Loads P_c (kN)	(8) Ratio $\frac{P_t}{P_c}$
80.0	30.5	8.6	0.0	334.52	67.19	64.49	1.04
80.0	30.5	8.6	0.0	324.86	65.86	62.87	1.05
80.0	30.5	8.6	12.7	342.10	64.52	63.98	1.01
80.0	30.5	8.6	19.1	324.86	62.96	60.23	1.05
80.0	30.5	8.6	26.4	342.10	62.52	61.86	1.01
80.0	30.5	8.6	31.8	355.55	61.41	63.10	0.97
80.0	30.5	8.6	38.1	334.52	56.29	58.64	0.96
80.0	30.5	8.6	44.5	355.55	60.52	60.68	0.99
80.0	30.5	8.6	12.7	342.10	68.97	63.98	1.07
80.0	30.5	8.6	26.4	334.52	65.32	60.65	1.08
80.0	30.5	8.6	38.1	334.52	64.52	58.64	1.10
79.3	29.8	8.2	26.4	328.31	109.47	98.73	1.11
79.3	29.8	8.2	38.1	328.31	106.80	94.59	1.13
79.3	29.8	8.2	0.0	324.17	124.15	105.49	1.18

Table 5.8 Comparision of ultimate loads predicted by equation 5.16 with experimental results of Loov(1984)

(1) Total Web (mm)	(2) Total Flange (mm)	(3) Total lip (mm)	(4) Thick- ness (mm)	(5) Yield Stress Fy (MPa)	(6) Test Loads Pt (kN)	(7) Calculated Loads Pc (kN)	(8) Ratio Pt / Pc
63.8	42.6	12.5	2.01	384.0	103.62	103.40	1.002
63.8	42.6	12.5	2.01	384.0	103.62	103.40	1.002
63.8	42.6	12.5	2.01	384.0	102.40	103.40	0.990
63.7	42.2	13.0	1.42	382.9	78.65	72.16	1.090
63.7	42.2	13.0	1.42	382.9	76.00	72.16	1.053
63.5	42.4	12.1	1.21	268.5	44.76	43.00	1.041
63.5	42.4	12.1	1.21	268.5	43.87	43.00	1.020
63.5	42.4	12.1	1.21	268.5	42.8	43.00	0.995
92.3	42.2	12.5	1.21	268.5	46.92	47.28	0.992
92.3	42.2	12.5	1.21	268.5	48.11	47.28	1.017
92.3	42.2	12.5	1.21	268.5	48.20	47.28	1.020
92.1	42.2	13.0	1.42	382.9	72.00	78.96	0.912
92.1	42.2	13.0	1.42	382.9	76.40	78.96	0.968
92.1	42.2	13.0	1.42	382.9	78.90	78.96	0.999
92.4	42.4	12.8	2.01	384.0	119.20	119.27	0.999
92.4	42.4	12.8	2.01	384.0	118.00	119.27	0.989
92.4	42.4	12.8	2.01	384.0	118.20	119.27	0.991
152.8	42.1	12.7	1.21	268.5	51.52	50.61	1.018
152.8	42.1	12.7	1.21	268.5	52.53	50.61	1.038
152.8	42.1	12.7	1.21	268.5	52.46	50.61	1.037
152.5	41.9	12.8	1.42	382.9	84.10	83.81	1.003
152.5	41.9	12.8	1.42	382.9	83.40	83.81	0.995
152.5	41.9	12.8	1.42	382.9	86.70	83.81	1.034
152.6	42.2	12.9	2.01	384.0	128.30	131.19	0.978
152.6	42.2	12.9	2.01	384.0	130.00	131.19	0.991
152.6	42.2	12.9	2.01	384.0	125.20	131.19	0.954
203.7	42.1	12.5	1.21	268.5	51.33	51.66	0.994
203.7	42.1	12.5	1.21	268.5	48.70	51.66	0.943
203.7	42.1	12.5	1.21	268.5	46.02	51.66	0.891
203.0	41.9	12.9	1.42	382.9	87.20	85.86	1.016
203.0	41.9	12.9	1.42	382.9	81.70	85.86	0.952
203.0	41.9	12.9	1.42	382.9	86.70	85.86	1.010
204.0	42.7	12.9	2.01	384.0	133.00	136.48	0.975
204.0	42.7	12.9	2.01	384.0	133.50	136.48	0.978
204.0	42.7	12.9	2.01	384.0	135.40	136.48	0.992

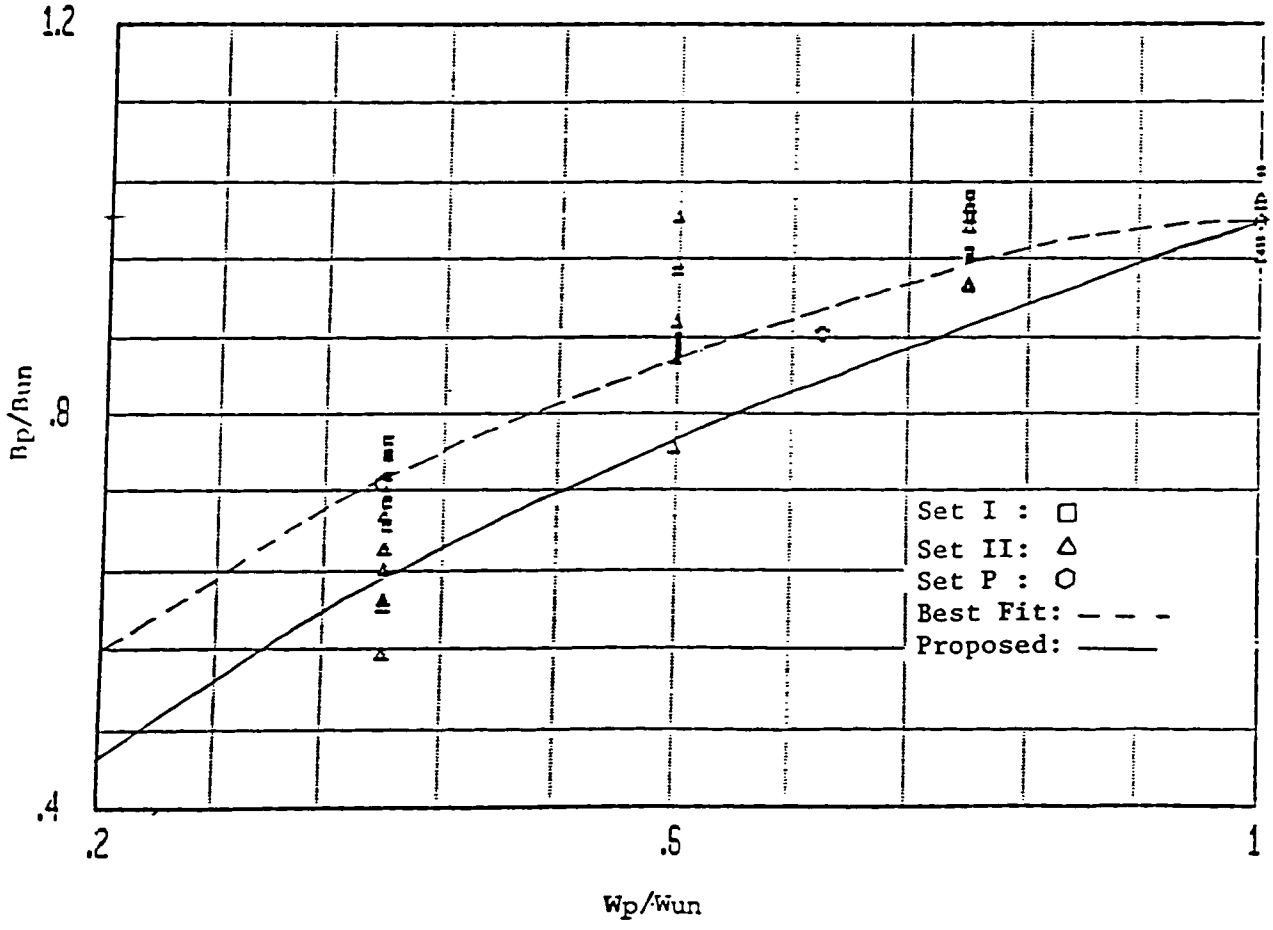

Fig. 5.1 Comparision of proposed relationship with experimental data

CHAPTER 6

CONCLUSIONS

6.1 SUMMARY

The main purpose of this research is to study the effect of perforations on the behaviour of axially compressed cold formed steel sections. To achieve this objective, 55 stub column tests were performed. These specimens were divided into three different sets depending on the value of the flat width-to-thickness ratio of their unperforated webs. These specimens were further sub-divided into sub-sets depending on the size and shape of the specimens. Three types of holes (circular, square, and slotted) were made in the webs of the specimens. The size of holes varied from 0 to 60% of the flat width of the webs of the specimens. The length of the stub columns was selected in such a way that failure of the specimens occurs by local buckling at their mid-heights, so that instruments such as tranducers and strain gauges could be mounted at pre-determined locations.

The material properties of most of the specimens were obtained through tests in the laboratory. The specimens were subjected to axial compressive loads until failure on a Tinius-Olson Universal testing machine. The test data includes axial shortening, web and flange out-of-plane

deflection, load readings and ultimate loads. Experimental buckling loads of the specimens were determined using Strain Reversal Method and Maximum Surface Strain Method. Graphs were drawn for load vs axial shortening and load vs out-of-plane deflection of the webs of these specimens. The experimental ultimate loads were compared with the calculated ultimate load values of perforated and unperaforted specimens using provisions of AISI- 1986 and by modifying provisions of CAN3-S136-M84. Based on the analysis new simplified equation was proposed to calculate the effective width of a perforated stiffened element with a circular, or square opening. The ultimate loads of the specimens were calculated using this relation, and results compared with the other available experimental results.

6.2 CONCLUSIONS

Based on the observations made during this study, the following conclusions can be drawn:

1. The failure of the unperforated specimens took place by local buckling, forming three half buckle waves. The length of the buckle wave is slightly less than the average of the width of the web and the width of flange. The mode of buckling is affected by the size of the hole. However, this was not investigated to any greater extent.

2. It is difficult to determine experimentally the buckling loads of the specimens, perhaps due to plate imperfections and difficulty in predicting the exact location of the

failure prior to testing. It may be said that the buckling load of the specimens is reduced as a small size hole is made in the webs. However, if the size of the hole increases, the buckling load increases as well.

3. There is a loss in stiffness of the sections due to an increase of size of hole. This is more evident from the load vs axial shortening curves especially closer to failure of the specimens. The stiffness of the sections is sensitive to the longitudinal size of the hole along the direction of loading. This is evident from the load vs axial shortening curves of the specimens with slotted holes. These specimens had the least stiffness among those within their respective sets.

4. There is no significant effect on the ultimate loads of the specimens with circular holes having a diameter up to 20% of the flat width of the specimens. However, the ultimate loads reduced with an increase in the diameter of the hole. The specimens with square holes had slightly lower ultimate loads than did those with circular holes, when the dimension of the side of the square was equal to the diameter of the circle. Due to the reduced stiffness of the specimens with slotted holes, the ultimate loads of these specimens were considerably less than those with circular or square holes, which had even larger sized holes in the transverse direction.

5. The effective width method is an excellent way of

estimating the ultimate loads of the specimens. The loads of the unperforated specimens calculated using the effective width equation given in North American codes were up to 6 % more than the experimental loads. Based on the test results of this study, it appears that there is need to revise this equation.

The ultimate loads of the perforated sections having circular openings calculated using provisions of the AISI (1986), were less than the experimental loads. The same was true for specimens with square holes, when the equation for calculating effective width of elements having circular holes was applied to these sections. On the whole, the provisions of the AISI (1986) for perforated elements are conservative.

The ultimate loads, calculated by modifying the provisions of CAN3-S136-M84, were also conservative for perforated sections. The loads predicted by this method were more accurate for sections with large size holes than for specimens with small size holes.

6. Equation 5.12 is proposed for the design of perforated cold formed steel sections based on the experimental ultimate loads of the specimens. The same equation, when applied to test data of other investigators, also gives quite reasonable results. Therefore, the effective width of a perforated web at ultimate loads can be calculated using equation 5.12.

6.3 SUGGESTIONS FOR FURTHER STUDY

To date, limited experimental and theoretical research has been done to study the effect of perforations on the behaviour of cold formed steel sections. Based on the observations of this work, the following points are suggested for further investigation:

1. The members were found to be very sensitive to the dimension of the hole parallel to the longitudinal axis of the specimen; hence, it is suggested that further tests be done to estimate the effect of varying this parameter.
2. The maximum flat width-to-thickness ratio of the webs of the specimens of this study was 112. Further testing should be done to investigate whether equation 5.12 is suitable for specimens with flat width-to-thickness ratios greater than 112.
3. It appears that the size of the hole is more important than the shape of the hole. However, specimens should be tested by cutting holes of other shapes such as the diamond, or cruciform, to confirm this.
4. The effective width equation for stiffened elements with circular or square openings proposed in this study is valid for estimating ultimate loads. The same effective width equation for perforated plate elements should be applicable at sub-ultimate loads. Further study should be done to confirm this.
5. It was not possible to propose an equation for finding

the buckle length due to the limited number of tests on unperforated specimens. More data should be collected through tests to better estimate the length of a buckle of a steel section.

REFERENCES

Allen, H.G. and Bulson, P.S. 1980. Background to buckling. Mcgraw Hill Book Company London, U.K..

American Iron and Steel Institute, 1986. Specification for design of cold-formed steel structural members. Washington, D.C., U.S.A..

American Society for Testing and Materials, 1985. Annual book of ASTM standards. Philadelphia, U.S.A..

Canadian Standards Association, 1984. Cold Formed Steel Structural Members, CAN3-S136-M84. Ontario, Canada.

Coan, J.M., 1951. Large-deflection theory for plates with small initial curvature loaded in edge compression. Journal of Applied Mechanics, Vol. 18, Transactions Of ASME, Vol. 73, pp. 143-157.

Column Research Council 1976. Guide to Stability Design Criteria for Metal Structures. Edited by Johnston, B.G. Wiley-Interscience, New York, U.S.A.

Fok, W.C., 1984. Evaluation of experimental data of plate buckling. ASCE Journal of Engineering Mechanics, Vol. 110, No. 4, pp. 577-588.

Fok, W.C. and Yuen, M.F., 1981. Modified pivotal plot for critical load calculations of a rectangular plate under edge compression. Journal Mechanical Engineering Science, Vol. 23 No. 4, pp. 167-170.

Johnson, A.L. and Winter, G., 1966. The structural performance of Austenitic stainless steel members. Report No. 327, Cornell University Ithaca, New York.

Korol, R.M. and Sherbourne, A.N., 1972. Strength prediction of plates in uniaxial compression. Journal of the Structural Division, Proc. of ASCE, Vol.98 (ST10), pp. 1965-1986.

Lee, H.P. and Harris, P.J., 1978. A finite element investigation of post-buckling strength of thin-walled structural members under compression. Canadian Journal of Civil Engineering, No. 5, pp. 595-610.

Little, G.H., 1977. Rapid analysis of plates collapse by Live-energy minimisation. International Journal of Mech. Sci., Vol. 19, No. 12, pp. 725-744.

Loov, R. 1984. Local buckling capacity of C-shaped cold-formed steel sections with punched webs. Canadian Journal of Civil Engineering, 11(1), pp 1-7.

Narayanan, R. and Chow, F.Y. 1984. Ultimate capacity of uniaxially compressed perforated plates. Thin walled Structures, 2, pp. 241-264.

Pekoz, T., 1986. Development of a unified approach to the design of cold-formed steel members. Committee of sheet steel producers. AISI, 1000 16th street, NW Washington, DC 20036. Report no SG 86-4.

Ritchie, D. and Rhodes, J., 1975. Buckling and post-buckling behaviour of plates with holes. Aeronautical Quarterly, November, pp. 281-296.

Robert, T.M. and Azizian, Z.G., 1984. Strength of perforated plates subjected to in-plane loading. Thin-Walled Structures 2(1984), pp. 153-164.

Rondal, J. and Maquoi, R., 1985. Stub-column strength of thin-walled square and rectangular hollow sections. Thin-Walled Structures, No 3, pp. 15-34.

Roorda, J. and Venkataramaiah, K.R. 1978. Effective width of stiffened steel plate components. Solid Mechanics Division, University of Waterloo, Ontario, Canada. Paper No. 148.

Schlack, A.L., 1964. Elastic stability of perforated square plates. Experimental Mechanics, June, 1964, pp. 167-172.

Schlack, A.L., 1968. Experimental critical loads for perforated square plates. Experimental Mechanics, Feb., pp. 69-74.

Sherbourne, A.N. and Korol, R.M., 1972. Post buckling of axially compressed plates. Journal of the Structural Division, Proc. of ASCE, Vol. 98 (ST9), pp. 2223-2234.

Souza, M.A., Fok, W.C., and Walker, A.C., 1983. Review of the experimental techniques for thin walled structures liable to buckling, Part II- Stable buckling. Experimental Techniques, October, pp. 36-39.

Spencer, H.H. and Walker A.C., 1974. Critique of Southwell plots with proposal for alternative methods. Experimental Mechanics, 15, pp. 303-310.

Stowell, E.Z., Heimerl, G.J., Libove, C., and Lundquist, E.E., 1951. Buckling Stresses for flat plates and sections. Proc. of ASCE, Vol. 77, pp. 545-578.

Vilnay. O. and Rockey, K.C., 1981. A generalised effective width method for plates loaded in compression. Journal of Constructional Steel Research, Vol. 1 No. 3, pp. 3-12.

Von Karman, T., Sechler, E. E., and Donnell, L. H., 1932. The strength of thin plates in compression. Transactions, ASME, Vol. 54, APM 54-5.

Walker, A.C., 1975. Design and analysis of cold-formed sections, John Wiley and Sons, New York, U.S.A..

Wang, S.T. and Winter, G., 1969. Cold-rolled Austenitic stainless steel: material properties and structural performance. Report No. 324, Cornell University Ithaca, New York.

William, D.G. and Walker, A.C., 1975. Explicit Solutions for the design of initially deformed plates subjected to compression. Proc. of the Institution of Civil Engineers, Part 2, Vol. 59, pp. 763-787.

Winter, G. 1947. Strength of thin steel compression flanges. Transactions ASCE pp.527-554.

Yu, W.W., 1985. Cold-formed steel design. John Wiley and Sons, New York, U.S.A..

Yu, W.W. and Davis, Charles S., 1973. Cold-formed steel members with perforated elements. ASCE, Journal of Structural Division, 99 (ST10), pp. 2061-2077.